

**Enhancement of thermoelectric properties in *p*-type  
conducting polymer-based composites**

*p* 型導電性高分子系熱電複合素子の特性向上

**51427354**

**MAY THU ZAR MYINT**

Division of Industrial Innovation Sciences

Graduate School of Natural Science and Technology

OKAYAMA UNIVERSITY

This dissertation is submitted for the degree of Doctor of

Engineering

**2019, September**

## DECLARATION

The material presented in this thesis is the outcome of my own research under the supervision of Professor Yasuhiko HAYASHI at Okayama University. It has not been previously submitted, in part or whole, to any university or institution for any degree or other qualification.

Signed:

Name: May Thu Zar Myint

Date: 20 September 2019

## **Enhancement of thermoelectric properties in *p*-type conducting polymer-based composites**

### **Abstract**

As the ability of recycling waste-heat to electricity, conducting polymers have great interests for thermoelectric applications. On the other hand, thermoelectric performance of conducting polymers is lower in comparison with inorganic thermoelectric materials and is still needed to improve before broad applications in thermoelectric devices. Among the conducting polymers, poly (3,4-ethylenedioxythiophene): poly (4-styrenesulfonic acid) (PEDOT:PSS) has become extensive attention due to its high electrical conductivity, stability, processability and flexibility. Addition of polar solvents such as ethylene glycol, dimethylsulfoxide, dimethyl formamide to PEDOT:PSS can enhance the electrical conductivity of this material owing to the realignment of polymer chain. Furthermore, post-treatment of PEDOT:PSS with various mineral acids can also increase the electrical conductivity, resulting in high thermoelectric power factor.

Another material of interest is poly (3-hexylthiophene) (P3HT) which has very low electrical conductivity due to less amount of carrier in it. Doping with 2,3,5,6-tetrafluoro-7,7,8,8-tetracyanoquinodimethane (F4TCNQ) to P3HT and making organic/inorganic hybrid composite with CNT yarn becomes a possible solution to simultaneously improve both electrical conductivity and Seebeck coefficient of this material. Owing to its narrow band gap energy and high charge carrier mobility, carbon

nanotube (CNT) yarn emerges as potential material to make composite with conducting polymers.

In this thesis, N<sub>2</sub> pressure-induced nitric acid treatment of PEDOT:PSS and doping of CNT yarn with P3HT and F4TCNQ are discussed to optimize their thermoelectric power factor. For PEDOT:PSS, N<sub>2</sub> pressure-induced nitric acid treatment was used to simultaneously improve the electrical conductivity and Seebeck coefficient. Upon this treatment, PEDOT:PSS changes from semiconductor to metal-like behavior and simultaneously enhances the electrical conductivity and Seebeck coefficient, resulting in an increase in thermoelectric power factor from 0.08 to 121  $\mu\text{Wm}^{-1}\text{K}^{-2}$  at 150°C. This is due to the conformational change of PEDOT and the removal of insulating extra PSS. In order to highlight the effect of N<sub>2</sub> gas pressure on the improvement of thermoelectric properties of PEDOT:PSS, it was treated with the same procedure of HNO<sub>3</sub> treatment and then dried in the vacuum chamber, immersion in deionized (DI) water or N<sub>2</sub> gas passing. Among them, the optimum thermoelectric properties were obtained after N<sub>2</sub> gas passing.

Other acids such as sulfuric acid (H<sub>2</sub>SO<sub>4</sub>) and hydrochloric acid (HCl) were also used to investigate the influence of the pressure of nitrogen (N<sub>2</sub>) gas on the structure and thermoelectric properties of acid treated PEDOT:PSS. As a result, the improvement of electrical conductivity was also related to the pressure of N<sub>2</sub> gas passing. Therefore, the two reasons for the conformation of PEDOT are the removal of insulating PSS by acid treatments and the pressure of N<sub>2</sub> gas. Acid treatment plays a major role in the removal of the insulating PSS, resulting in the conformation of PEDOT while the pressure of N<sub>2</sub> gas is mainly responsible for the additional conformation of polymer favoring the linear orientation of the structure. Therefore, mechanical forces such as the pressure of N<sub>2</sub> gas can influence the structure of acid-treated PEDOT:PSS regardless of the types of acids.

For P3HT, we propose a novel technique herein, doping of P3HT with CNT yarn after Joule annealing in the vacuum chamber. Joule annealing can heal the structural defects and remove the amorphous carbon on the surface of the CNT yarn which also facilitates the doping with P3HT and F4TCNQ. In addition, Seebeck coefficient significantly improved due to the Joule annealing and electrical conductivity significantly improved due to the doping with F4TCNQ. After doping CNT yarn with P3HT alone, it showed semiconductor behavior. After doping with both P3HT and F4TCNQ, it showed metal-like nature owing to the formation of dopant-linked semi-crystalline polymer.

In addition, thermoelectric performance of acids treated PEDOT:PSS films at an elevated temperature are also discussed in this thesis and it is worth studying so that we can broaden the applications of acids treated PEDOT:PSS films at various temperatures. For CNT yarn/P3HT/F4TCNQ composite, Joule annealing of CNT yarn favors the enhancement of Seebeck coefficient while *p*-type doping is responsible for the improvement of electrical conductivity. Therefore, combination of joule annealing and doping can pave a way to enhance the thermoelectric performance of carbon based materials. Finally, the effort of this research will greatly contribute in the practical applications for low temperature energy harvesting.

## Table of Contents

<b>Abstract</b> .....	<b>iii</b>
<b>Contents</b> .....	<b>vi</b>
<b>Chapter 1 Introduction</b> .....	<b>1</b>
1.1 Preface .....	1
1.2 Purpose of the thesis .....	2
1.3 Organization of the thesis .....	2
<b>Chapter 2 Research Background</b> .....	<b>4</b>
2.1 Thermoelectricity .....	4
2.2 Conducting (conjugated) Polymers.....	6
2.2.1 Various kinds of conducting polymers .....	7
2.2.2 Mechanism of conduction in conducting polymers.....	8
2.2.3. Poly (3,4-ethylenedioxythiophene): poly (styrene sulfonate) (PEDOT:PSS).....	9
2.2.4. Poly (3-hexylthiophene) (P3HT) .....	10
2.3 Carbon Nanotube (CNT) yarn.....	12
2.3.1. Carbon Nanotube (CNT).....	12
2.3.2. Fabrication of Carbon Nanotube (CNT) Yarn .....	14
<b>Chapter 3 Enhancement of Thermoelectric Properties of PEDOT:PSS by N<sub>2</sub> Pressure-Induced Nitric Acid Treatment</b> .....	<b>16</b>
3.1 Introduction .....	16
3.2 Experimental Details .....	17
3.2.1 Materials and Methods .....	17

3.2.2	Preparation and Treatment of PEDOT:PSS Films .....	17
3.2.3	Measurement of Thermoelectric Properties and Characterization .....	18
3.3	Results and Discussion .....	20
3.3.1	Thermoelectric Properties .....	20
3.3.2	Characterization for the Improvement of Thermoelectric Properties of PEDOT:PSS Films .....	22
3.4	Conclusion .....	33
<b>Chapter 4</b>	<b>Influence of Pressure of Nitrogen Gas on Structure and Thermoelectric Properties of Various Acid-treated PEDOT:PSS Films .....</b>	<b>34</b>
4.1	Introduction .....	34
4.2	Experimental Details .....	35
4.2.1	Materials .....	35
4.2.2	Acid Treatments and Characterization .....	35
4.3	Results and Discussion .....	37
4.3.1	Thermoelectrics Properties .....	37
4.3.2	Influence of Pressure of Nitrogen Gas on Various Acids-treated PEDOT: PSS Films .....	43
4.4	Conclusions .....	52
<b>Chapter 5</b>	<b>Enhancement of Thermoelectric Performance of Poly (3- hexylthiophene) (P3HT)/ CNT Yarn Composite via Joule Annealing and Doping .....</b>	<b>54</b>
5.1	Introduction .....	54
5.2	Experimental details .....	54
5.2.1	Materials and Methods .....	54

5.2.2. Measurement and Characterization .....	56
5.3. Results and discussion .....	56
5.3.1 Effect of Resistance Annealing and <i>P</i> -type Doping on Thermoelectric Properties of Carbon Nanotube Yarn .....	56
5.4. Conclusions .....	71
<b>Chapter 6 Summary .....</b>	<b>73</b>
<b>Acknowledgments .....</b>	<b>75</b>
<b>References .....</b>	<b>77</b>
<b>List of publications .....</b>	<b>89</b>
<b>List of Oral and Poster Presentation .....</b>	<b>89</b>

# CHAPTER 1

## Introduction

### 1.1 Preface

The global energy demand is increasing very fast year by year owing to the continuous industrialization and population growth. Currently, world depends primarily on fossil fuels to fulfill the energy requirements. However, more than half of the fossil fuels combusted and dissipated as waste-heat into the atmosphere and on the other hand, the environmental problems resulted by the combustion of fossil fuels become a critical issue. Therefore, the only way to fulfill the global energy demand is to harvest the energy from the sustainable energy sources. Thermoelectric (TE) generators can convert directly heat into electricity through the Seebeck's effect without producing any polluting matter into the environment. Thermoelectric materials have attracted great attention as an environmentally friendly material to restore energy from low-grade industrial waste-heat or natural heat [1-6].

Inorganic semiconductors or alloy materials such as SiGe, PbTe, Bi<sub>2</sub>Te<sub>3</sub>, GeTe and clathrates have been using as thermoelectric materials since a long time ago. However, these materials have some limitations such as high density, low flexibility, rigidity, bulkiness, and high toxicity. These characteristics restrict the use of such inorganic materials for energy harvesting because many heat sources including human body do not usually have flat surfaces. Therefore, the demand for flexible and lightweight organic materials for TE applications has become crucial [7-11].

There are various conjugated polymers, polyacetylenes (PAC), poly p-phenylene vinylene (PPV), poly pyrroles (PPY), poly anilines (PANI), poly thiophenes (PT) and poly 3,4-ethylenedioxythiophene (PEDOT), which have broad potentials for thermoelectric applications [12-14]. Moreover, the electrical conductivity of the conjugated polymers still needs to improve for thermoelectric applications. Research

groups are approaching to optimize thermoelectric performance based on two main strategies: (1) improving the power factor by energy filtering, secondary doping, texturing and post-treatment with acids and polar solvents and, (2) reducing the thermal conductivity through heterostructuring, nanostructuring, strain and defect scattering [6,15].

## 1.2 Purpose of the Thesis

Many research groups have been reporting various techniques to improve the thermoelectric performance of the conjugated polymers. It was shown that the post-treatment with polar solvents such as ethylene glycol (EG), dimethylsulfoxide (DMSO), N, N-dimethyl formamide (DMF) and some acids to PEDOT:PSS films significantly improve the electrical conductivity.

The main purpose of this thesis is to simultaneously improve the thermoelectric properties of conducting polymers (PEDOT:PSS and P3HT) towards high performance applications. To study how the pressure of N<sub>2</sub> gas influences on the thermoelectric properties and the structure of PEDOT:PSS is also an important part of this thesis. In addition, Joule annealing of CNT yarn and doping with *p*-type polymers is one of the innovations in this thesis to enhance the electrical conductivity and Seebeck coefficient simultaneously.

## 1.3 Organization of the Thesis

The chapter contents of this thesis are briefly described as follows;

**Chapter 1** includes preface and brief description of the purposes and organization of thesis.

**Chapter 2** reviews on the research background of thermoelectricity, conducting (conjugated) polymers: PEDOT:PSS and P3HT, and carbon nanotube (CNT) yarn.

**Chapter 3** describes the enhancement of thermoelectric properties of PEDOT:PSS by N<sub>2</sub> pressure-induced nitric acid (HNO<sub>3</sub>) treatment. HNO<sub>3</sub> treatment of PEDOT:PSS films followed by vacuum dry and immersion in deionized (DI) water are also explained comparatively.

**Chapter 4** presents the influence of pressure of nitrogen (N<sub>2</sub>) gas on structure and thermoelectric properties of acids-treated PEDOT:PSS films using various acids as well as various pressures of N<sub>2</sub> gas.

**Chapter 5** establishes the enhancement of thermoelectric properties of P3HT/CNT yarn composite via Joule annealing and doping with *p*-type molecular dopant.

**Chapter 6** incorporates the summary of whole research works.

## CHAPTER 2

### Research Background

#### 2.1. Thermoelectricity

The performance of the thermoelectric materials is determined by dimensionless figure of merit,  $ZT$ .

$$ZT = \frac{S^2 \sigma}{k} T \quad (2.1)$$

where,  $S$  is the Seebeck coefficient,  $\sigma$  is the electrical conductivity,  $k$  is the thermal conductivity and  $T$  is the absolute temperature. According to the definition of  $ZT$ , a higher electrical conductivity, a higher Seebeck coefficient and a lower thermal conductivity contribute a greater  $ZT$  [16-19]. Power factor,  $S^2 \sigma$  is occasionally used as alternative way instead of  $ZT$  to estimate the thermoelectric performance when the thermal conductivity of the materials is significantly low among the comparable materials [20-21]. Seebeck coefficient is defined by

$$S = \frac{8\pi^2 k_B^2}{3eh^2} m^* T \left( \frac{\pi}{3n} \right)^{2/3} \quad (2.2)$$

where,  $k_B$  is the Boltzmann constant,  $e$  is the electron charge,  $h$  is the Plank's constant,  $m^*$  is the effective mass and  $n$  is the carrier concentration. Thus, Seebeck coefficient relates to the carrier concentration and decreases with increasing carrier concentration. However, electrical conductivity is given by

$$\sigma = ne\mu \quad (2.3)$$

where,  $\mu$  is the carrier mobility. Electrical conductivity increases with increasing carrier concentration and carrier mobility [21]. Thermal conductivity,  $k$  comprises a lattice contribution,  $k_l$  and an electronic contribution,  $k_e$ , i.e;  $k=k_l+k_e$ . According to the Wiedemann-Franz law,

$$k_e = L\sigma T \quad (2.4)$$

where  $L$  is the Lorentz constant. The electronic contribution,  $k_e$  increases with increasing carrier concentration because charge carrier also carries heat. But for semiconductors, the lattice or phonon contribution,  $k_l$  is more important [22-23].

Thermoelectric power results primarily from two physical effects; Seebeck effect, the potential differences created per degree of temperature gradient across the material, and Peltier effect, the temperature differences produce current when passing through the hot side to the cold side [24]. A simple thermoelectric generator (TEG) works based on  $p$ - $n$  junction through Seebeck effect as shown in Figure 2.1. When one end of the thermoelectric materials is heated, electrons or holes move away from the hot end to the cold end, by this way electricity is generated. The power conversion efficiency is given by

$$P_{out} = \eta Q_{in} \quad (2.5)$$

where,  $P_{out}$  is the power generated by the device,  $\eta$  is the maximum efficiency of the device and  $Q_{in}$  is the amount of heat which passes through the device. On the other hand, the efficiency of the device primarily depends on the temperature difference,  $\Delta T = T_h - T_c$  and relates to the Carnot limit,  $\eta_c = \Delta T / T_h$ . Therefore, the efficiency of the thermoelectric generator in terms of the Carnot efficiency is

$$\eta = \eta_c \frac{\sqrt{1+ZT}-1}{\sqrt{1+ZT}+1} \quad (2.6)$$

Therefore, according to the equation (2.6) the maximum efficiency depends on both the Carnot efficiency,  $\eta_c$  and the figure of merit,  $ZT$  [13, 25]. In general, metals as well as heavily doped semiconductors that typically have half-filled bands can have high electrical conductivities, but the Seebeck coefficients are usually low. Additionally, the resulting thermoelectric performance is also low due to high thermal conductivity. Therefore, the research for the combination of organic and inorganic thermoelectric materials to achieve the high thermoelectric performance has accelerated in recent year.

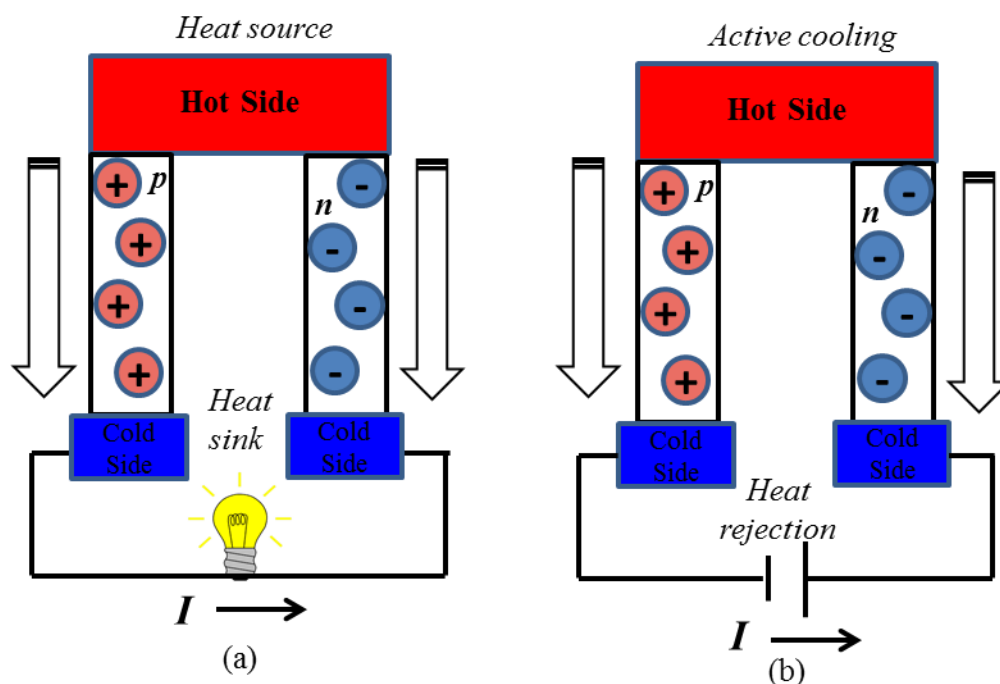


Figure 2.1: Simple thermoelectric module: (a) Seebeck effect and (b) Peltier effect.

Among them, some of the potential candidates for the combination of organic and inorganic hybrid materials are conjugated polymers and carbon nanomaterials [26].

## 2.2. Conducting (conjugated) polymers

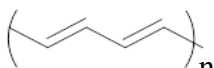
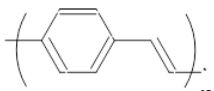
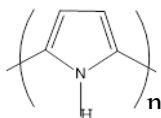
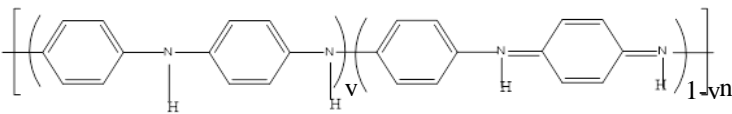
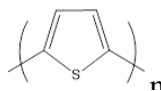
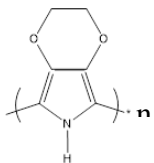
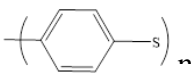
Most organic polymers have been long realized as insulators and are usually used in electronic devices to coat and insulate it. However, there are three types of semiconducting polymers that have been developed. They are electro-conducting polymers, proton-conducting polymers and ion-conducting polymers. The electrical conductivity of these polymers is due to the presence of alternating single and double bonds ( $\pi$ - $\pi$  interaction) along the polymer backbone, called conjugated bonds which are composed of aromatic rings connected to each other via carbon-carbon single bonds [27]. Neutral or undoped conjugated polymers have electrical conductivity close to insulators, it becomes conductive, sometimes like metals while its oxidized or doped

state. There are two possible ways to improve the doping level of a conjugated polymer for conducting, electrochemical doping and chemical doping [28].

### 2.2.1. Various Kinds of Conducting Polymers

There are various types of conducting polymers that can be used for thermoelectric application. Among them, some typical conducting polymers such as poly acetylene (PAC), poly p-phenylene vinylene (PPV), poly pyrroles (PPY), poly aniline (PANI), poly thiophene (PT), poly 3,4-ethylenedioxythiophene (PEDOT) and poly phenylene sulfide

Table 2.1: Chemical structures of some typical conducting polymers.

Names	Polymer structures
Poly acetylene(PAC)	
Poly p-phenylene vinylene (PPV)	
Poly pyrroles (PPY)	
Poly aniline (PANI)	
Poly thiophene (PT)	
Poly 3,4-ethylene dioxylthiophene (PEDOT)	
Poly phenylene sulfide (PPS)	

sulfide (PPS) have been well-known for electronic applications. Chemical structures of these conductive polymers are listed in Table (2.1) [29-32].

### 2.2.2. Mechanism of Conduction in Conducting Polymers

In general, conducting polymers include electronically conducting polymers and ionically conducting polymers. Ionically conducting polymers are usually called polymer electrolytes. Electronically conducting polymers include conjugated conducting polymers and the insulating polymers blending with conducting materials [33]. A distinct characteristic of conducting polymers is the presence of conjugated double bonds in their backbone. Conjugated polymers become conducting polymers after doping. The atoms along backbone contain single and double bonds alternatively and both involved in strongly localized  $\sigma$ -bonds while double bonds consisting of weakly localized  $\pi$ -bonds. The  $p$ -orbitals in the  $\pi$ -bond overlap each other, accepting the electrons to be more easily delocalized and move freely between the atoms. A simple schematic diagram of conjugated backbone is shown in Figure (2.2). During doping, the

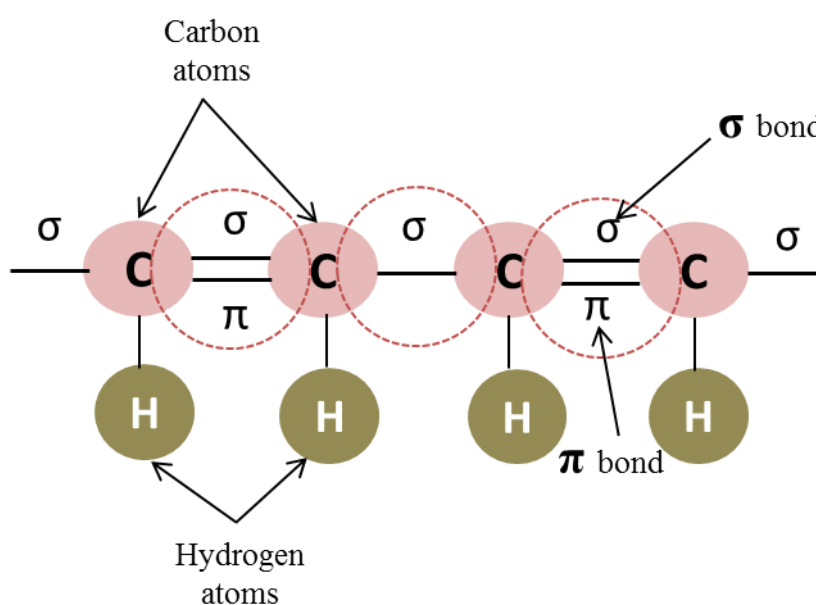


Figure 2.2: Schematic diagram of conjugated backbone of polymer, containing alternate single and double bond.

neutral polymer chain oxidized or reduced to either positively or negatively charges, resulting in a highly conducting state of the polymer. The properties of the conductive polymer depend on the type and molecular size of the dopants. Therefore, polaron length, chain length, charge transfer to adjacent molecules and conjugation length can affect the doping process. The presence of dopant molecules in the polymer causes the backbone stabilized and the charge neutralized. Dopants play as charge carriers and introduce charge transfer from dopant molecules to polymer chain, relocalizing as polarons (molecular chain containing one positive charge in a conjugated system) or bipolarons (molecular chain containing two positive charge in a conjugated system) in the chain. Generally, conducting polymers can be doped into two ways: *p*-doping and *n*-doping. In *p*-doping, polymer is oxidized and will have positive charge whereas in *n*-doping, polymer is reduced and will possess negative charge[34-35].

### 2.2.3. Poly (3,4-ethylenedioxythiophene): poly (styrene sulfonate) ( PEDOT:PSS)

Poly (3,4-ethylenedioxythiophene) (PEDOT), derivative of polythiophene, is the most popular TE polymer due to high thermoelectric properties at its doped state. Nevertheless, as-prepared PEDOT:PSS has low thermoelectric properties with the electrical conductivity  $<1 \text{ Scm}^{-1}$  and Seebeck coefficient of  $15 \mu\text{VK}^{-1}$  [36], which are related to the excess PSS that is needed to stabilize PEDOT:PSS in water. PEDOT:PSS consists of grains with a hydrophobic conducting PEDOT-rich core and a hydrophilic insulating PSS-rich shell [37]. Generally, a high concentration of PSS is used for stable dispersion of PEDOT:PSS and such PSS worsen the electrical conductivity [38]. Therefore, selective removal of insulating PSS is one of the methods to enhance electrical conductivity of PEDOT:PSS [39]. Using secondary dopants with high dielectric constant such as dimethyl sulfoxide (DMSO), ethylene glycol (EG), N,N-dimethyl formamide (DMF) and tetrahydrofuran (THF) become promising methods to

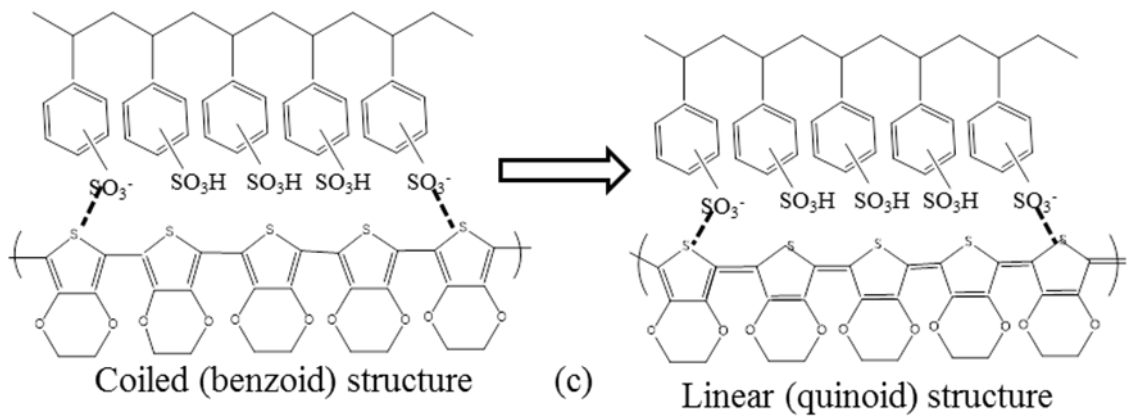


Figure 2.3: Benzoid (coiled) and quinoid (linear) structure of PEDOT:PSS.

remove insulating PSS in PEDOT:PSS dispersion [40]. Post-treatment of PEDOT:PSS with various acids are also the effective routes for the removal of insulating PSS [41-44]. During the secondary doping and post-treatment, the coulombic interaction between the positively charged PEDOT and negatively charged PSS chains are reduced through screening effect of acids and dopants, which in turn enable the removal of non-conductive PSS and led to a three-dimensional conjugated network of highly conjugated PEDOT [40]. Moreover, the improvement in conductivity of PEDOT:PSS is due to the change of the polymer structure from coiled (benzoid) to linear (quinoid) structure resulted in the removal of PSS [36, 45-46]. The change from benzoid to quinoid structures are illustrated in Figure (2.3).

#### 2.2.4. Poly (3-hexylthiophene) (P3HT)

Poly (3-hexylthiophene) (P3HT) (Figure 2.4 (a)) has been widely used in the fabrication of optoelectronic devices due to its excellent electrical properties, appropriate energy gap, doping reversibility and easy processability [40]. However, owing to the very low electrical conductivity of P3HT ( $\approx 10^{-7} \text{ Scm}^{-1}$ ) [47], molecular dopant such as 2, 3, 5, 6-tetrafluoro-7, 7, 8, 8-tetracyanoquinodimethane (F4TCNQ) (Figure 2.4 (b)) has been used as electron acceptor to P3HT due to its high electron

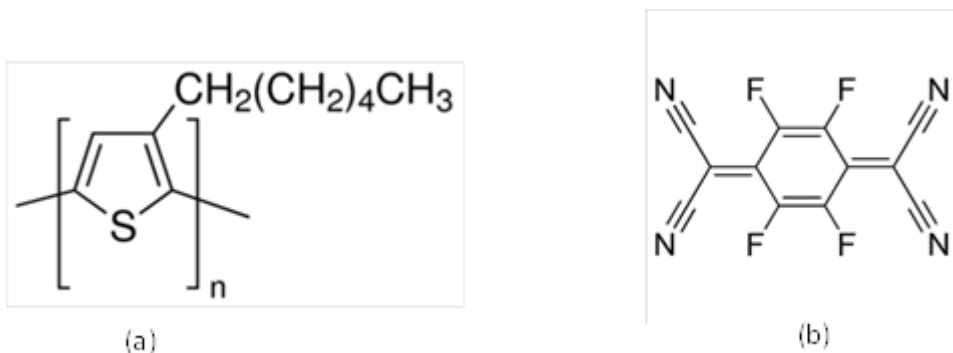


Figure 2.4: Chemical structure of (a) P3HT and (b) F4TCNQ.

affinity of 5.24 eV [48]. F4TCNQ undergo ground-state charge transfer with P3HT, yielding polarons or bipolarons and the dopant anions remain as counter-ions [49]. Doped P3HT is conducted by an electron exchange process between F4TCNQ as an electron acceptor and P3HT as an electron donor. Upon doping, P3HT polymer chains self-organised into a more ordered structure, resulting an enhancement in electron transport, improving the TE performance [40]. Generally, there are two possible donor-acceptor ground-state interactions between P3HT and F4TCNQ, which are sketched in Figure 2.5 (a) and (b). In Figure 2.5 (a), an electron is completely transferred from

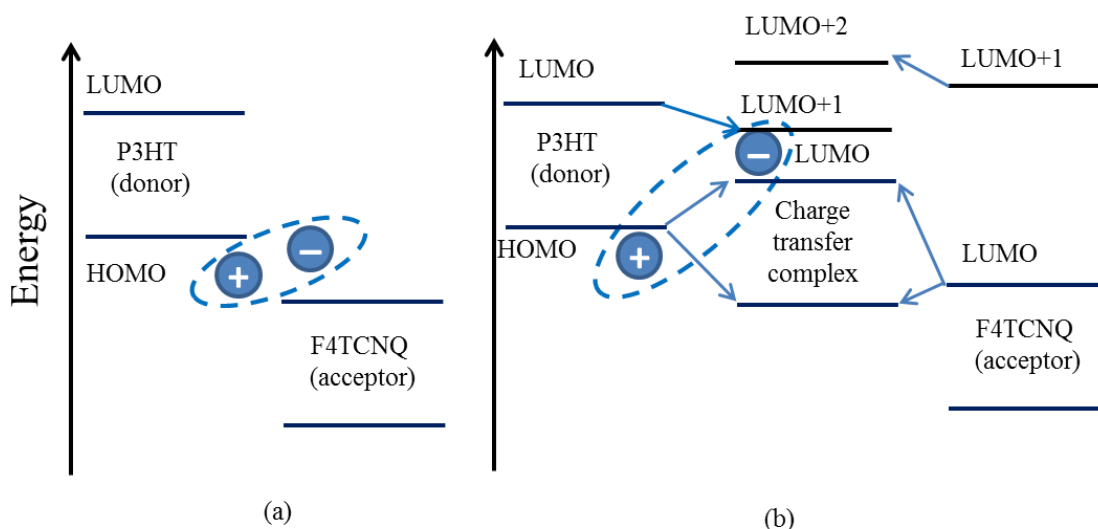


Figure 2.5: Donor-acceptor ground-state interactions between P3HT and F4TCNQ. (a) Complete charge transferred from P3HT donor to the F4TCNQ acceptor, and (b) partial charge transfer between P3HT and F4TCNQ.

P3HT donor to the F4TCNQ acceptor. The transferred electron remains fixed at the F4TCNQ molecule since the concentration of F4TCNQ in the P3HT matrix is typically low. The associated hole on P3HT can be either coulombically bound by the F4TCNQ anion or may move freely within the matrix of P3HT. On the other hand, partial charge transfer between P3HT and F4TCNQ can be created and a supramolecular charge transfer complex is formed. Highest occupied and lowest unoccupied molecular orbitals, HOMO and LUMO are acquired from both the neutral P3HT HOMO and F4TCNQ LUMO as in Figure 2.5 (b). In this case, holes are created due to the electron deoccupation of P3HT HOMO as a consequence of Fermi-Dirac statistics [48].

## 2.3. Carbon Nanotube (CNT) Yarn

### 2.3.1. Carbon Nanotubes (CNT)

CNT is an allotrope of carbon and its name comes from its cylindrical structure [50]. There are two main types of carbon nanotubes; single-walled carbon nanotubes (SWCNT) and multi-walled carbon nanotube (MWCNT) depending on how the grapheme sheet rolled up to form the tube which can determine it is metallic or

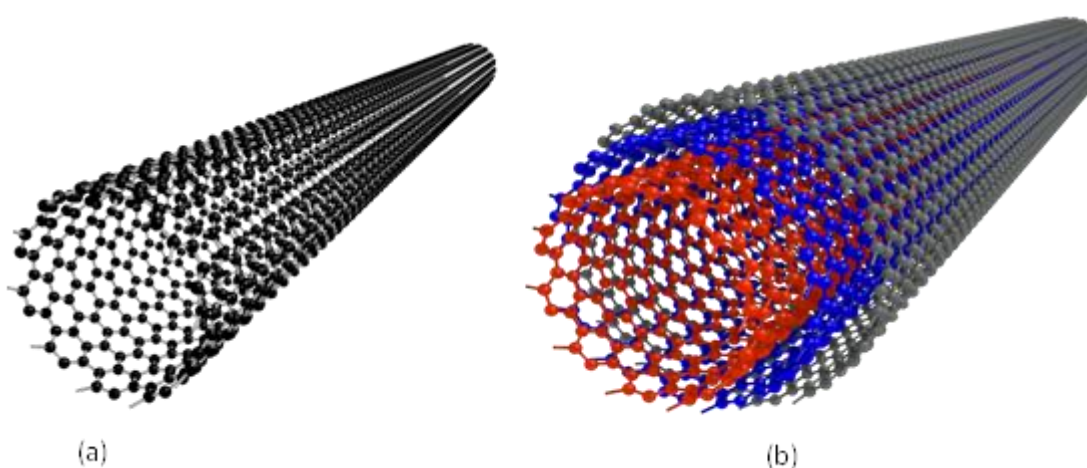


Figure 2.6: Structure of single-walled carbon nanotube (SWCNT) and multi-walled carbon nanotubes (MWCNT).

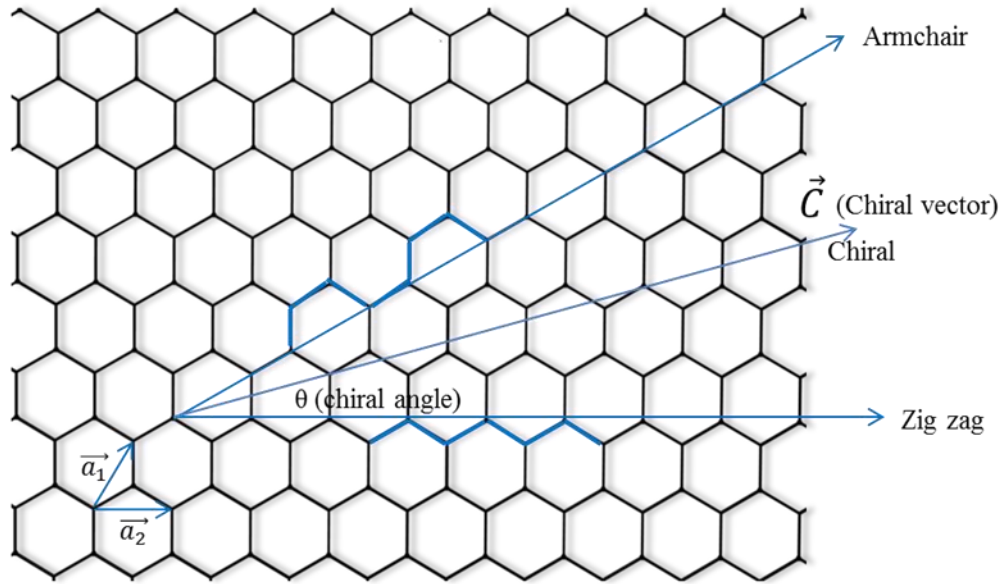


Figure 2.7: Schematic illustration of graphite sheet and formation of various types of carbon nanotubes.

semiconductor. Single-walled carbon nanotube consists of a single-layered graphene which is rolled up seamlessly into a cylindrical tube. Multi-walled carbon nanotube consists of multiple layers of graphene which are rolled concentrically into tubes. Schematic diagrams of single-walled and multi-walled carbon nanotubes are shown in Figure 2.6. The configuration of the carbon nanotube may be expressed by the tube chirality, or helicity by chiral vector. The chiral vector can be defined by

$$C = na_1 + ma_2 \quad (2.7)$$

where,  $a_1$  and  $a_2$  are the two translational lattice,  $n$  and  $m$  are integers.  $m = 0$  ( $\theta = 30^\circ$ ) are called zig-zag tubes,  $n = m$  ( $\theta = 0^\circ$ ) are called armchair tubes and  $n \neq m$  are called chiral tubes. The value of  $n$  and  $m$  determines the chirality and affects the electrical properties of CNT. CNT with  $|n-m| = 3q$  has metallic like nature as in (10, 10) tube,  $|n-m| = 3q \pm 1$  has semiconducting like nature as in (10, 0),  $q$  is an integer (Figure 2.7) [50-53]. The zig-zag, armchair and chiral tubes are illustrated in Figure 2.8.

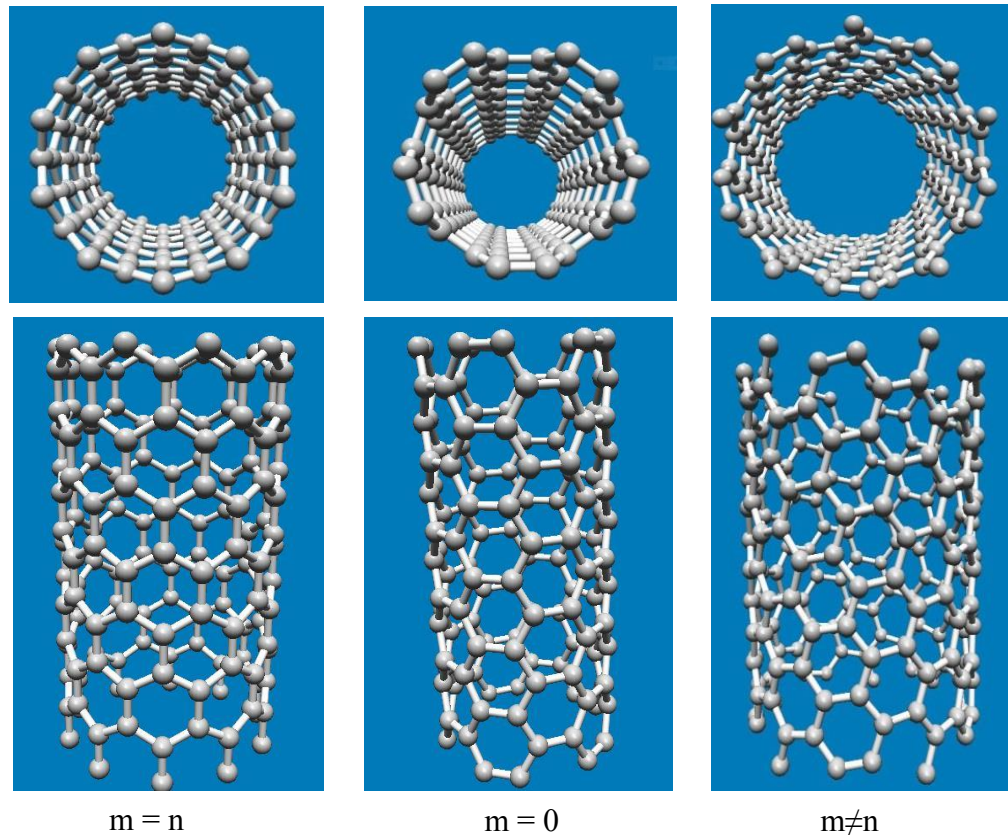


Figure 2.8: Structure of (a) zig-zag, (b) armchair and (c) chiral tubes.

### 2.3.2. Fabrication of CNT Yarn

Long and continuous CNT yarn can be fabricated from many spinning procedures including wet spinning, spinning directly from chemical vapor deposition (CVD) reactor and dry spinning from vertically aligned CNT forests. Among them, the latter method is very simple, easily controllable, and furthermore, fabricates long and continuous CNT yarn with mass production ability [54]. A remarkable advantage of dry-spun CNT yarn is that CNTs in yarn connects themselves with each other, thereby forming continuous and highly conductive CNT yarns naturally [55]. However, there are large interspaces and voids in the yarns during the spinning process which reduces van der Waals interactions between CNTs leading lower mechanical strength [54]. Moreover, not all the CNT arrays can be spun into fibers and the degree of spinnability of CNTs is closely related to the morphology of the CNT arrays. In addition, the entangle structures

at the ends of CNT bundles are key parameter for the continuous drawing process [56].

## CHAPTER 3

### **Enhancement of Thermoelectric Properties of PEDOT:PSS by N<sub>2</sub> Pressure-Induced Nitric Acid Treatments**

#### **3.1 Introduction**

Commercially available inorganic thermoelectric materials are not suitable for the recovery of low-temperature waste heat because they can effectively operate only at high temperature. Nevertheless, a large amount of waste heat in our surroundings is below 200°C. Therefore, organic thermoelectric materials which can provide high performance at low temperature have become excellence in order to restore the huge amount of low temperature waste heat [9, 17].

Recently, among the conducting polymers, many research groups have focused on poly (3,4-ethylenedioxythiophene): poly styrenesulfonate (PEDOT:PSS) due to its unique properties [57-59]. However, there are numerous restrictions for this material to overcome before broad application in thermoelectric devices, i.e., both electrical conductivity and Seebeck coefficient of PEDOT:PSS usually need further improvement to accomplish high thermoelectric properties [60]. Generally, high carrier concentration and/or high carrier mobility enables to obtain high electrical conductivity. But high carrier concentration tends to decrease Seebeck coefficient [58, 61-62]. The existence of a large amount of non-ionized dopants can considerably decrease the carrier mobility as well as Seebeck coefficient, and hence reduces the thermoelectric power factor. Despite the fact that secondary doping can significantly increase the carrier mobility without altering the carrier concentration or doping state, it is still challenging to simultaneously improve the electrical conductivity and Seebeck coefficient [63-64].

In this chapter, facile and cost-effective approach to simultaneously improve the electrical conductivity and Seebeck coefficient of PEDOT:PSS films via N<sub>2</sub> pressure-induced treatment with HNO<sub>3</sub> is reported. The conformational change of PEDOT and

the removal of insulating extra PSS by the combined effect of nitric acid treatment and passing of N<sub>2</sub> gas significantly enhanced the electrical conductivity from < 1 Scm<sup>-1</sup> to 2696 Scm<sup>-1</sup> at room temperature with a pressure of 0.1 MPa. For comparative study, the PEDOT:PSS film was treated with the same procedure with HNO<sub>3</sub> and then dried in the vacuum chamber or immersion in deionized (DI) water to remove insulating PSS. In that case, the optimum electrical conductivity measured at room temperature was 2018 Scm<sup>-1</sup> and 988 Scm<sup>-1</sup> for the vacuum dry and DI water washing, respectively. Therefore, the improvement in thermoelectric properties is not only the effect of the acid but also the pressure of the N<sub>2</sub> gas. To our best knowledge, it is the first demonstration of the effect of pressure on the thermoelectric properties of the treated PEDOT:PSS film. Furthermore, many research groups reported on the room temperature thermoelectric properties of acid treated PEDOT:PSS films but report on the thermoelectric properties of PEDOT:PSS film in wide temperature range is very rare [65]. For this reason, it is worth studying the performance of nitric acid treated PEDOT:PSS films at an elevated temperature so that we can broaden the applications of acid treated PEDOT:PSS films.

## **3.2 Experimental Details**

### *3.2.1 Materials and Methods*

PEDOT:PSS (Clevios PH 1000) was purchased from Heraeus, Germany. Nitric acid (HNO<sub>3</sub>, 69%) was purchased from Wako Pure Chemical Industries, Ltd. (Japan). All chemicals in this study were used directly without further purification.

### *3.2.2 Preparation and Treatment of PEDOT:PSS Films*

The glass substrates (20 mm × 20 mm) were cleaned with deionized water, ethanol and acetone, and then put in the ultra-violet (UV) ozone cleaner (Filgen) for 20 min to facilitate a better film formation. PEDOT:PSS (100 μl) was spin-coated onto the

glass substrate by spin-coating at a spin speed of 600 rpm for 30 s followed by 2000 rpm for 20 s and dried at 50°C for 30 min. The treatment of PEDOT:PSS films with HNO<sub>3</sub> was done according to the following methods.

**Treatment 1:** HNO<sub>3</sub> (100 μl) was dropped onto the PEDOT:PSS film at room temperature and kept for 10 min followed by passing N<sub>2</sub> gas [66] with various pressures using gun. The distance between the tip of the gun and the sample was fixed at 20 mm. N<sub>2</sub> gas was sprayed in order to cover all area of the film.

**Treatment 2:** HNO<sub>3</sub> (100 μl) was dropped onto the PEDOT:PSS film at room temperature and kept for 10 min, then dried in the vacuum chamber for 24 hr.

**Treatment 3:** HNO<sub>3</sub> (100 μl) was dropped onto the PEDOT:PSS film at room temperature and kept for 10 min, then dried at 50°C for 30 min. The samples were washed with DI water followed by drying at 100°C for 15 min and cooled down to room temperature.

### *3.2.3 Measurement of Thermoelectric Properties and Characterization*

Seebeck coefficient, electrical conductivity and power factor of the PEDOT:PSS films were measured by ZEM-3M8 ULVAC Seebeck Coefficient Measurement System (ADVANCED RIKO, Inc.) with thin film measurement attachment in the helium environment. Configuration of the thin film measurement is shown in Figure 3.1. Before the ZEM-3 measurement, DektakXT profilometer was used to measure the average thickness of the films. The samples were then cut into 4 mm × 16 mm size for the measurement of thermoelectric properties.

The Hall measurement (Lake Shore Model 8403, AC/DC Hall effect measurement system) was conducted to investigate the carrier concentration and carrier mobility. X-ray photoelectron spectroscopy (XPS, JEOL JPS 9030, Tokyo, Japan) was performed to analyze the change in composition of the PEDOT:PSS before and after treatment. Ultra-

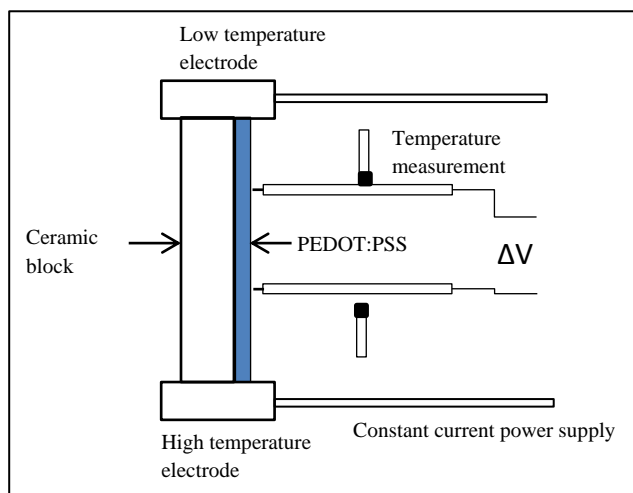


Figure 3.1: Schematic of configuration of thin film measurement for thermoelectric properties.

violet-visible (UV-vis) (JASCO V-670 Spectrophotometer) absorption bands were recorded to analyze the neutral, polaron and bipolaron states of the PEDOT. The morphology and surface roughness were characterized by Scanning Probe Microscope (SPM, Nano Navi SII). Contact angle was measured with Drop Master DMe-211 to characterize the surface wettability of the films. X-ray diffraction measurement (XRD) was performed by RIGAKU SmartLab X-ray diffractometer with  $\text{CuK}_\alpha$  radiation ( $\lambda = 1.5418 \text{ \AA}$ ) at a scanning rate of 1 degree per minute to investigate the change in crystallinity of PEDOT:PSS films before and after  $\text{HNO}_3$  treatment. Raman spectroscopy (JASCO NRS450 NMDS) with a wavelength of 532.21 nm (green laser) was used to analyze the conformational change of the PEDOT chains after treatment. Cyclic voltammetry (CVs, Princeton Applied Research VERSA STAT 4-100) was used to characterize the electrochemical activity of the PEDOT:PSS before and after treatment.

### 3.3 Results and Discussion

#### 3.3.1 Thermoelectric Properties

The PEDOT:PSS films were treated with HNO<sub>3</sub> at different conditions in order to ensure the synergetic effect of HNO<sub>3</sub> and the pressure of N<sub>2</sub> gas on the thermoelectric properties of PEDOT:PSS. Electrical conductivity, Seebeck coefficient and power factor of the PEDOT:PSS films before and after different treatments are shown in Figure 3.2. In Figure 3.2 (b), the Seebeck coefficient of pristine PEDOT:PSS film does not change too much in the temperature range between 25°C and 200°C. Meanwhile the electrical conductivity of the pristine PEDOT:PSS film increases from 0.8 Scm<sup>-1</sup> at room temperature to 3.5 Scm<sup>-1</sup> at 200°C, indicating the semiconductor behavior. After the treatment, in contrast to the pristine film, the electrical conductivity decreases with increasing temperature while the Seebeck coefficient increases with increasing temperature, exhibiting the metallic or semi-metallic behavior of the PEDOT:PSS films.

The post treatment of PEDOT:PSS films with HNO<sub>3</sub> for 10 min followed by N<sub>2</sub> gas passing gives the highest electrical conductivity (2693 Scm<sup>-1</sup> at 25°C), whereas that of the films with the same treatment followed by vacuum dry renders the electrical conductivity of 2018 Scm<sup>-1</sup> only. When the films were treated with HNO<sub>3</sub> at 25°C for 10 min followed by rinsing with DI water, the resulted electrical conductivity is only 988 Scm<sup>-1</sup>, which is the lowest among different treatment conditions. During the acid treatment, HNO<sub>3</sub> causes the protonation of PSS resulting in the formation of PSSH, which can be easily phase-segregated from PEDOT due to a weak Coulombic interaction. The reaction can be express as follows:



The conformational change of the PEDOT chain also occurs due to not only the phase segregation of PSSH but also the pressure of the N<sub>2</sub> gas. A better film condition was

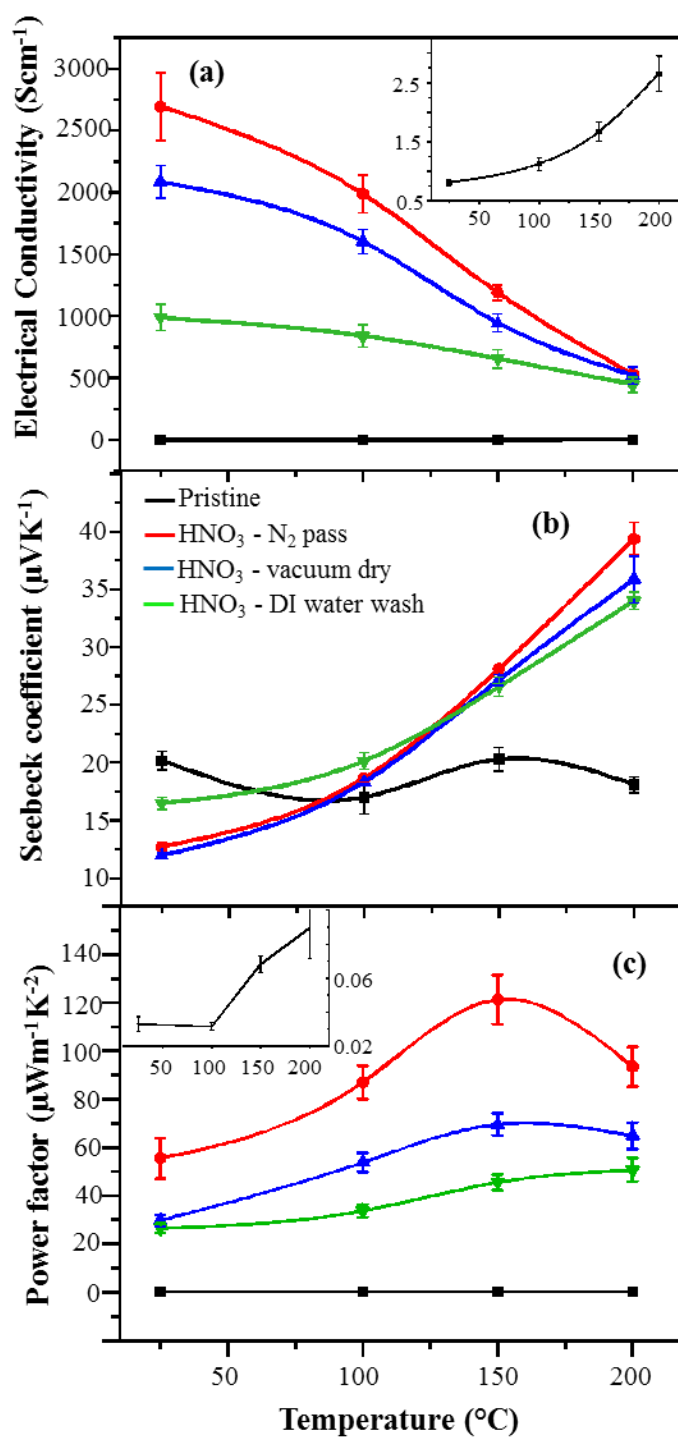


Figure 3.2: (a) Electrical conductivity, (b) Seebeck coefficient, and (c) power factor of the pristine and  $\text{HNO}_3$  treated PEDOT:PSS films at different conditions as a function of measurement temperatures. The insets in (a) and (c) are electrical conductivity and power factor of pristine PEDOT:PSS as a function of measurement temperature to show the variation in parameters clearly.

also obtained without wrinkling or peeling off after N<sub>2</sub> gas passing. Therefore, we observed that N<sub>2</sub> pressure influences the phase segregation as well as the conformational change of the PEDOT chain and hence improves the mobility, resulting in an increase in electrical conductivity [66]. In order to confirm this, the Hall effect measurement was conducted. The carrier concentration of pristine PEDOT:PSS is around 10<sup>17</sup> cm<sup>-3</sup> and the mobility is <1 cm<sup>2</sup>V<sup>-1</sup>s<sup>-1</sup> in previous reports [40, 63, 65-66]. As measured by the Hall effect measurement, even though we failed to measure the pristine PEDOT:PSS films, the carrier concentration is 2.5 x 10<sup>21</sup> cm<sup>-3</sup> for N<sub>2</sub> gas pass sample, 2.1 x 10<sup>21</sup> cm<sup>-3</sup> for vacuum dry sample and 1.5 x 10<sup>21</sup> cm<sup>-3</sup> for the DI water wash sample respectively. The carrier mobility of N<sub>2</sub> gas pass sample is 6.7 cm<sup>2</sup>V<sup>-1</sup>s<sup>-1</sup>, that of vacuum dry and DI water wash samples are 5.8cm<sup>2</sup>V<sup>-1</sup>s<sup>-1</sup> and 4.2 cm<sup>2</sup>V<sup>-1</sup>s<sup>-1</sup>, respectively. The carrier concentration and the carrier mobility values of N<sub>2</sub> gas pass sample are the highest among those of other treatment conditions. This may be due to the effect of the pressure of N<sub>2</sub> gas which leads to better phase separation between PEDOT and PSS and giving more chance for the PEDOT chain to be linearly reoriented.

### *3.3.2 Characterization for the Improvement of the Thermoelectric Properties of PEDOT:PSS Films*

The influence of HNO<sub>3</sub> treatment on the removal of extra PSS was confirmed by the XPS analysis as shown in Figure 3.3. The photoelectron peaks consisting of the doublet S 2p<sub>1/2</sub> and S 2p<sub>3/2</sub> observed at 168.6 eV and 167.7 eV originates from the sulphur atoms of the sulfonate group in PSS. The deconvoluted peaks of S 2p, O 1s, C 1s core-level spectra of the pristine and HNO<sub>3</sub> treated PEDOT:PSS at different conditions are shown in Figure 3.4. After the treatment with HNO<sub>3</sub>, the S 2p peak of PSS shifts about 0.8 eV to the lower binding energy and the PSS peak intensity decreases significantly after HNO<sub>3</sub> treatment [64]. The lowest intensity of PSS was

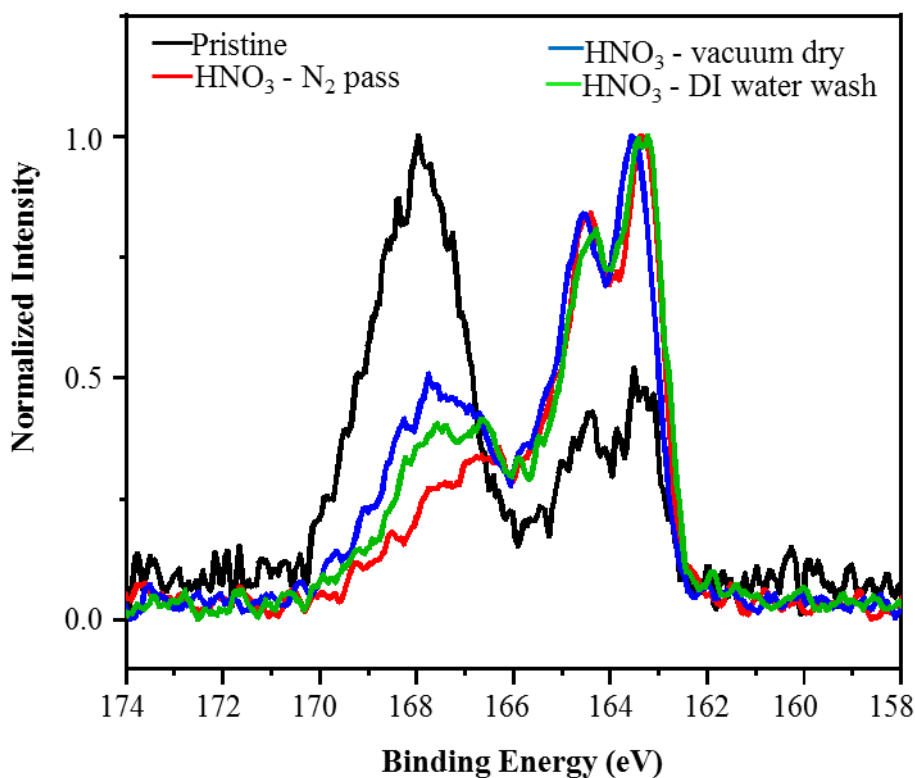


Figure 3.3: S 2p core-level XPS spectra of the pristine PEDOT:PSS and HNO<sub>3</sub> treated PEDOT:PSS films at different conditions.

observed after HNO<sub>3</sub> treatment followed by N<sub>2</sub> gas pass, indicating that HNO<sub>3</sub> treatment followed by N<sub>2</sub> gas pass can remove PSS more effectively than other treatments. Removing insulating PSS from the PEDOT:PSS film generally results in an increase in electrical conductivity, which agrees well with the conductivity measurement of the samples. The O 1s peak at the binding energy 532.4 eV corresponds to oxygen atom in PEDOT unit while 531.5 eV corresponds to the oxygen atom attached to the sulfur atom with double bond (O=S=O) in PSSH (Figure 3.4 (b)). The peak at 531.5 eV shifts about 0.4 eV to a lower binding energy and the intensity decreases while the peak at 532.4 eV shifts to 0.4 eV to a higher binding energy and the intensity increases. This indicates the formation of PSSH which segregates from the PEDOT:PSS chains [65]. The peaks at 285.7 eV and 284 eV in C 1s spectra (Figure 3.4 (c)) are associated with C-O bonds in

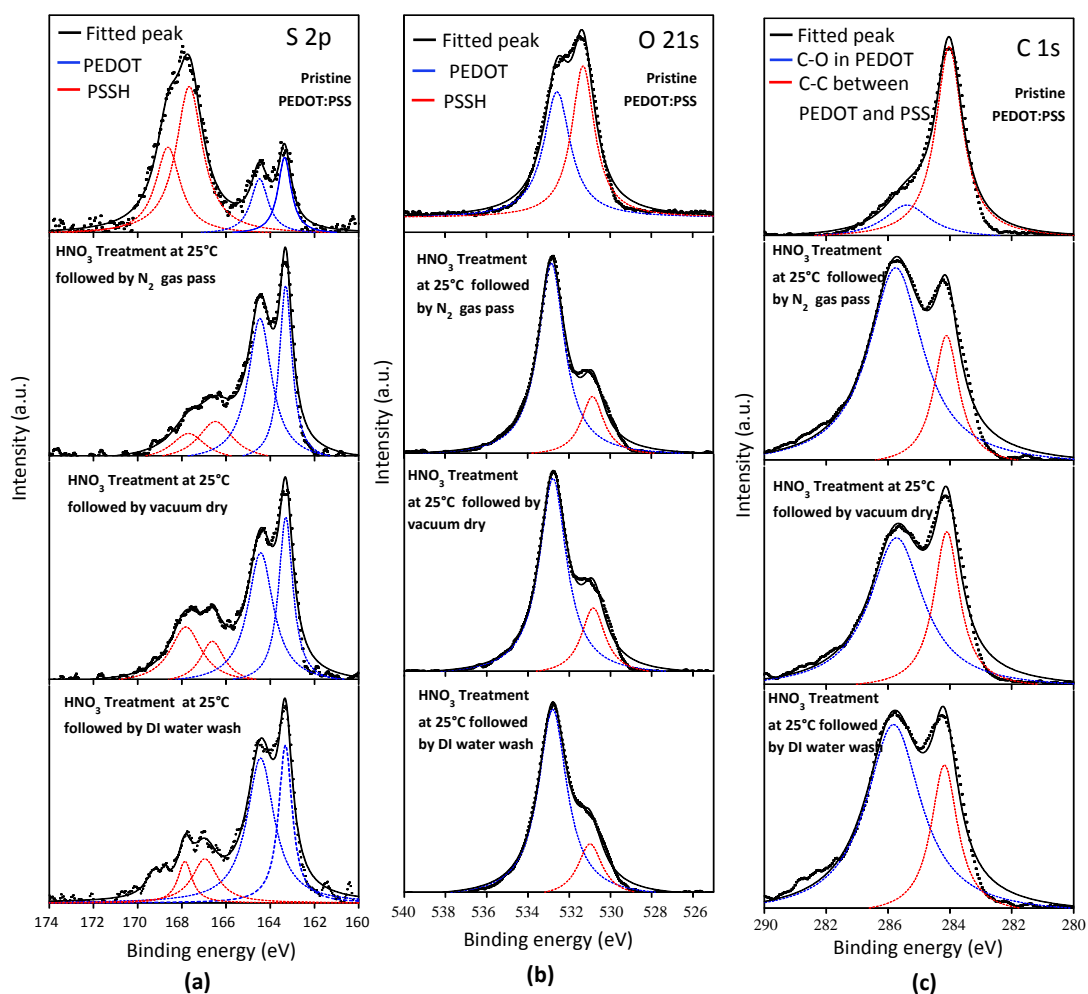


Figure 3.4: (a) S 2p, (b) O 1s and (c) C 1s core-level spectra of the pristine PEDOT:PSS and HNO<sub>3</sub> treated PEDOT:PSS at different conditions. The dotted curves represent the experimental results and the blue and red curves correspond to the deconvoluted peaks for the PEDOT and PSSH.

PEDOT and C-C bonds in PEDOT:PSS. The intensity peak of C-C bond in PEDOT:PSS decreases while that of C-O bonds in PEDOT increases after the treatment with HNO<sub>3</sub> which is consistent with the previous report [68]. Composition of the pristine PEDOT:PSS and PEDOT:PSS films treated at different conditions obtained by XPS analysis are listed in Table 3.1.

In order to confirm the segregation of PSS rich domains from PEDOT:PSS, the surface morphology of the PEDOT:PSS films were analyzed by SPM. SPM Images are

Table 3.1: Composition of the pristine PEDOT:PSS films and HNO<sub>3</sub> treated PEDOT:PSS films at different treatment conditions obtained by XPS analysis.

Photoelectron peaks	Atom %			
	Pristine PEDOT:PSS	Treatment with HNO <sub>3</sub> followed by N <sub>2</sub> gas passing	Treatment with HNO <sub>3</sub> followed by vacuum dry	Treatment with HNO <sub>3</sub> followed by DI water wash
S 2p <sub>3/2</sub>	5.9	6.3	6.3	6.3
S 2p <sub>1/2</sub>	16.1	18.3	17.9	19.1
O 1s	24.5	24.2	24.3	23.6
C 1s	51.0	51.3	51.3	50.2

scanned for three times for each sample. The pristine PEDOT:PSS film shows a very smooth surface with root mean square (rms) roughness of 1.21 nm as shown in Figure 3.5. After the treatment, the films become rougher, and rms roughness increases to 1.7 nm, 1.5 nm and 1.9 nm, for the films processed by N<sub>2</sub> gas pass, vacuum dry and DI water wash, respectively (Figure 3.5 (b), (c), (d)). Interestingly, the roughness of the films processed by N<sub>2</sub> gas pass is lower than that of films DI water wash sample. It

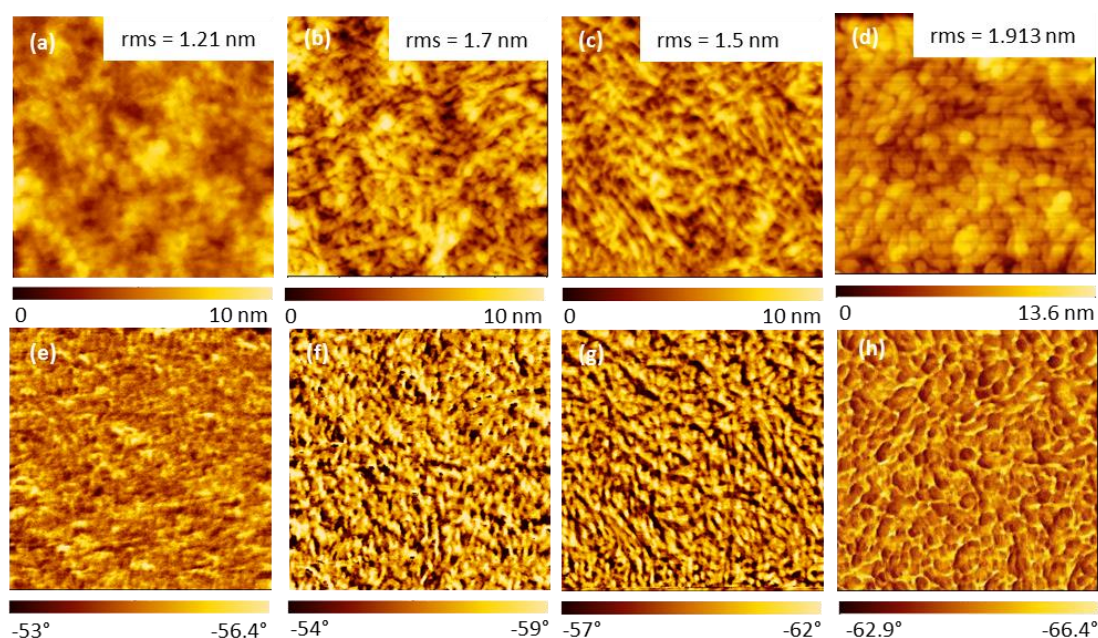


Figure 3.5: Topographic and phase images of (a), (e) pristine and those of HNO<sub>3</sub> treated PEDOT:PSS films followed by (b), (f) N<sub>2</sub> gas pass, (c), (g) vacuum dry, (d), (h) DI water wash. All images are scanned at 5 μm × 5 μm area.

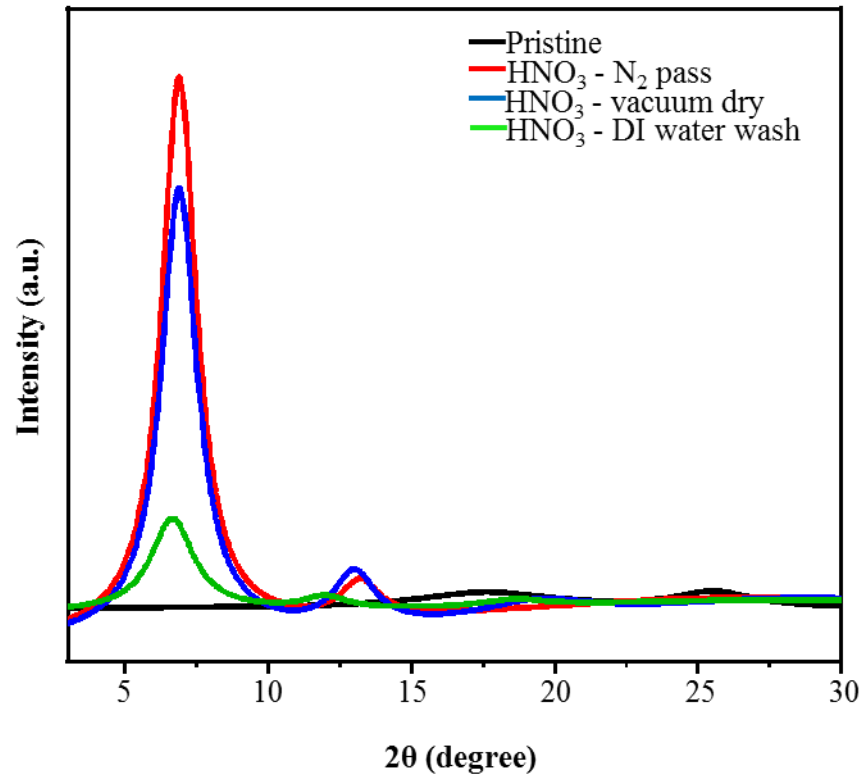


Figure 3.6: XRD patterns of the pristine and that of HNO<sub>3</sub> treated PEDOT:PSS films at different conditions.

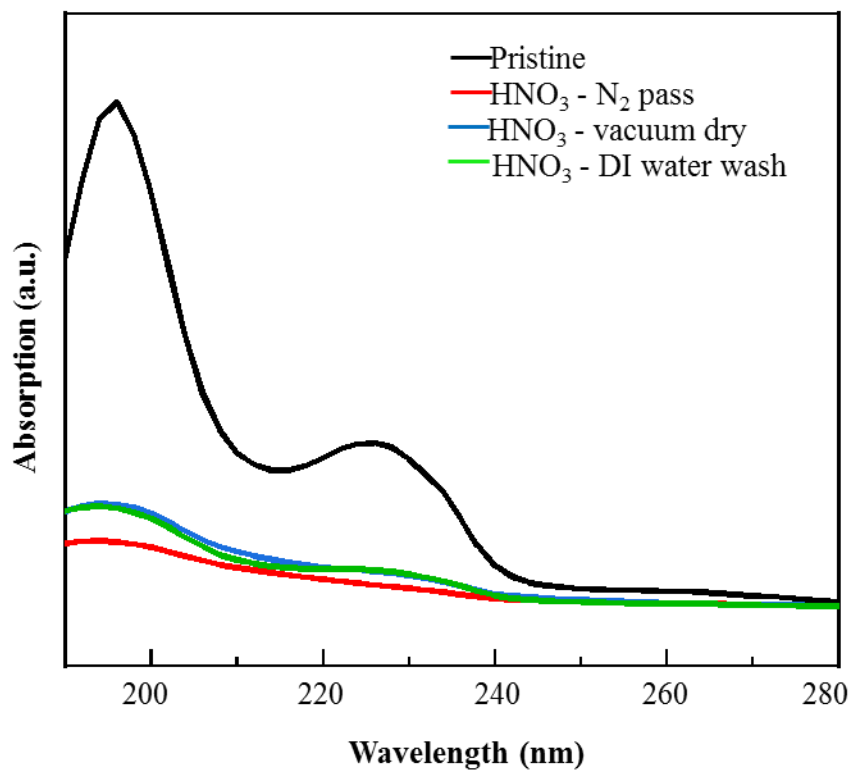
may be ascribed to the pressure of the N<sub>2</sub> gas, which makes the films become smoother. In addition, nanosized fibrous structures are observed after the treatments as shown in the phase images of the films (Figure 3.5 (f), (g), (h)), An increase in rms roughness and the formation of fibrous structures are the evidences of the phase segregation between PEDOT-rich domains and PSS-rich domains in addition to the removal of the non-complex PSS [64, 66, 69]. SPM results are also consistent with the XRD results as indicated in Figure 3.6. The pristine PEDOT:PSS film shows two diffraction peaks at 18.1° and 25.8° which originates from the amorphous halo diffraction of PSS and the inter-chain ring stacking of PEDOT. After the treatment with HNO<sub>3</sub>, new peaks appeared at 6.9° and 12° which correspond to the lamellar stacking of PEDOT and PSS respectively [42, 66, 68]. The results in Table 3.2 are calculated using the Bragg's law

Table 3.2: Interplanar spacing and grain size of the PEDOT:PSS films at various 2 $\theta$  values before and after treatment.

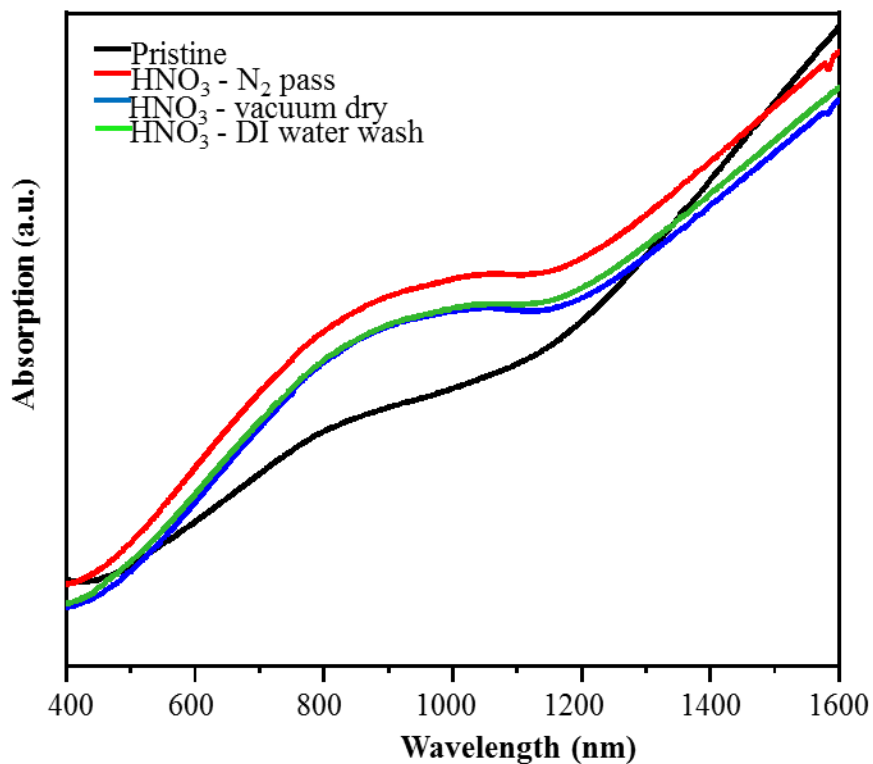
Treatment condition	Plane indices	2 $\theta$ (degree)	d-spacing (nm)	grain size (nm)
pristine	(100)	–	–	–
N <sub>2</sub> gas pass		6.9°	1.28	5.04
vacuum dry		6.9°	1.28	4.7
DI water wash		6.6°	1.34	3.6
pristine	(200)	–	–	–
N <sub>2</sub> gas pass		13.2°	0.67	5.07
vacuum dry		13°	0.68	4.71
DI water wash		12°	0.74	3.62
pristine	amorphous halo diffraction of PSS	17.5°	0.51	0.87
N <sub>2</sub> gas passing		–	–	–
vacuum dry		18.3°	0.48	4.74
DI water wash		18.7°	0.47	3.65
pristine	(010)	25.6°	0.35	0.91
N <sub>2</sub> gas passing		–	–	–
vacuum dry		25.9°	0.34	4.8
DI water wash		–	–	–

and Scherrer equation. The grain sizes at 6.9° and 13.2° are 5.04 nm and 5.07 nm respectively after treatment with HNO<sub>3</sub> followed by N<sub>2</sub> gas passing, which is the biggest grain size in comparison with other treatments, indicating the higher crystallinity among other treatment conditions because of the removal of amorphous phase PSS.

UV-Vis-NIR absorption spectra (Figure 3.7 (a) and (b)) are also recorded at the visible and near infrared region to investigate the influence of HNO<sub>3</sub> treatments on PEDOT:PSS films systematically. The absorption bands at 195.7 nm and 225.7 nm in Figure 3.7 (a) come from the PSS moiety. Hence, the decrease in the intensities of these two bands after HNO<sub>3</sub> treatment can be attributed to the removal of PSS from the PEDOT:PSS, resulting in the enhancement of the electrical conductivity [66, 70-71]. The intensities of the two bands become the lowest in the sample with HNO<sub>3</sub> treatment followed by N<sub>2</sub> gas pass. This indicates that HNO<sub>3</sub> treatment followed by N<sub>2</sub> gas pass is more effective than other methods for the removal of PSS. The absorption bands



(a)



(b)

Figure 3.7: (a) UV absorption and (b) Vis-NIR spectra of pristine PEDOT:PSS and HNO<sub>3</sub> treated PEDOT:PSS at different conditions.

around 600 nm, 900 nm and 1200 nm in Figure 3.7 (b) specifically show the neutral, polaron, and bipolarons states of the PEDOT chains, as previously reported in the literatures [64, 70]. After the HNO<sub>3</sub> treatment, the absorption intensity at  $\approx 900$  nm increases significantly, indicating an increase in its oxidation level to polaronic states [71-72]. UV-Vis-NIR measurement is also consistent with the Raman analysis as illustrated in Figure 3.8. Raman spectroscopy is a useful technique to investigate the conformational changes in polymers. The peak positions at 1225, 1336, 1396 and 1472 cm<sup>-1</sup> show the vibrational mode of C<sub>α</sub>-C<sub>α</sub> (inter- ring stretching), C<sub>β</sub>-C<sub>β</sub> (stretching), C<sub>α</sub>=C<sub>β</sub> (symmetric) and C<sub>α</sub>=C<sub>β</sub> (asymmetric) of the PEDOT. The characteristics peak at 1538 cm<sup>-1</sup> comes from the vibrational modes of PSS chains. The peak at 1396 cm<sup>-1</sup> in pristine PEDOT:PSS shifts to a higher wavenumber; 1404 cm<sup>-1</sup>, 1399 cm<sup>-1</sup>

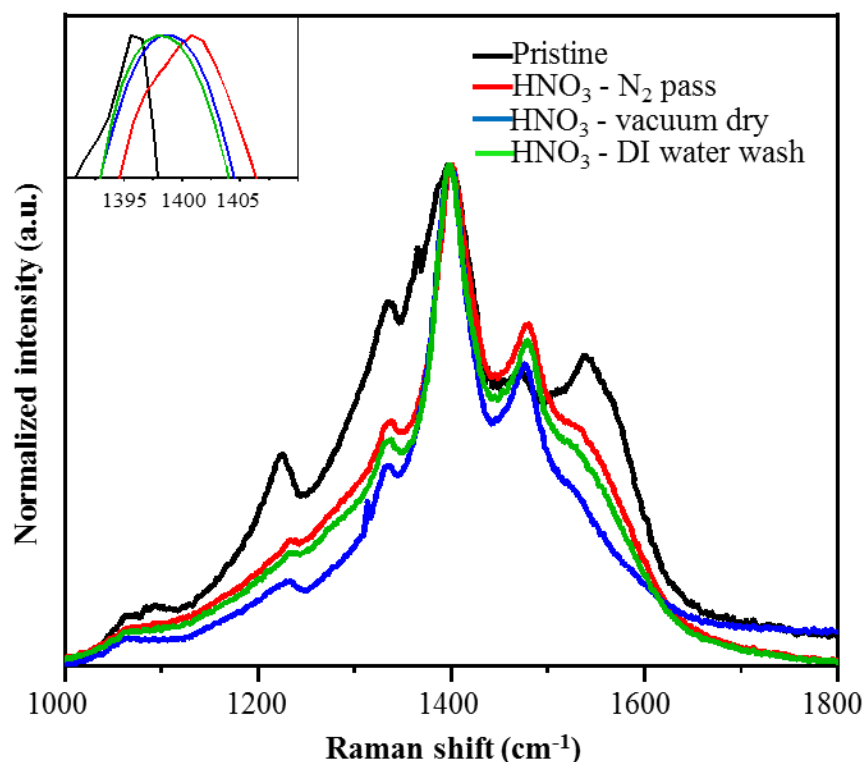


Figure 3.8: Raman spectra of PEDOT:PSS before and after treated with HNO<sub>3</sub> at different conditions. The inset curve shows the peak shift from 1396 cm<sup>-1</sup> to 1398 cm<sup>-1</sup>, 1399 cm<sup>-1</sup> and 1404 cm<sup>-1</sup> after different HNO<sub>3</sub> treatments.

and  $1398\text{ cm}^{-1}$  after the treatment with  $\text{HNO}_3$  followed by  $\text{N}_2$  gas pass, vacuum dry and DI water wash, respectively. It may be the conformational change of the thiophene rings of PEDOT from coiled structure (benzoid) to extended coiled or linear structure (quinoid), resulting in an increase in electrical conductivity [65]. The peak shift is more significant for the sample treated with  $\text{HNO}_3$  followed by  $\text{N}_2$  gas pass than that of other samples. Therefore, the pressure of the  $\text{N}_2$  can partially assist the conformational change of the PEDOT chain.

Contact angle measurement (Figure 3.9 and Table 3.3) was also performed to confirm the removal of amorphous phase PSS. The pristine PEDOT:PSS film shows the contact angle of  $35.2^\circ$  within 5s and decreases very quickly to  $18.5^\circ$  within 65 s, showing the hydrophilic nature of PSS. After the treatment with  $\text{HNO}_3$  followed by  $\text{N}_2$  gas pass, contact angle becomes  $63^\circ$  within 5 s and  $60.5^\circ$  within 65 s indicating the hydrophobic nature. PEDOT:PSS films were characterized by CV as the removal of

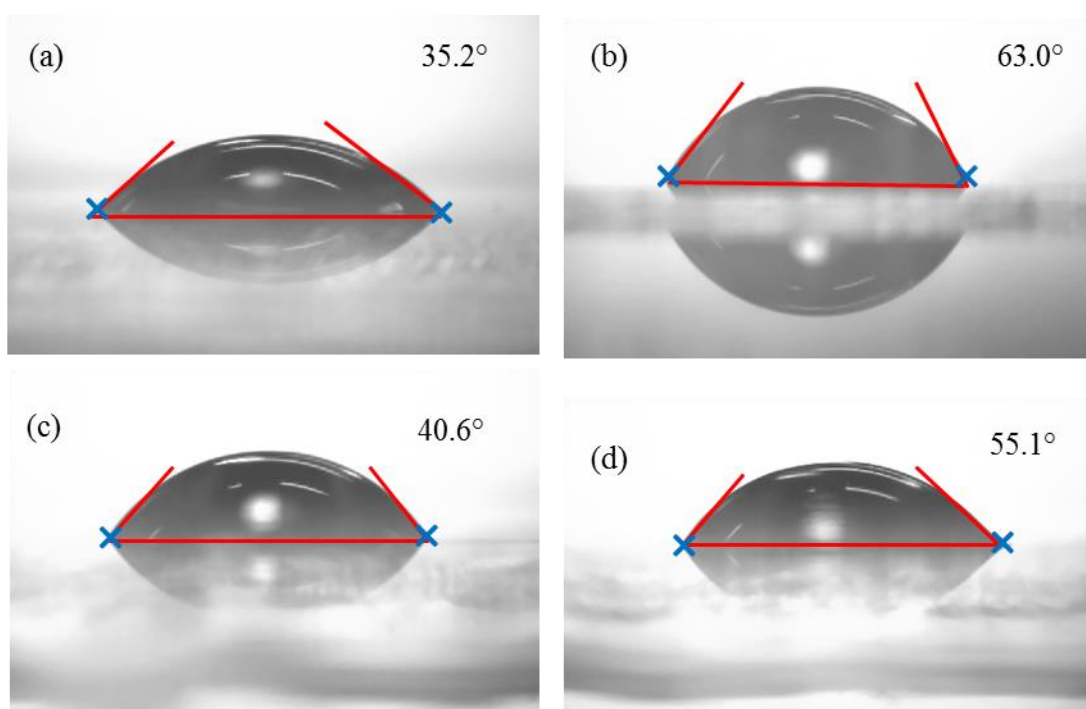


Figure 3.9: Contact angle measurement of (a) pristine PEDOT:PSS and  $\text{HNO}_3$  treated PEDOT:PSS followed by (b)  $\text{N}_2$  gas passing, (c) vacuum dry, and (d) DI water wash. (Measurements were performed with 5s).

Table 3.3: Contact angles of the PEDOT:PSS films before and after HNO<sub>3</sub> treatment at various conditions.

Time	Contact angle (°)			
	Pristine	Treatment with HNO <sub>3</sub> at 25°C followed by N <sub>2</sub> gas passing	Treatment with HNO <sub>3</sub> at 25°C followed by vacuum dry	Treatment with HNO <sub>3</sub> at 25°C followed by DI water wash
5 s	35.2	63	40.6	55.1
15 s	33.5	63.4	40.4	54.7
25 s	22.0	62.3	39.4	53.4
65 s	18.5	60.5	38.4	51.9

PSS can affect the electrochemical activity of the PEDOT chains. Cyclic voltammograms (CVs) of pristine PEDOT:PSS and HNO<sub>3</sub> treated PEDOT:PSS films at different conditions are shown in Figure 3.10. The electrochemical activity of pristine PEDOT:PSS was detected in the potential range from -0.1 to 0.4V Vs Ag/AgCl. Additional electrochemical activity was detected below -0.1 V Vs Ag/AgCl after

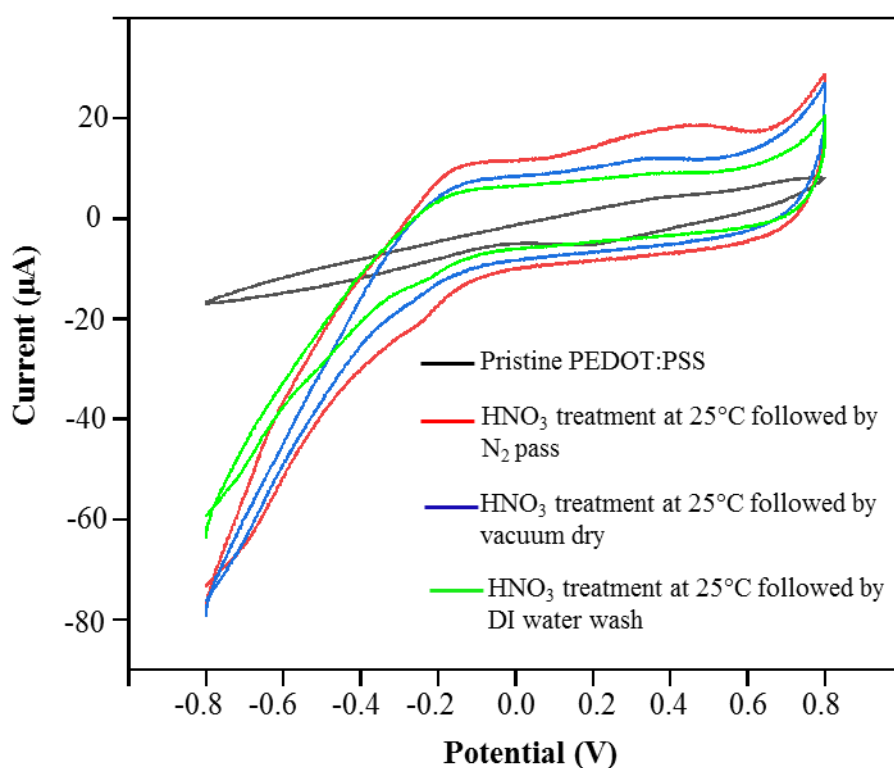


Figure 3.10: Cyclic voltammograms (CVs) of pristine PEDOT:PSS and HNO<sub>3</sub> treated PEDOT:PSS films at different conditions in 0.1 M NaCl solution.

treatment with HNO<sub>3</sub> at different conditions. As conjugated PEDOT chains are surrounded by insulating PSS, PSS may hamper the charge transfer between the working electrode and PEDOT chains [73]. After the treatment with HNO<sub>3</sub>, the removal of insulating PSS results in an increase in electrochemical activity of PEDOT chains. In addition, HNO<sub>3</sub> treated sample followed by N<sub>2</sub> gas pass results in an enlargement of area for the electrochemical activity among the different treatment conditions. It can be attributed that the pressure triggered by N<sub>2</sub> gas passing can assist the removal of excess insulating PSS, which has a weak Coulombic attraction with PEDOT during the HNO<sub>3</sub> treatment.

Based on the various characterizations, we attribute the simultaneous increase in electrical conductivity and Seebeck coefficient at an elevated temperature to the following reasons. The N<sub>2</sub> pressure-induced HNO<sub>3</sub> treatment effectively segregates PEDOT from PSS and removes PSS, resulting in conformational change and in turn an increase in mobility. Concurrently, the treatment also increases the oxidization and doping states of the PEDOT film which is evident from Vis-NIR absorption spectrum. An increase in doping also agrees well with an increase in carrier concentration, which is characterized by the Hall measurement. Both mobility and doping enhance the electrical conductivity, according the relationship  $\sigma = q\mu n$ , where  $\sigma$ ,  $q$ ,  $\mu$  and  $n$  are electrical conductivity, elementary charge, mobility and carrier concentration (doping states), respectively. The significant improvement in electrical conductivity suggests that the semiconducting polymer is transformed into a (semi)metallic one, which is also evident from the temperature dependent electrical conductivity measurement. However, an increase in doping after the treatment also results in decrease in Seebeck coefficient at room temperature. Nevertheless, the Seebeck coefficient increases again at higher temperature due to the (semi)metallic

behaviour of the material. Therefore, above 100°C, the electrical conductivity and Seebeck coefficient increase simultaneously and the optimum power factor is obtained at 150°C.

### **3.4 Conclusion**

In summary, nitric acid treatment of PEDOT:PSS films with the aid of N<sub>2</sub> gas pass gives the highest electrical conductivity at room temperature and decreased with increasing measurement temperature while the Seebeck coefficient increases with increasing measured temperature. The conductivity improvement is due to the increase in polaronic states (doping) and the phase segregation of the PSSH from PEDOT and the removal of insulating PSS resulting in the conformational change of the PEDOT chains. The optimum power factor of  $121 \pm 10 \mu\text{Wm}^{-1}\text{K}^{-2}$  was obtained at a measured temperature of 150°C and pressure of 0.1 MPa, then decrease again at 200°C because of the decrease in electrical conductivity. Electrical conductivity improvement is not only due to the HNO<sub>3</sub> treatment but also N<sub>2</sub> gas pass after treatment. While the Coulombic attraction between PEDOT and extra PSS is weaker because of HNO<sub>3</sub>, the pressure of N<sub>2</sub> gas facilitates to remove such weakly bonded PSS too. In addition, the pressure of the N<sub>2</sub> gas is also responsible for the conformational change of the PEDOT chain while HNO<sub>3</sub> is responsible for the removal of insulating PSS.

## CHAPTER 4

### **Influence of Pressure of Nitrogen Gas on Structure and Thermoelectric Properties of Various Acid-treated PEDOT:PSS Films**

#### **4.1 Introduction**

Owing to the discovery and development of conducting polymers by Heeger, Macdiarmid and Shirakawa, it has been used in a wide range of electronic applications [74-75]. Poly (3,4-ethylenedioxythiophene) (PEDOT): poly styrene sulfonate (PSS) has advantages over other conductive polymers due to its outstanding properties such as easy processing, high electrical conductivity, stability and flexibility [76-77]. On the other hand, TE performance of PEDOT:PSS are still lower for its practical uses due to the excess insulating PSS in the PEDOT:PSS dispersion. Moreover, PSS molecules play an important role in PEDOT:PSS as counter ions as well as dispersion agent for PEDOT. Previous works have employed the post-treatment of PEDOT:PSS films with various acids to improve the TE properties by controlling the doping level. Nevertheless, only the effect of acids or organic solvents on the structure and thermoelectric properties of the PEDOT:PSS are focused in their reports [41-43, 46, 78]. In chapter (3), N<sub>2</sub> pressure-induced HNO<sub>3</sub> treatment of PEDOT:PSS followed by different conditions such as vacuum dry, N<sub>2</sub> gas passing and DI water washing were discussed. In this chapter, post-treatment of PEDOT:PSS films with various acids followed by N<sub>2</sub> gas-passing is explained. The influence of the pressure of N<sub>2</sub> gas on the structure and thermoelectric properties of PEDOT:PSS at various pressures are also discussed.

The electrical conductivity significantly improved from less than 1 Scm<sup>-1</sup> to 1810±200 Scm<sup>-1</sup> for H<sub>2</sub>SO<sub>4</sub>, 1175 ± 23 Scm<sup>-1</sup> for HNO<sub>3</sub> and 846 ± 72 Scm<sup>-1</sup> for HCl treatments followed by N<sub>2</sub> gas-passing with the pressure of 0.1 MPa at a measurement temperature of 150°C. Corresponding power factor of 97 ± 8 μWm<sup>-1</sup>K<sup>-2</sup>, 121 ± 10

$\mu\text{Wm}^{-1}\text{K}^{-2}$  and  $32 \pm 1 \mu\text{Wm}^{-1}\text{K}^{-2}$  were observed for  $\text{H}_2\text{SO}_4$ ,  $\text{HNO}_3$ , and  $\text{HCl}$  treatments, respectively. Based on our results, acids are mainly responsible for the removal of insulating PSS resulting in the conformational change of the PEDOT polymer chain while  $\text{N}_2$  pressure is responsible for the additional conformation of PEDOT polymer favoring the linearly oriented structure. Therefore, mechanical force such as  $\text{N}_2$  pressure after post-treatment of PEDOT:PSS with various acids can lead to additional conformation of the polymer and can result in higher thermoelectric performance.

## 4.2 Experimental Details

### 4.2.1. Materials

PEDOT:PSS (Clevios PH 1000) was purchased from Heraeus Deutschland GmbH & Co. KG (Germany). Sulfuric acid (95%), nitric acid (69%) and hydrochloric acid (37%) from Wako Pure Chemical Industries Ltd. (Japan) were used as received in our experiment.

### 4.2.2. Acid Treatments and Characterization

The glass substrates were washed with deionized (DI) water, ethanol, and acetone and finally cleaned in the Filgen UV ozone cleaner for 20 min. PEDOT:PSS film (100  $\mu\text{l}$ ) was prepared by spin-coating, which is the same procedure as in Chapter 3.

**$\text{H}_2\text{SO}_4$  treatment:** PEDOT:PSS film was put on the hot plate at a temperature of  $160^\circ\text{C}$ , then 100  $\mu\text{l}$  of  $\text{H}_2\text{SO}_4$  was dropped onto it. After 10 min,  $\text{N}_2$  gas was passed with a pressure of 0.1 MPa using gun. Then, the films were thoroughly rinsed with DI water and dried on the hot plate at a temperature of  $120^\circ\text{C}$  for 15 min.

**$\text{HNO}_3$  treatment:**  $\text{HNO}_3$  treatment was performed as in Chapter 3 [36].

**$\text{HCl}$  treatment:**  $\text{HCl}$  treatment was done the same procedure as the  $\text{H}_2\text{SO}_4$  treatment except the treatment temperature was at  $70^\circ\text{C}$ .

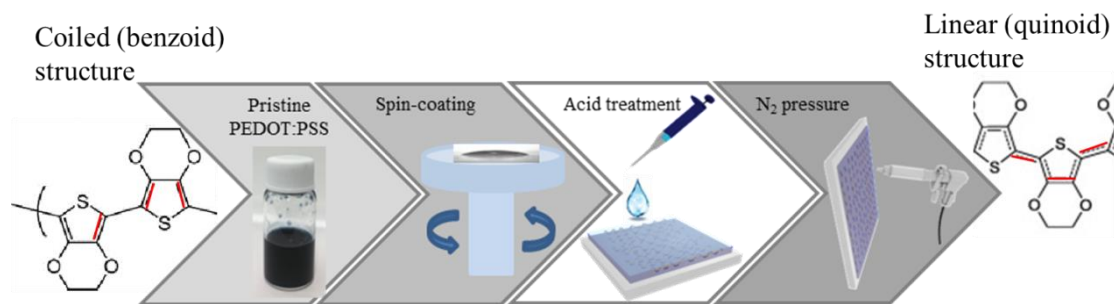


Figure 4.1: Schematic illustration of the experimental details.

The films were fixed at 20 mm away from the gun for all experiments. All treatments were done at their optimized treatment temperatures and conditions. Figure 4.1 shows the process of N<sub>2</sub> gas-passing on the PEDOT:PSS films after treatment with various acids. Electrical conductivity, Seebeck coefficient (thermo power) and power factor of the films were measured in a helium environment by ZEM-3M8 ULVAC (ADVANCED RIKO, Inc.), which is attached to the sample holder for the thin film measurement. Surface of the films was observed by digital microscope (OLYMPUS BX53M) at a magnification of 7.5×. Carrier concentration and carrier mobility were measured to examine the effect of N<sub>2</sub> gas on the improvement of electrical conductivity using (Lake Shore Model 8403) AC/DC Hall effect measurement system. The change in bonding condition before and after treatment was analyzed by Raman spectroscopy (JASCO, NRS 450 NMDS) with a green laser (wavelength 532.21 nm). The morphology and surface roughness of the PEDOT:PSS films were observed by Scanning Probe Microscopy (SPM, Nano Navi SII). The removal of insulating PSS was confirmed by X-ray photoelectron spectroscopy (XPS, JEOL JPS 9030, Japan). UV-vis-NIR (JASCO V-670 spectrophotometer) was performed to observe the doping states of the PEDOT. The change in crystallinity of PEDOT:PSS films after treatment at various pressures of N<sub>2</sub> gas was characterized by RIGAKU SmartLab X-ray diffractometer with CuK<sub>α</sub> radiation ( $\lambda = 1.5418^\circ \text{ \AA}$ ) at a scanning rate of 1 degree per minute.

### 4.3 Results and Discussion

#### 4.3.1 Thermoelectric Properties

Electrical conductivity, Seebeck coefficient and power factor of the HNO<sub>3</sub> treated PEDOT:PSS films followed by N<sub>2</sub> gas pass at different pressures such as 0.05, 0.1, 0.15, 0.2 and 0.25 MPa are shown in Figure 4.2. The electrical conductivity increases when the pressure is increased from 0.05 to 0.25 MPa and the highest electrical conductivity (2693 Scm<sup>-1</sup> at 25°C) is attained at a pressure of 0.1 MPa. The electrical conductivity, however, decreases at a pressure of 0.25 MPa, probably due to the damage of the film, which will be discussed later. On the other hand, the Seebeck coefficient is the lowest at a pressure of 0.2 MPa. Despite this, the Seebeck coefficient increases at an elevated temperature and hence the treated film shows a higher Seebeck coefficient than the pristine does. The optimum power factor of 121±10 μWm<sup>-1</sup>K<sup>-2</sup> was obtained at 150°C but it decreases again at 200°C (Figure 4.2 (c)) because of the decrease in electrical conductivity.

Electrical conductivity, Seebeck coefficient and power factor of pristine PEDOT:PSS are around 1.7 ± 0.2 Scm<sup>-1</sup>, 20 ± 1 μVK<sup>-1</sup> and 0.07 ± 0.005 μWm<sup>-1</sup>K<sup>-2</sup> at a measurement temperature of 150° C. Electrical conductivity of H<sub>2</sub>SO<sub>4</sub>, HNO<sub>3</sub> and HCl treated PEDOT:PSS films are 1400 ± 210 Scm<sup>-1</sup>, 656 ± 75 Scm<sup>-1</sup> and 632 ± 27 Scm<sup>-1</sup> respectively after washing with DI water. Electrical conductivity increased to 1810 ± 200 Scm<sup>-1</sup> for H<sub>2</sub>SO<sub>4</sub> treated, 1175 ± 23 Scm<sup>-1</sup> for HNO<sub>3</sub> treated and 846 ± 72 Scm<sup>-1</sup> for HCl treated PEDOT:PSS films after N<sub>2</sub> gas-passing with a pressure of 0.1 MPa as illustrated in Figure 4.3 (a). The improvement in electrical conductivity after acids treatment followed by DI water-washing can be attributed to the removal of the insulating PSS, also resulting in the conformational change of the PEDOT polymer chain from benzoid (coiled) to quinoid (linear) structure [65, 79-80]. In contrast, the

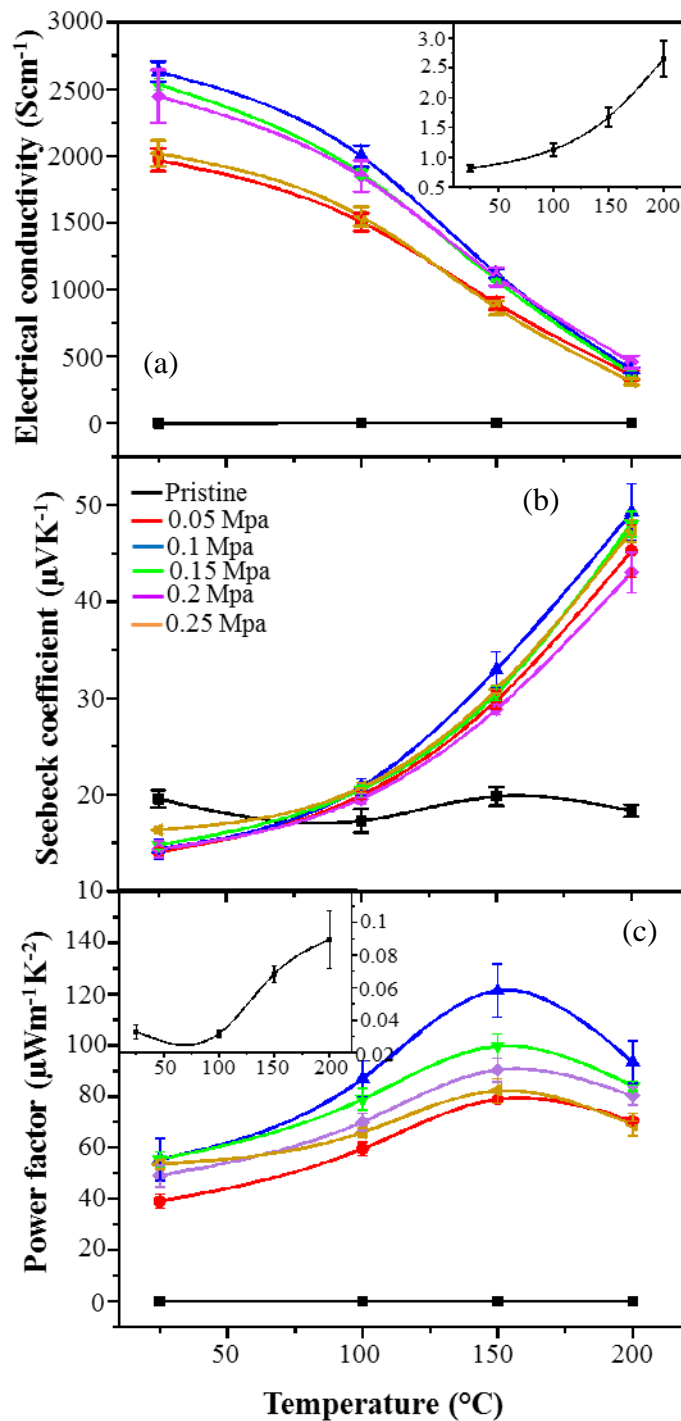


Figure 4.2: (a) Electrical conductivity, (b) Seebeck coefficient, and (c) power factor of PEDOT:PSS films after  $\text{HNO}_3$  treatment followed at different pressures of  $\text{N}_2$  gas. The insets in (a) and (c) are the electrical conductivity and power factor of pristine PEDOT:PSS as a function of measurement temperatures to show the variation in parameters clearly.

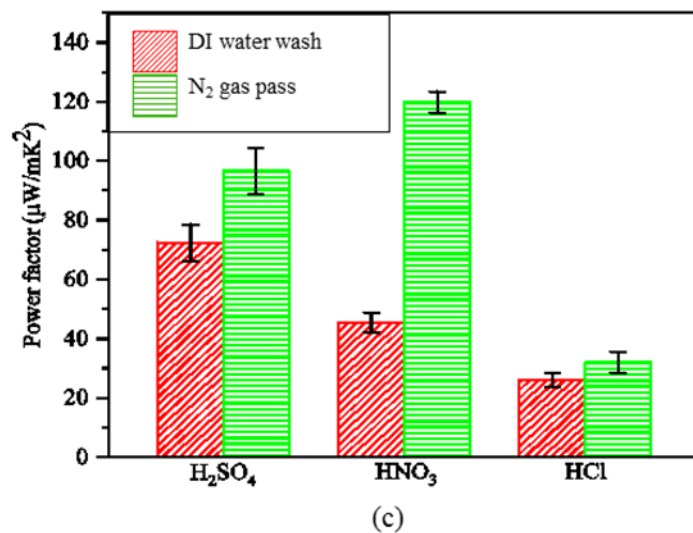
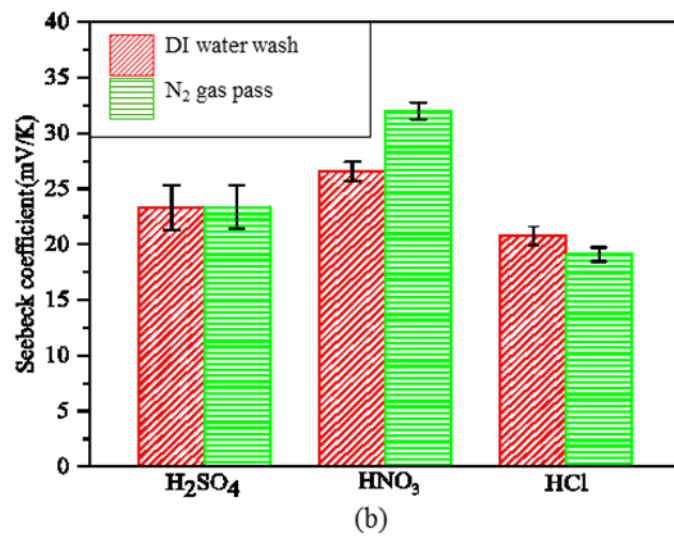
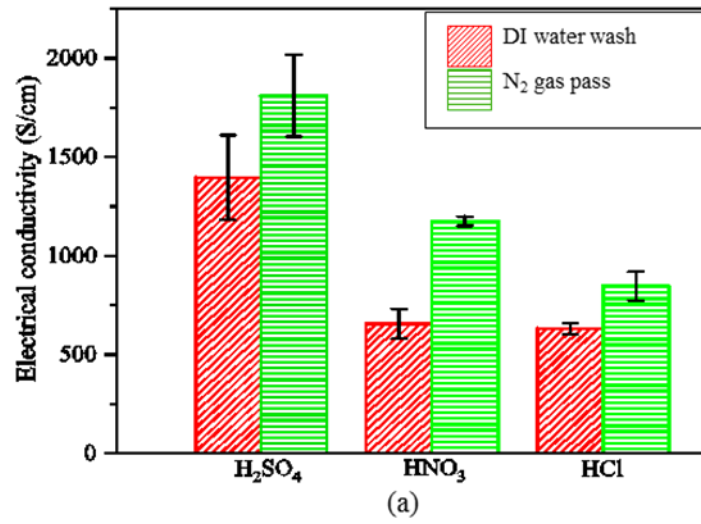


Figure 4.3: (a) Electrical conductivity, (b) Seebeck coefficient and (c) power factor of the PEDOT:PSS films treated with various acids followed by DI water-washing and passing with the pressure of N<sub>2</sub> gas (0.1 MPa) at a measurement temperature of 150° C.

improvement in the electrical conductivity after acids treatment followed by N<sub>2</sub> gas-passing can be ascribed as the additional conformational change of the PEDOT due to the pressure of N<sub>2</sub> gas. It is confirmed by Raman spectroscopy as shown in Figure 4.7. Seebeck coefficient does not change significantly for all acids except for HNO<sub>3</sub> from  $27 \pm 1 \mu\text{VK}^{-1}$  to  $32 \pm 1 \mu\text{VK}^{-1}$  (Figure 4.3 (b)) after DI water-washing and N<sub>2</sub> gas-passing respectively, but which is still unclear why. The power factor improved from  $72 \pm 6$  to  $97 \pm 8 \mu\text{Wm}^{-1}\text{K}^{-2}$  for H<sub>2</sub>SO<sub>4</sub>, from  $46 \pm 3$  to  $121 \pm 10 \mu\text{Wm}^{-1}\text{K}^{-2}$  for HNO<sub>3</sub> and  $26 \pm 1$  to  $32 \pm 1 \mu\text{Wm}^{-1}\text{K}^{-2}$  for HCl treated PEDOT:PSS films (Figure 4.3 (c)) after corresponding acid treatments followed by DI water-washing and N<sub>2</sub> gas-passing at a pressure of 0.1 MPa. Therefore, N<sub>2</sub> gas-passing after acid treatments can give the higher thermoelectric power factor values rather than DI water- washing after acid treatments.

Electrical conductivity increases at the pressure range of 0.1 to 0.2 MPa and then decreases beyond 0.2 MPa. This is probably due to the film damage or some defects on the surface of the films because of the high pressure of N<sub>2</sub> gas. These surface defects are observed by digital microscope as in Fig. 4.4. Smooth surface are observed in pristine PEDOT:PSS film and the film treated with a pressure of 0.1 MPa. Some pinholes or micropores are observed on the surface of the films treated at pressure of 0.15 and 0.2 MPa while big scratches are observed on the film treated with a pressure of 0.25 MPa.



Figure 4.4: Digital micrographs of HNO<sub>3</sub> treated PEDOT:PSS films showing the surface conditions at various pressures of N<sub>2</sub> gas. The scale bars in all photos are 500  $\mu\text{m}$ . All photos were captured at a magnification of 7.5X.

Electrical conductivity, Seebeck coefficient and power factor of  $\text{HNO}_3$ ,  $\text{H}_2\text{SO}_4$  and  $\text{HCl}$  treated PEDOT:PSS films followed by both  $\text{N}_2$  pass and DI water wash are measured at elevated temperatures (Figure 4.5 and 4.6). Electrical conductivity decreases and

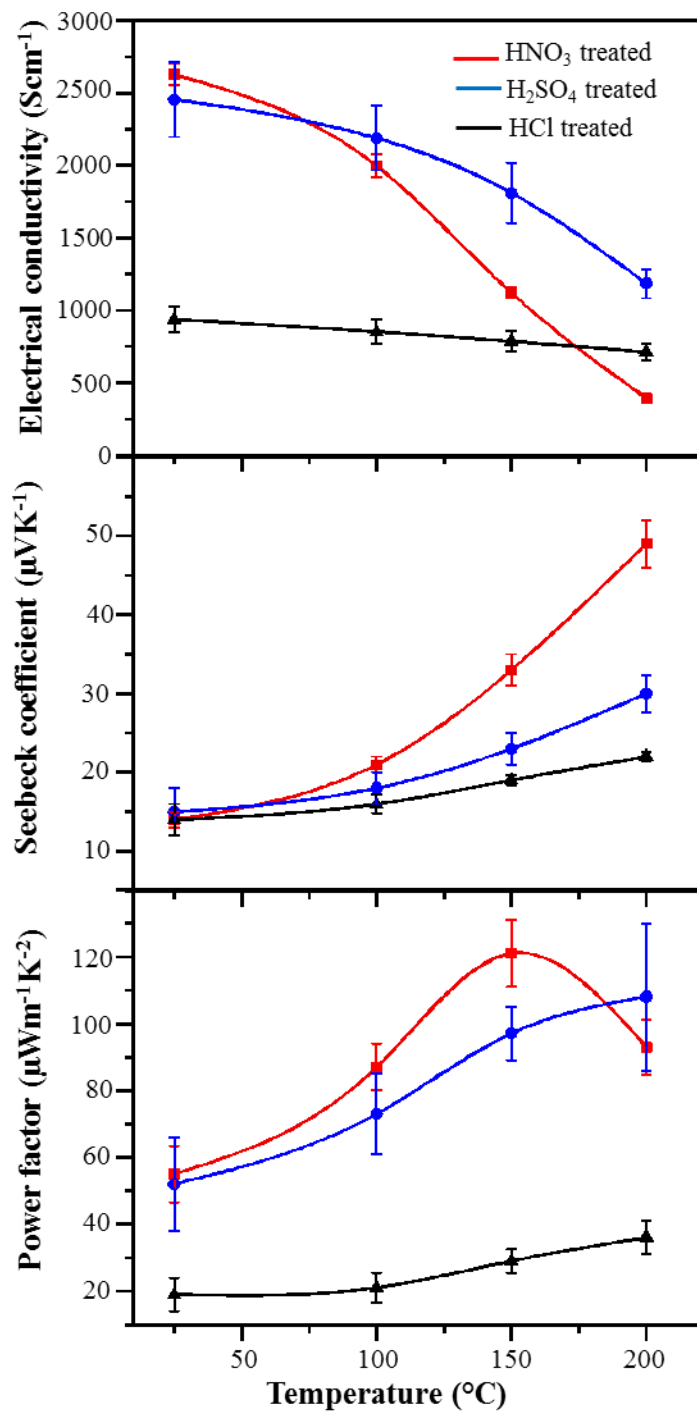


Figure 4.5: Electrical conductivity, Seebeck coefficient and power factor of the  $\text{HNO}_3$ ,  $\text{H}_2\text{SO}_4$  and  $\text{HCl}$  treated PEDOT:PSS films followed by passing with a pressures of 0.1 MPa as a function of measurement temperatures.

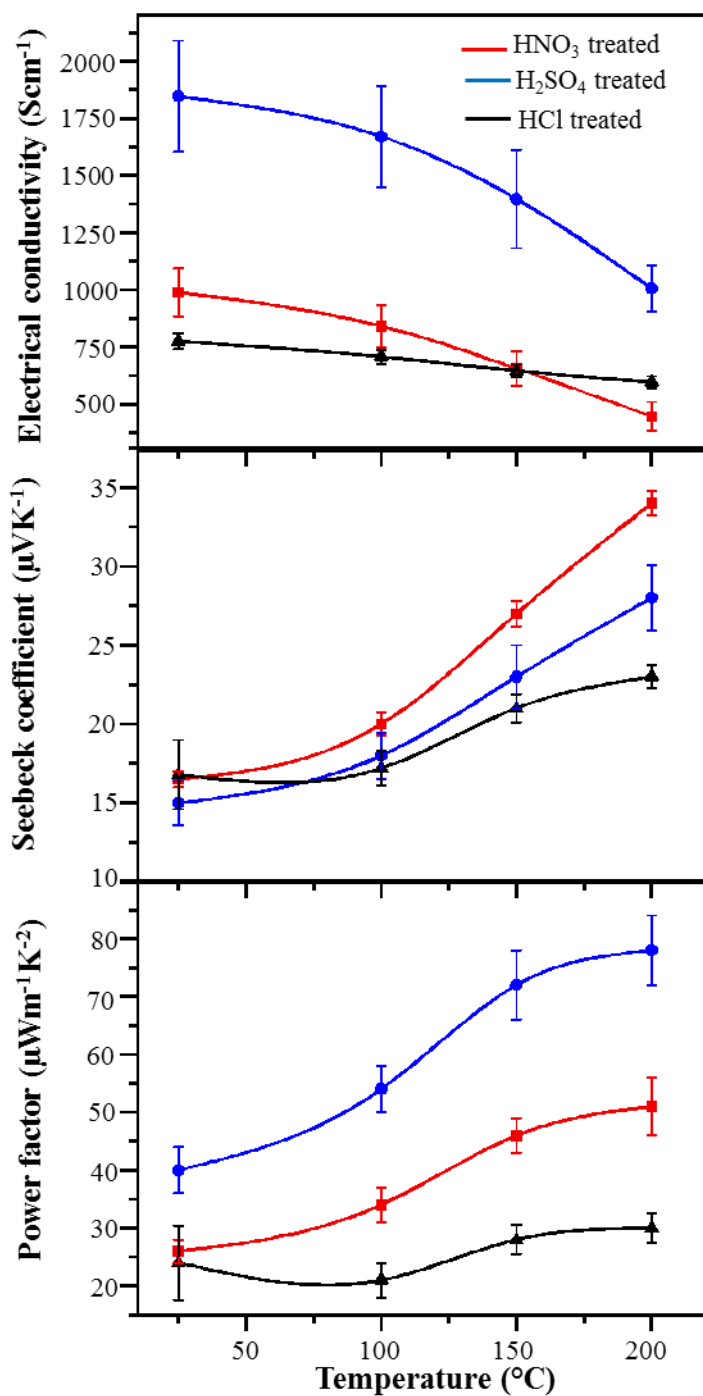


Figure 4.6: Electrical conductivity, Seebeck coefficient and power factor of HNO<sub>3</sub>, H<sub>2</sub>SO<sub>4</sub> and HCl treated PEDOT:PSS films followed DI water washing as a function of measurement temperature.

Seebeck coefficient increases with increasing measurement temperature after treatment with various acids followed by both N<sub>2</sub> gas pass and DI water wash, showing metal-like

behavior.

The optimum Seebeck coefficient of  $32 \pm 1 \mu\text{VK}^{-1}$  was obtained at a pressure of 0.1 MPa due to the increasing measurement temperature when treated with  $\text{HNO}_3$ . Seebeck coefficient is defined by

$$S = \frac{\pi^2 k_B^2 T}{3e} \left. \frac{\partial \ln \sigma(E)}{\partial E} \right|_{E_F} \quad (4.1)$$

where  $\sigma(E)$  is the conductivity of the material at Fermi energy  $E_F$ ,  $k_B$  is the Boltzmann constant and  $e$  is the charge of the electron [15, 62]. Based on this equation, Seebeck coefficient also depends on the local band structure of the material. The removal of PSS may transform the local band structure of PEDOT:PSS and such a probable change in the band structure may be responsible for the improvement in the Seebeck coefficient [81]. Nevertheless, the optimum power factor of  $121 \pm 10 \mu\text{Wm}^{-1}\text{K}^{-2}$  was obtained by the treatment with  $\text{HNO}_3$  at a pressure of 0.1 MPa due to the high Seebeck coefficient.

#### *4.3.2. Influence of Pressure of $\text{N}_2$ Gas on the Structure and Thermoelectric Properties of Various Acids-treated PEDOT:PSS Films*

We observed that the pressure of  $\text{N}_2$  gas favors the phase segregation of PSS as well as the conformation of the PEDOT polymer chain resulting in the enhancement of the carrier concentration, especially the carrier mobility. It is confirmed by the Hall measurement as shown in Table 4.1. Pristine PEDOT:PSS film has hole mobility of around  $2.4 \pm 0.3 \text{ cm}^2\text{V}^{-1}\text{s}^{-1}$  and hole concentration of  $10^{17} \text{ cm}^{-3}$ . After treatment with  $\text{HNO}_3$  and passing with  $\text{N}_2$  gas at various pressures, the hole concentration enhanced to  $10^{21} \text{ cm}^{-3}$  and the hole mobility are also improved. The optimum carrier mobility of  $7 \pm 1.4 \text{ cm}^2\text{V}^{-1}\text{s}^{-1}$  is obtained for the sample treated at a pressure of 0.1 MPa while the carrier concentrations are not too much different at various pressures of  $\text{N}_2$  gas. Therefore, the pressure of the  $\text{N}_2$  gas can lead to the linear orientation of the polymer structure. The carrier mobility decreases again beyond the pressure of 0.1 MPa and this

Table 4.1- Carrier mobility and carrier concentration of the pristine PEDOT:PSS and those of HNO<sub>3</sub> treated films at various pressures of N<sub>2</sub> gas.

Sample	$\mu$ (cm <sup>2</sup> V <sup>-1</sup> s <sup>-1</sup> )	$n$ (cm <sup>-3</sup> )
pristine	2.4 ± 0.3	(7.4 ± 1.7) × 10 <sup>17</sup>
0.05 MPa	5.1 ± 0.7	(4.4 ± 0.02) × 10 <sup>21</sup>
0.1 MPa	6.9 ± 1.4	(2.1 ± 0.5) × 10 <sup>21</sup>
0.15 MPa	4.9 ± 0.2	(3.4 ± 0.3) × 10 <sup>21</sup>
0.2 MPa	5.6 ± 1.3	(2.7 ± 0.6) × 10 <sup>21</sup>
0.25 MPa	5.1 ± 0.7	(5.1 ± 0.6) × 10 <sup>21</sup>
0.3 MPa	5	3.3 × 10 <sup>21</sup>

may be attributed to the defects on the surface of the films such as pin holes and damages, which is also consistent with the digital micrographs.

Raman spectroscopy was also performed to confirm the effect of the pressure of N<sub>2</sub> gas on the conformation of the PEDOT polymer chain. Calibration was performed using Si substrate before and after sample measurement in order to investigate the potential heating effect on the spectrum. No significant peak shift was found for the calibration results, indicating that there was no potential heating effect on the spectral peak position. The peaks assigned at 1227 cm<sup>-1</sup> in Figure 4.7 come from C<sub>α</sub>- C<sub>α</sub> inter- ring stretching, 1337 cm<sup>-1</sup> from C<sub>β</sub>- C<sub>β</sub> inter-ring stretching, 1401 cm<sup>-1</sup> from C<sub>α</sub>= C<sub>β</sub> symmetric stretching, 1506 cm<sup>-1</sup> from C<sub>α</sub>= C<sub>β</sub> asymmetric stretching, respectively [65, 79-80, 82-83]. The peak at 1401 cm<sup>-1</sup> shifts to 1404 cm<sup>-1</sup>, 1406 cm<sup>-1</sup>, 1407 cm<sup>-1</sup>, 1408 cm<sup>-1</sup> and 1409 cm<sup>-1</sup>, respectively after treatment with HNO<sub>3</sub> and the pressure of N<sub>2</sub> gas at 0.05, 0.1, 0.15, 0.2 and 0.25 MPa respectively. These peaks shift reveal the conformation of the PEDOT from benzoid (coiled) to quinoid (linear) structure [65, 79-80]. Therefore, the pressure of N<sub>2</sub> gas after acid treatment can favor the linearly oriented structure of the PEDOT, resulting in the enhancement of the electrical conductivity which is also consistent with the Hall measurement. It was observed in the previous

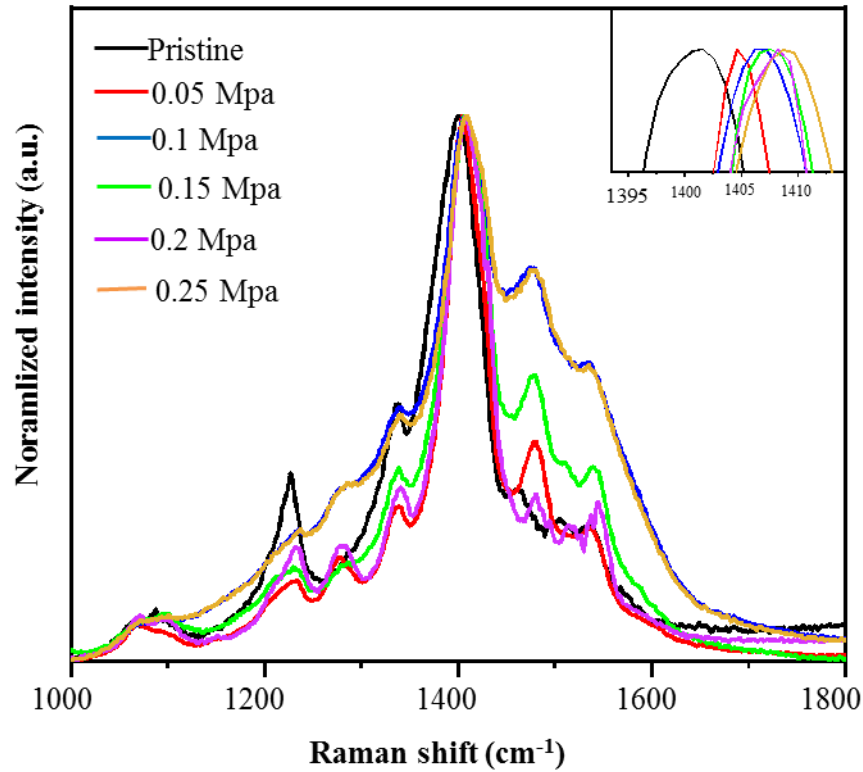


Figure 4.7: Raman spectra of pristine and  $\text{HNO}_3$  treated PEDOT:PSS films at different pressures of  $\text{N}_2$  gas. The inset illustrates the zoom-in view of the peaks shift of  $\text{C}\alpha=\text{C}\beta$  symmetric stretching.

reports that oriented mechanical forces induced by directional film deposition methods [84-85], mechanical rubbing [86] and capillary force [87] makes the polymer films highly aligned and causes anisotropic charge transport in the film. Similar to prior reports,  $\text{N}_2$  blown from one side of the sample might include oriented mechanical force, creating the anisotropic alignment in the PEDOT:PSS and leading to increase in electrical conductivity.

In order to observe the morphological changes of PEDOT:PSS at various pressures of  $\text{N}_2$  gas, the SPM images were scanned for the pristine PEDOT:PSS films and the  $\text{HNO}_3$  treated films. Figure 4.8 represents the topography and phase images of the pristine and  $\text{HNO}_3$ -treated PEDOT:PSS films at various pressures of  $\text{N}_2$  gas at 0.05,

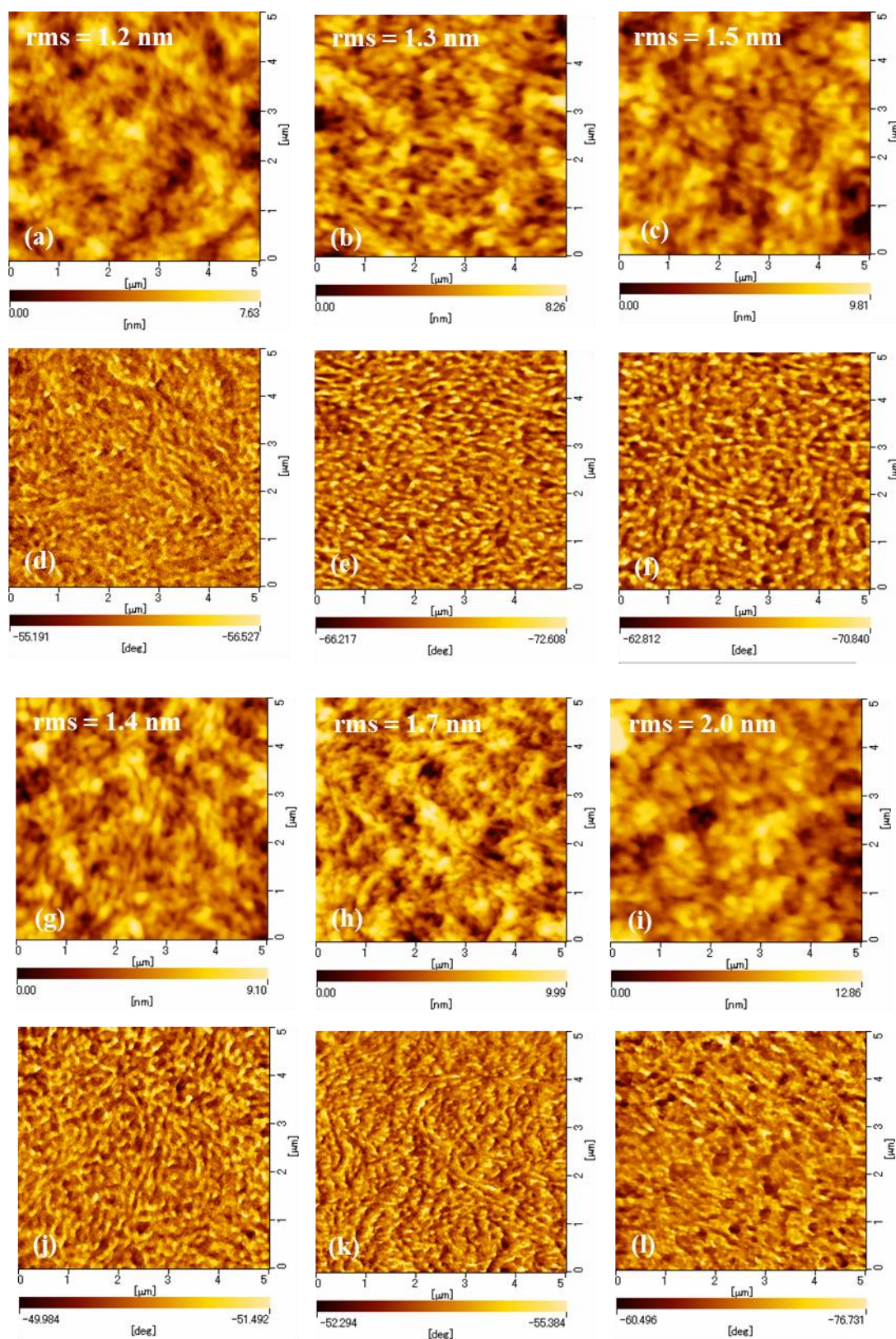
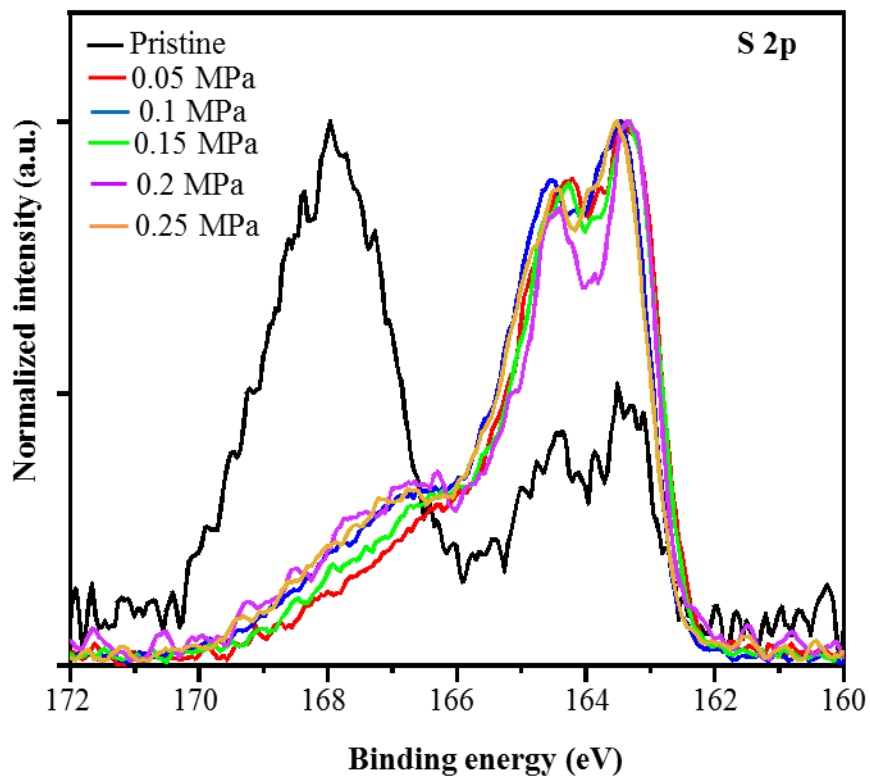


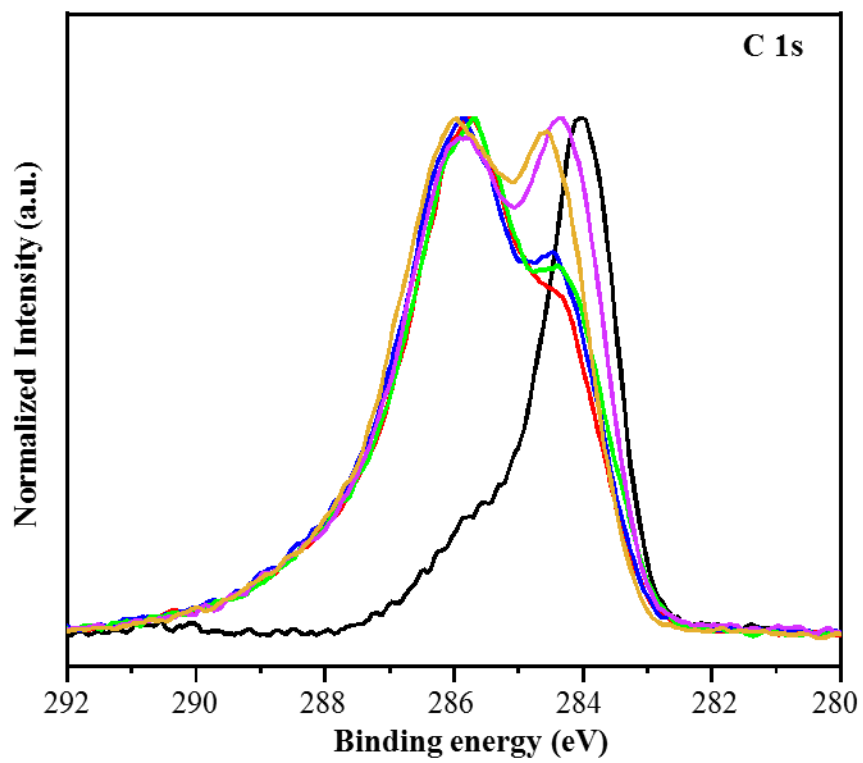
Figure 4.8: SPM topography images (a), (b), (c), (g), (h), (i) and phase images (d), (e), (f), (j), (k), (l) of pristine PEDOT:PSS film and those of  $\text{HNO}_3$  treated films at  $\text{N}_2$  gas pressure of 0.05, 0.1, 0.15, 0.2, and 0.25 MPa. The scanned area for each image is  $5\mu\text{m} \times 5\mu\text{m}$ .

0.1, 0.15, 0.2 and 0.25 MPa respectively. The bright region represents the PEDOT and the dark brown region represents the PSS in the phase images of the films. We can see clearly that some dark colored regions disappear after the treatment in the phase images. It can be attributed to the partial removal of PSS ions [88]. In the topographic images, the root mean square (rms) roughness of the pristine PEDOT:PSS film is 1.2 nm. However, the rms roughness of the treated films become 1.3, 1.5, 1.4, 1.7 and 2.0 nm at the N<sub>2</sub> pressures of 0.05, 0.1, 0.15, 0.2 and 0.25 MPa, respectively. It is an evidence of the phase separation of PSS from PEDOT indicating the removal of PSS phase [66]. Interestingly, the rms of the pristine and the HNO<sub>3</sub> treated samples at N<sub>2</sub> pressures of 0.05, 0.1 and 0.15 MPa are not too much different, nevertheless, those of the treated samples at 0.2 and 0.25 MPa significantly increase to 1.7 and 2.0 nm. Therefore, the pressure of N<sub>2</sub> gas favors the smoother surface morphology even though there is phase separation between the PEDOT and PSS grains. On the other hand, the higher pressure of N<sub>2</sub> gas leads to the surface defects like pin holes, resulting in the increase of rms values.

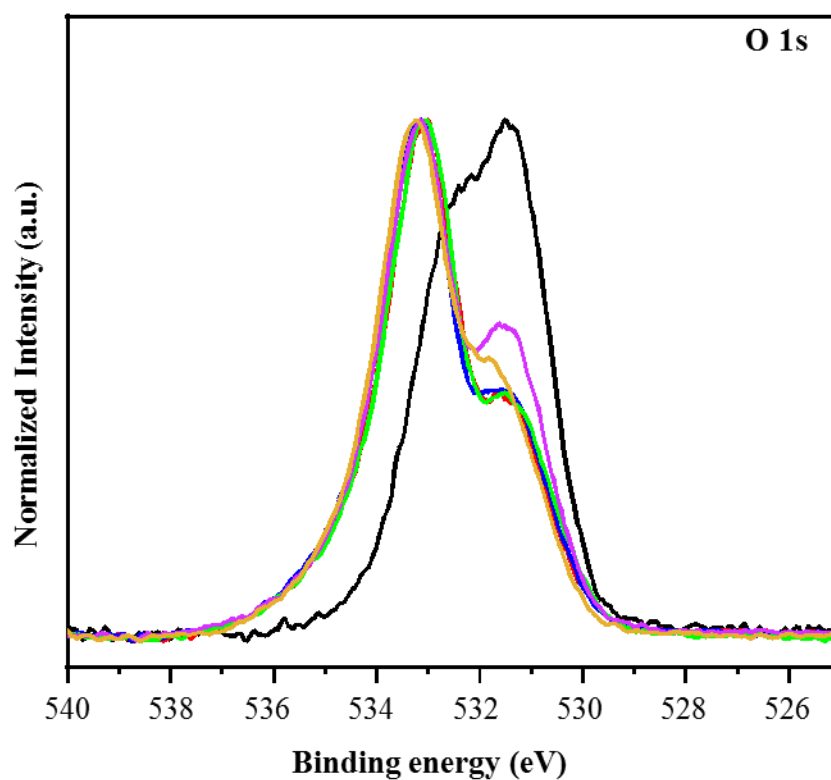
XPS was conducted to analyze the influence of the pressure of N<sub>2</sub> gas on the removal of extra PSS phase of the HNO<sub>3</sub> treated PEDOT:PSS films. XPS bands at 169.1 eV and 167.7 eV are the S2p bands of the sulfur atoms in PSS and the bands at 164.3 eV and 163.1 eV are the S2p bands of the sulfur atoms in PEDOT [89] as in Figure 4.9 (a). The S2p peaks of PSS shifts around 1 eV to the lower binding energy after the treatment with HNO<sub>3</sub> followed by passing at various pressures of N<sub>2</sub> gas. The atomic ratio of PEDOT:PSS was calculated from the area under the peaks using full width at half maximum (FWHM) of curve fitting. The ratio of PEDOT to PSS before treatment is 1:2.52. These ratios significantly increase to 1:0.41, 1:0.44, 1:0.58, 1:0.59 and 1:0.4 after treatment with HNO<sub>3</sub> followed by the pressure of N<sub>2</sub> gas at 0.05, 0.1, 0.15, 0.2 and 0.25 MPa, respectively. Nevertheless, the ratios are not significantly



(a)



(b)



(c)

Figure 4.9: (a) S2p, (b) C1s and (c) O1s core-level of the XPS spectra of the pristine and those of HNO<sub>3</sub> treated PEDOT:PSS films at different N<sub>2</sub> pressures.

different at different pressures of N<sub>2</sub> gas. Therefore, HNO<sub>3</sub> treatment is essentially responsible for the removal of insulating PSS and, on the other words, the pressure of N<sub>2</sub> gas after HNO<sub>3</sub> treatment does not play a major role in removing the extra PSS. The peaks at 285.7 eV and 284 eV in C1s spectra come from the C-O bond in PEDOT and C-C bond in PSS chain [90] (Figure 4.9 (b)). After treatment with HNO<sub>3</sub> and passing with various pressures of N<sub>2</sub> gas, the intensities of the peaks at 285.7 eV increase while the intensities of the peaks at 284 eV decrease, indicating the removal of thiophene group of PSS. The peaks at 531.4 eV and 532.5 eV in Figure 4.9 (c) come from the oxygen atom which is attached to the sulfur atom in PSS and the oxygen atom in PEDOT. After treatment, the intensities of the peaks at higher binding energy increases while the intensities of the peaks at lower binding energy decreases. It can be attributed

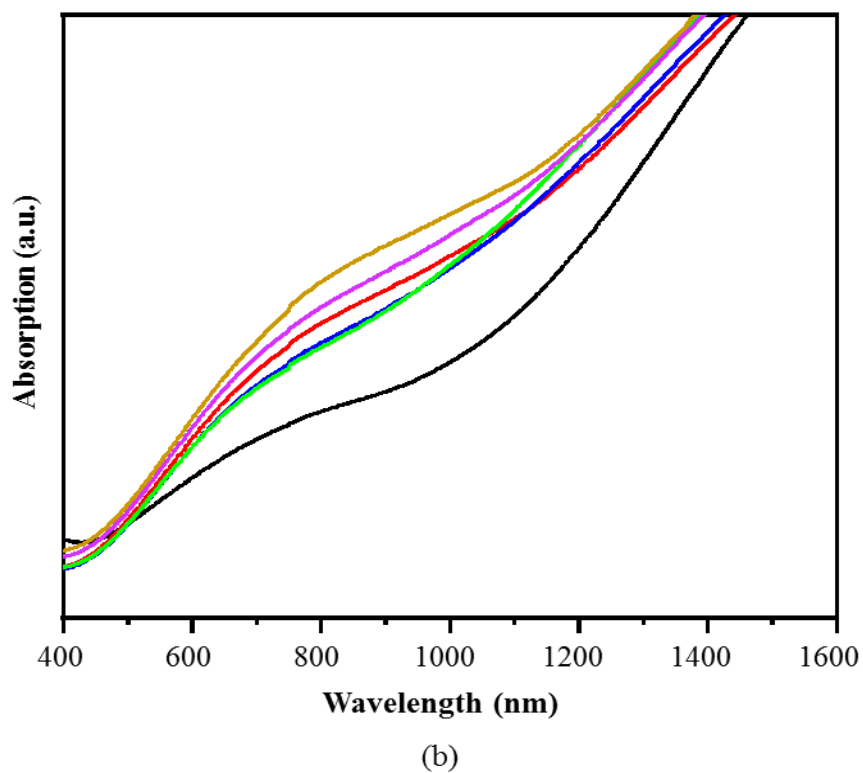
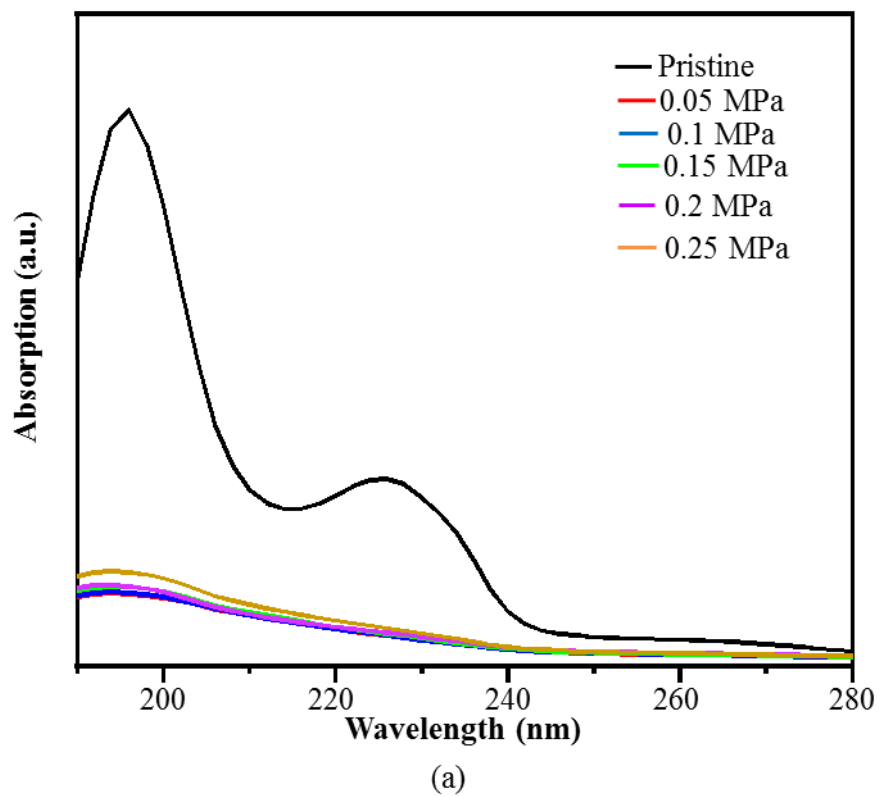


Figure 4.10: UV-vis-NIR spectra of pristine and HNO<sub>3</sub> treated PEDOT:PSS at different pressures of N<sub>2</sub> gas: (a) at UV region and (b) at vis-NIR region.

to the phase segregation of PSS from the PEDOT:PSS resulting in the formation of PSSH [66, 89]. However, by comparing the XPS results of the treated films at different pressures of N<sub>2</sub> gas, the intensities of the peaks are very similar to each other. It means that passing with N<sub>2</sub> gas after acid treatment does not play a major role in the removal of PSS.

UV-vis-NIR absorption spectra were recorded to confirm the above XPS analysis as illustrated in Figure 4.10 (a) and (b). The decrease in the intensities of the two absorption bands at 196 nm and 225.8 nm in the UV region (Figure 4.9 (a)) after acid treatment followed by passing with N<sub>2</sub> gas at various pressures indicates the removal of extra PSS from PEDOT:PSS, hence both bands come from the PSS moiety [90]. However, all the bands stack one upon another after HNO<sub>3</sub> treatment at various pressures of N<sub>2</sub> gas show that the amount of PSS removal is similar at different treatment pressures. The absorption bands at near infrared region were also recorded to examine the influence of N<sub>2</sub> pressure after treatment. The absorption bands around 600 nm, 900 nm and 1200 nm come from the neutral, polaron and bipolaron states of the PEDOT, which have reported in the previous literature [90]. The improvement of the absorption intensities at  $\approx$  900 nm after HNO<sub>3</sub> treatment and at various pressures of N<sub>2</sub> gas reveals an increase in its doping state to polaronic state. Therefore, the results of UV-vis-NIR measurement agree well with XPS measurement.

To investigate the mechanism of significantly increasing the electrical conductivity after acid treatment followed by N<sub>2</sub> gas-passing, X-ray diffraction (XRD) was performed as depicted in Figure 4.11. The pristine PEDOT:PSS film shows only the amorphous halo inter-chain stacking at  $2\theta$  value of 23.8°. After treatment with HNO<sub>3</sub> and at various pressures of N<sub>2</sub> gas, the new peaks appear at around 2.5° and 6.8°, which are attributed to the lamellae stacking of the alternating structure of PEDOT and PSS. Therefore, after acid treatment, PEDOT crystallites incline to a linear structure resulting

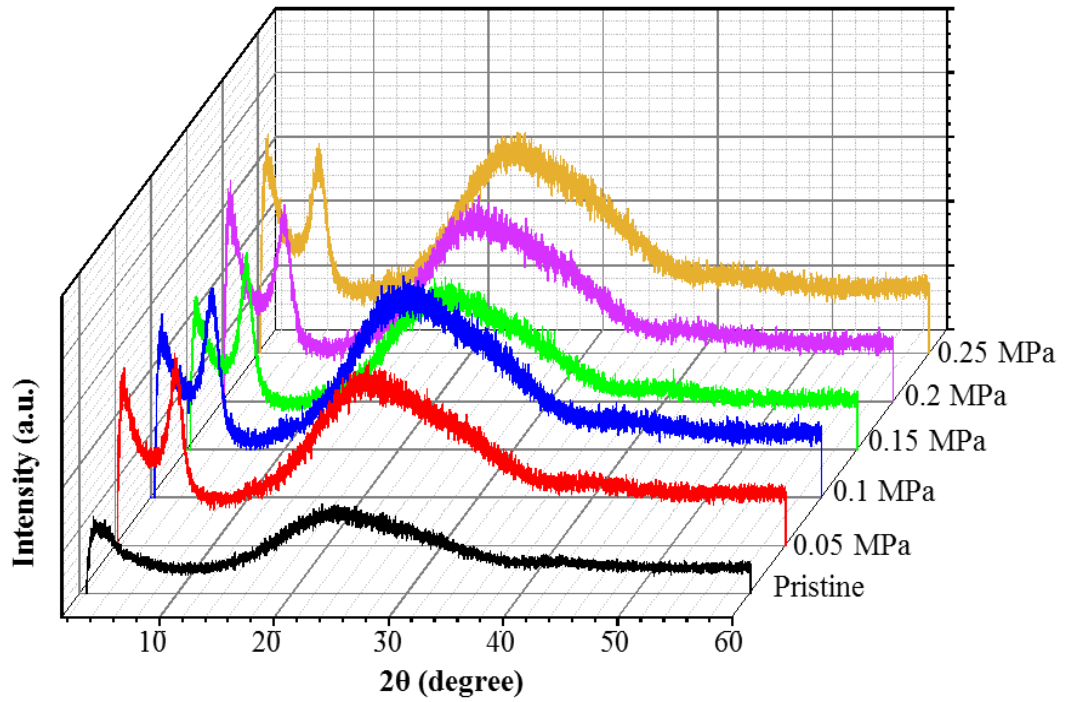


Figure 4.11: X-ray diffraction (XRD) pattern of pristine and those of HNO<sub>3</sub> treated PEDOT:PSS thin films followed by passing with different pressures of N<sub>2</sub> gas.

in more lamellae stacking [71, 91-92], which is consistent with the Raman spectroscopy results. Moreover, no significant peaks shifts are observed for the positions of both peaks resulting in no obvious changes of lattice spacing although different pressures of N<sub>2</sub> gas are used. Therefore, it can be ascribed as the pressure of N<sub>2</sub> gas has no significant influences on the removal of extra PSS.

#### 4.4. Conclusion

In summary, we have reported the influence of the pressure of N<sub>2</sub> gas after acid treatment on the structure and thermoelectric properties of PEDOT:PSS. The improvement of electrical conductivity is due to the removal of insulating extra PSS from PEDOT:PSS and the conformation of PEDOT polymer structure from benzoid (coiled) to quinoid (linear) structure. In our experiment, there are two reasons for the conformation of PEDOT: (1) the removal of PSS by acid treatments and (2) the pressure

of N<sub>2</sub> gas. Acid treatment plays a major role in the removal of the insulating PSS, resulting in the conformation of PEDOT while the pressure of N<sub>2</sub> gas is mainly responsible for the additional conformation of polymer favoring the linear orientation of the structure. Therefore, mechanical forces such as the pressure of N<sub>2</sub> gas can affect the structure of acid-treated PEDOT: PSS regardless of the types of acids. Applying mechanical forces after acid treatment can give higher thermoelectric performance rather than traditional DI water-washing for PEDOT:PSS films.

## CHAPTER 5

### Enhancement of Thermoelectric Properties of Poly (3-hexylthiophene) (P3HT)/Carbon Nanotube (CNT) Yarn Composite

#### 5.1 Introduction

As thermoelectric (TE) devices enable to convert waste heat to electricity from a variety of sources including human body, flexible, light-weighted and robust thermoelectric materials have much attraction for those applications [93-94]. CNT yarn is one of the potential materials owing to its narrow band gap energy and high charge carrier mobility, and it can be easily fabricated into flexible, wearable, light-weighted and robust materials [95]. Moreover, the carrier type of the CNT yarn can be easily altered by simple doping as well, paving it for using in various wearable or flexible TE applications [96-97]. Most of the research groups have reported about the TE performance of single-walled carbon nanotubes (SWCNTs) and double-walled carbon nanotubes [97-100]. The applications of MWCNTs in TE generators still needs to explore owing to low fabrication cost and availability of large quantity.

In this chapter, we propose a novel way herein, doping of CNT yarn composed of individual multi-walled carbon nanotube (MWCNTs) with *p*-type dopants, F4TCNQ and P3HT after Joule annealing in the vacuum condition.

#### 5.2 Experimental Details

##### 5.2.1. Materials and Methods

Chemical vapor deposition (CVD) method (Black Magic II, Aixtron Ltd.) was used to synthesize high-density and vertically aligned CNTs. A thin layer of iron was used as catalyst which was deposited on the substrate ( $\text{Al}_2\text{O}_3/\text{SiO}_2/\text{Si}$ ) by electron beam deposition (VTR-350M/ERH, ULVAC KIKO Inc.). CNT array was resulted on this

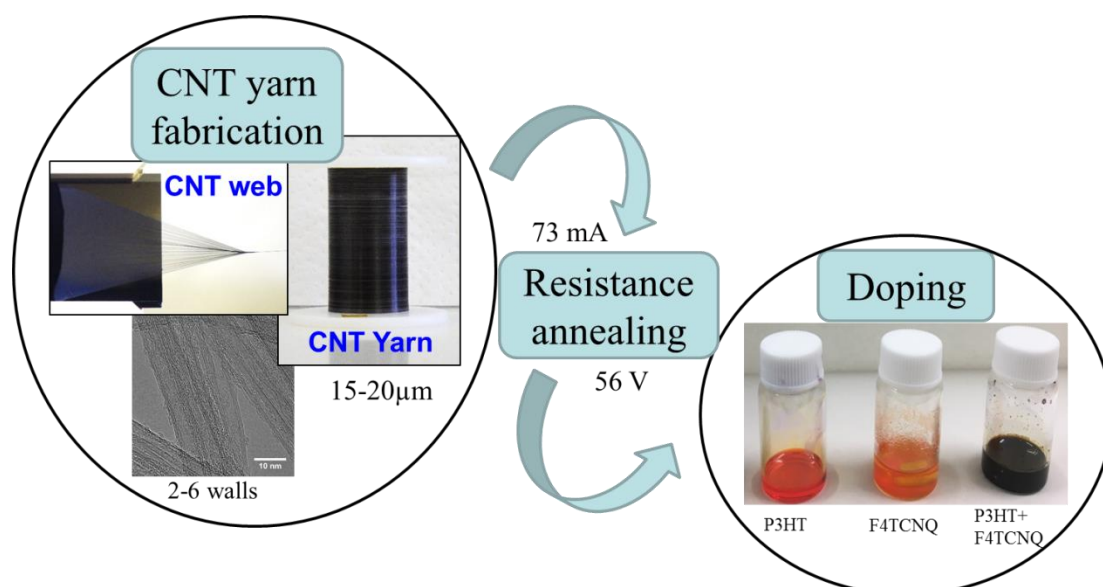


Figure 5.1: Fabrication, resistance annealing and doping of CNT yarn

substrate in vertical orientation [101]. CNT yarn was composed of much more individual MWCNTs with average tube diameter of 4-6 nm and wall number of approximately 2-6 observed by transmission electron microscopy (TEM) as shown in Figure 5.1. Then, CNT yarn which has the diameter of 15-20  $\mu\text{m}$  were fabricated from this array using dry spinning method with rotation speed of 500 rpm and drawing speed of 300 mm/min. Joule heating was accomplished by passing a current of  $\sim 73$  mA and voltage of 56 V under vacuum condition at around  $1-2 \times 10^{-4}$  Pa [102] for 1 min.

P3HT (regioregular) was purchased from Tokyo Chemical Industry Co. Ltd. F4TCNQ was purchased from Luminescence Technology Corporation. Chlorobenzene (99%) was purchased from Wako Pure Chemical Industries, Ltd. P3HT (5 mg/ml) was dissolved in chlorobenzene solution by magnetic stirring at  $70^\circ\text{C}$  for 10 min at 300 rpm. F4TCNQ was also dissolved in chlorobenzene solution by probe sonication for 10 min followed by magnetic stirring at  $110^\circ\text{C}$  for 20 min at 300 rpm. Moreover, F4TCNQ solution was added into the P3HT solution with various weight ratios of 5 %, 10 % and 17 % respectively by bath sonication for 10 min in order to prepare F4TCNQ doped P3HT solution [103-104]. Then CNT yarns were dipped into P3HT, F4TCNQ and

F4TCNQ doped P3HT solutions respectively for 6 hrs. As a consequence, CNTYs were dried in an oven at 80°C for 15 min.

### 5.2.2. Measurement and Characterization

ZEM-3M8 ULVAC Seebeck Coefficient Measurement System (ADVANCED RIKO, Inc) was used to measure the thermoelectricity such as Seebeck coefficient, electrical conductivity and power factor, which has special sample attachment to measure the thin film or wire. Measurement was performed in the helium environment. Analytical scanning electron microscope (SEM, JEOL, JSM-6060LA) was used to measure the diameter as well as to analyze the surface condition of the CNT yarn. Raman spectroscopy (JASCO, NRS450 NMDS) was performed using 523 nm excitation (green) lasers to characterize short/long-range order/disorder in CNT yarns. Transmission electron microscopy (JEOL JEM-2100F HR-TEM) was used to analyze the number of walls as well as the presence of amorphous carbon in CNT yarn. The presence of carbonaceous entities before and after Joule heating was quantitatively estimated by thermal gravimetric analysis (TGA) (DTG-60, SHIMADZU). TGA was performed at 10 °C/min from 25 to 1000 °C under air flow rate of 300 ml/min.

## 5.3. Results and Discussion

### 5.3.1. Effect of Resistance Annealing and P-type Doping on Thermoelectric Properties of Carbon Nanotube Yarn

Electrical conductivity, Seebeck coefficient and power factor of pristine CNT yarn has 637 Scm<sup>-1</sup>, 23μVK<sup>-1</sup> and 34 μWm<sup>-1</sup>K<sup>-2</sup>, respectively at room temperature. After joule heating at around 4 W (73 mA × 56 V), Seebeck coefficient significantly improves to 114 μVK<sup>-1</sup> while electricity conductivity is still lower (592 Scm<sup>-1</sup>) than the pristine one. Therefore, power factor increased to 776 μWm<sup>-1</sup>K<sup>-2</sup> after joule heating at 4 W at

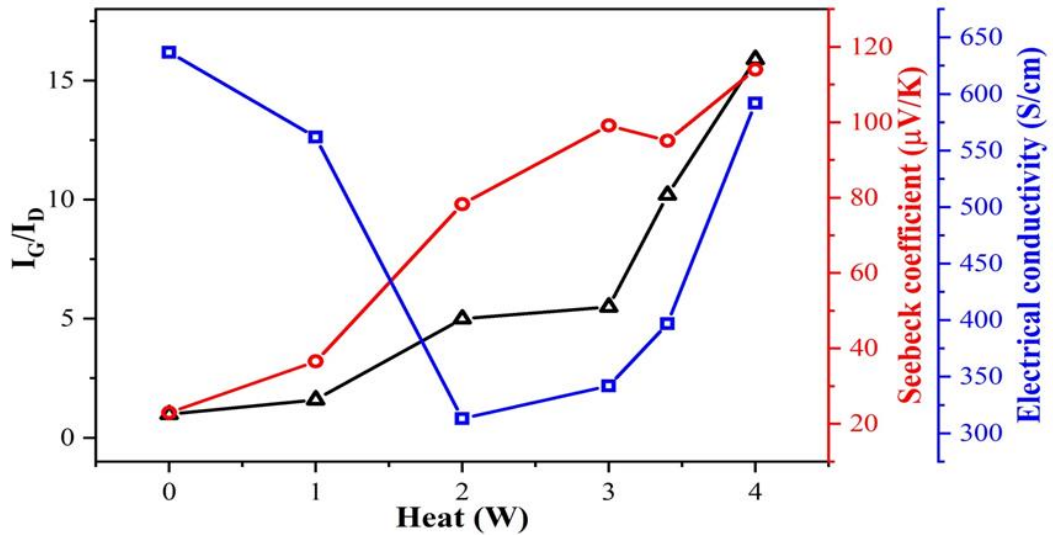


Figure 5.2: Effect of joule heating on Seebeck coefficient, electrical conductivity and graphitic structure of CNT yarns.

room temperature. CNT yarn was broken when continuously heating to 5 W. The effect of joule heating at various amount of heat on the Seebeck coefficient and electrical conductivity is shown in Figure 5.2. When the amount of heat is gradually increased, Seebeck coefficient increased and electrical conductivity decreased first until 2 W and then increased again gradually.

After joule heating, some part of amorphous carbon on the surface of the CNT yarn changed to graphene-like structure and some of the defective six-membered ring carbon atoms are also cured during joule heating, which are confirmed by Raman spectroscopy as in Figure 5.9. Therefore, the surface of the CNT yarn becomes a perfect graphene-like structure after Joule heating. Because of the formation of graphene-like structure on the surface of the CNT yarn, dopant materials can be easily attached to the surface of the CNT yarn. Nevertheless, amorphous carbon and other impurities may decrease the carrier mobility which cause scattering and contact resistant [105]. On the other hand, electrical conductivity slightly increases again beyond 2W as the formation of graphene-like structure and removal of amorphous carbon not only on the surface of

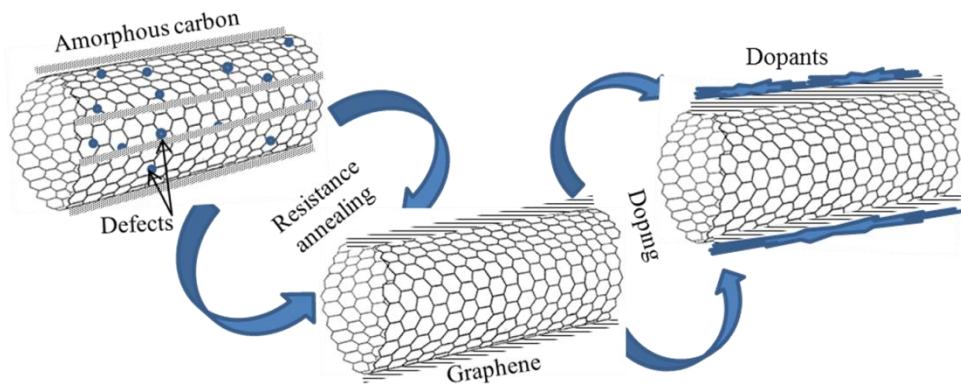


Figure 5.3: Possible mechanism of morphology change of CNT yarn after joule heating and *p*-type doping.

outside fibre but also on the surface of inner fibre since CNT yarn composes of many individual fibres. Possible mechanism of morphology change during joule heating and *p*-doping is demonstrated in Figure 5.3.

In order to increase the electrical conductivity after joule heating, CNT yarns are doped with *p*-type molecular dopant, F4TCNQ, *p*-type conductive polymer, P3HT and both. Firstly, doping is performed with various concentrations of F4TCNQ such as 1, 2.5, 5 and 10 mg/ml respectively. The highest power factor of  $2250 \mu\text{Wm}^{-1}\text{K}^{-2}$  (electrical conductivity of  $1812 \text{ Scm}^{-1}$  and Seebeck coefficient of  $111 \mu\text{VK}^{-1}$ ) was obtained at a measurement temperature of  $150^\circ\text{C}$  when doped with 2.5 mg/ml F4TCNQ (Figure 5.4). Electrical conductivity decreases again at high concentrations of F4TCNQ due to the aggregate formation on the surface of the CNT yarns, which is observed by SEM as in Figure 5.14. Seebeck coefficient still remains unchanged at high concentration of F4TCNQ. After doping with F4TCNQ, in contrast to the Joule annealed CNT yarns, the electrical conductivity decrease with increasing temperature while the Seebeck coefficient increases with increasing temperature, showing the metallic behavior (Figure 5.5 (a) and (b)). Moreover, when CNT yarns were doped with *p*-type conducting polymer (5 mg/ml P3HT), it shows the power factor of  $1030 \mu\text{Wm}^{-1}\text{K}^{-2}$

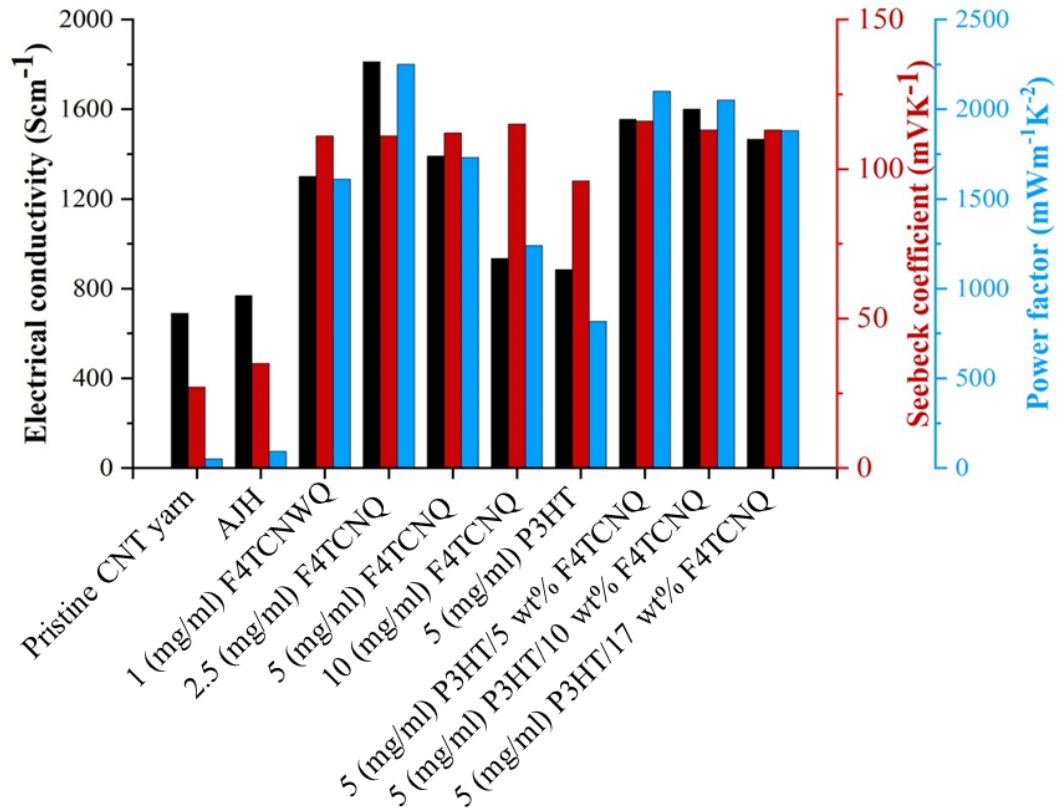
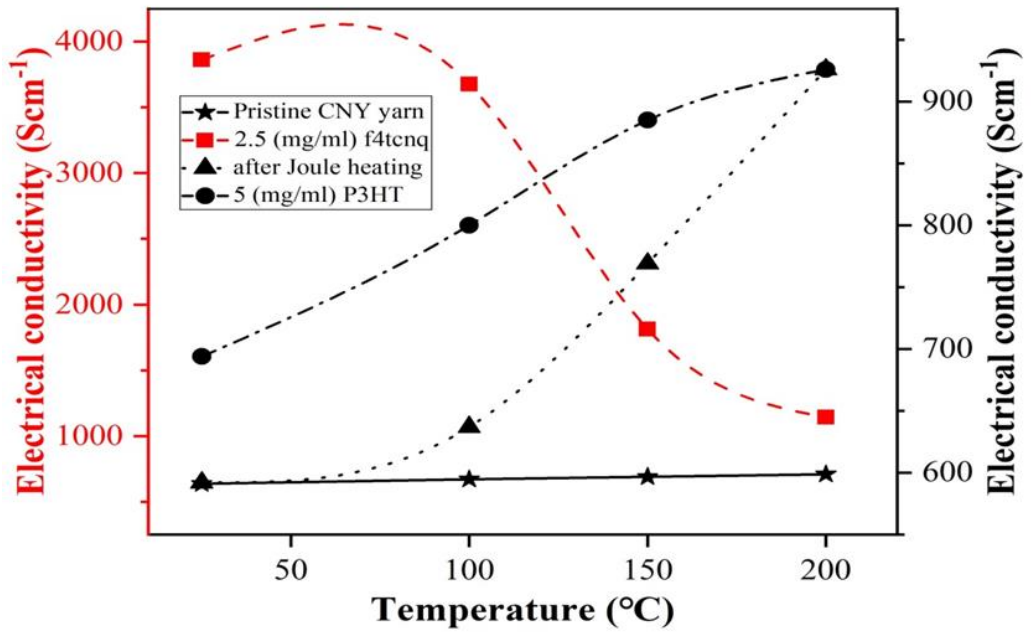
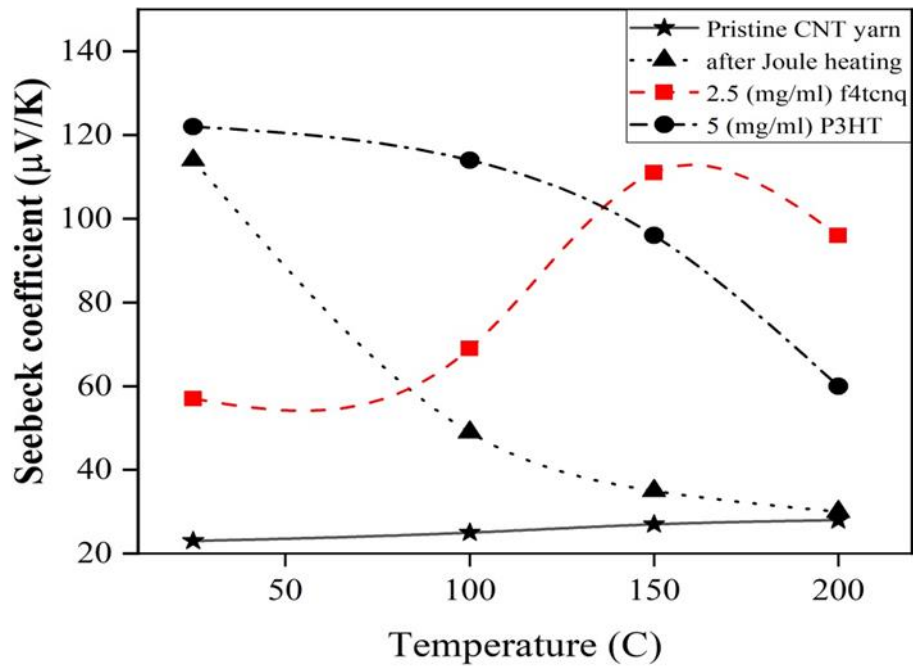


Figure 5.4: Electrical conductivity (black column), Seebeck coefficient (red column) and the corresponding power factor (blue column) of pristine, resistance-annealed, F4TCNQ doped, P3HT doped, and F4TCNQ and P3HT doped CNT yarns. All measurements were done at 423 K.

<sup>1</sup>K<sup>-2</sup> (electrical conductivity of 694 Scm<sup>-1</sup> and Seebeck coefficient of 122  $\mu$ VK<sup>-1</sup>) at room temperature and then decreases at measurement temperature of 423 K (power factor of 330  $\mu$ Wm<sup>-1</sup>K<sup>-2</sup>, Seebeck coefficient of 60  $\mu$ VK<sup>-1</sup> and electrical conductivity of 926 Scm<sup>-1</sup>), still exhibiting the semiconductor behavior (Figure 5.5 (a) and (b)). When doping with both P3HT and F4TCNQ, the maximum power factor of 2100  $\mu$ Wm<sup>-1</sup>K<sup>-2</sup> (electrical conductivity of 1555 Scm<sup>-1</sup> and Seebeck coefficient of 116  $\mu$ VK<sup>-1</sup>) was rendered at the measurement temperature of 423 K. The highest electrical conductivity of 3861 Scm<sup>-1</sup> was attained when doped with 2.5 mg/ml F4TCNQ and the highest Seebeck coefficient of 122  $\mu$ VK<sup>-1</sup> was obtained when doped with P3HT at room temperature.



(a)



(b)

Figure 5.5: (a) Electrical conductivity and (b) Seebeck coefficient of pristine, resistance-annealed, F4TCNQ doped and P3HT doped CNTYs at various measurement temperatures, showing semiconductor and metallic behavior, respectively.

In order to explain the significant improvement of Seebeck coefficient and electrical conductivity qualitatively after joule heating and  $p$ -type doping, we use the numerical calculation as below. Seebeck coefficient or thermopower with  $j = 0$  can be express as

$$S = \frac{E}{\partial T / \partial x} \quad (5.1)$$

where  $E$  is the total electric field. When no external electric field is applied, the total electric field becomes,

$$E = \frac{1}{e} \frac{\partial E_F}{\partial x} \quad (5.2)$$

If  $n$  electrons with charge  $e$  move in the  $x$ -direction with a velocity, we have equation for the electric current density  $j$ ,

$$j = \pm \frac{1}{e} \int_0^\infty \sigma(E) \frac{\partial f_0}{\partial E} \left( \frac{\partial E_f}{\partial x} + \frac{E - E_f}{T} \frac{\partial T}{\partial x} \right) dE \quad (5.3)$$

The Fermi energy is much greater than zero (conduction band edge) in metals (degenerate materials) while it is much less than zero in semiconductors (nondegenerate materials). Parabolic single band model covers both degenerate and nondegenerate materials. Using the assumption of the power-law model, the electron relaxation time is a function of energy as

$$\tau = \tau_{const} E^r \quad (5.4)$$

where  $r$  is called the scattering parameter, and  $\tau_{const}$  is independent of energy but it may be dependence on effective mass and temperature. There are three fundamental scattering mechanisms:  $r = -1/2$  for the acoustic phonon scattering (most materials),  $r = 3/2$  for ionized impurity scattering, and  $r = 1/2$  for polar optical phonon scattering. Using the reduced energy,  $E^* = E/k_B T$  and the reduced Fermi energy,  $E_F^* = E_F/k_B T$  since the electron energy is approximately the order of  $k_B T$ , the electron relaxation time  $\tau$

becomes

$$\tau = \tau_{const} (k_{\beta} T)^r E^{*r} = \tau_0 E^{*r} \quad (5.5)$$

The density of states  $g(E)$  with the degeneracy can be expressed as

$$g(E) = \frac{N_v}{2\pi^2} \left( \frac{2m_d^*}{\hbar^2} \right)^{\frac{3}{2}} (k_{\beta} T)^{\frac{1}{2}} E^{*\frac{1}{2}} \quad (5.6)$$

where,  $N_v$  is the degeneracy (multiple valleys or the number of bands). The electron concentration,  $n$  can be express as

$$n = \frac{N_v}{2\pi^2} \left( \frac{2m_d^* k_{\beta} T}{\hbar^2} \right)^{\frac{3}{2}} \int_0^{\infty} \frac{E^{*\frac{1}{2}}}{e^{(E^* - E_F^*) + 1}} dE^* \quad (5.7)$$

For the sake of simplicity, the Fermi integral can be written as

$$F_s = \int_0^{\infty} \frac{E^{*s}}{e^{(E^* - E_F^*) + 1}} dE^* \quad (5.8)$$

Using the Fermi integrals, the electron concentration  $n$  is express as

$$n = \frac{N_v}{2\pi^2} \left( \frac{2m_d^* k_{\beta} T}{\hbar^2} \right)^{\frac{3}{2}} F_{1/2} \quad (5.9)$$

Therefore, Seebeck coefficient,  $S$  can be derive as

$$S = - \left( \frac{k_{\beta}}{e} \right) \left[ \frac{\left( r + \frac{5}{2} \right) F_{r+3/2}}{\left( r + \frac{3}{2} \right) F_{r+1/2}} - E_f^* \right] \quad (5.10)$$

where,  $S$  is the temperature dependent Seebeck coefficient,  $e$  is the charge of electron ( $1.602 \times 10^{-19}$  C),  $k_{\beta}$  is the Boltzmann constant,  $T$  is the temperature at which Seebeck coefficient is measured and  $E_f$  is the Fermi energy. Since,  $(E - E_f) > 3$  for nongenerate semiconductors, an approximation  $F_j(E_f) \approx e^{E_f} \varphi(j + 1)$  can be used, where  $\varphi(j)$  is the gamma function, we obtained

$$S = - \left( \frac{k_{\beta}}{e} \right) \left[ \frac{r + \frac{5}{2}}{r + \frac{3}{2}} \frac{\varphi\left(r + \frac{3}{2} + 1\right)}{\varphi\left(r + \frac{1}{2} + 1\right)} - E_f \right] \quad (5.11)$$

Then, we can simplify the equation (5.11) as

$$S = -\frac{1}{eT} \left[ \left( \frac{5}{2} + r \right) k_{\beta} T - E_f \right] \quad (5.12)$$

From equation (5.12) we obtained Fermi energy,  $E_f$  and scattering parameter,  $r$  [106, 108]. Fitted values of temperature dependent Seebeck coefficient used for this calculation is shown in Figure 5.6 (a), (b) and (c). To better understand the numerical results, parabolic single band model is created using these Fermi energy values as shown in Figure 5.7. Fermi energy of the pristine CNT yarn is 0.0037 eV, which is very near to the top of the valence band, showing the semi-metallic nature. After Joule heating,  $E_f$  becomes -0.071 eV and shifted to the opposite side of the valence band, creating energy gap between valence band and conduction band. On the other hand, it shows the semiconductor nature. After doping,  $E_f = 0.053$  eV is obtained, which

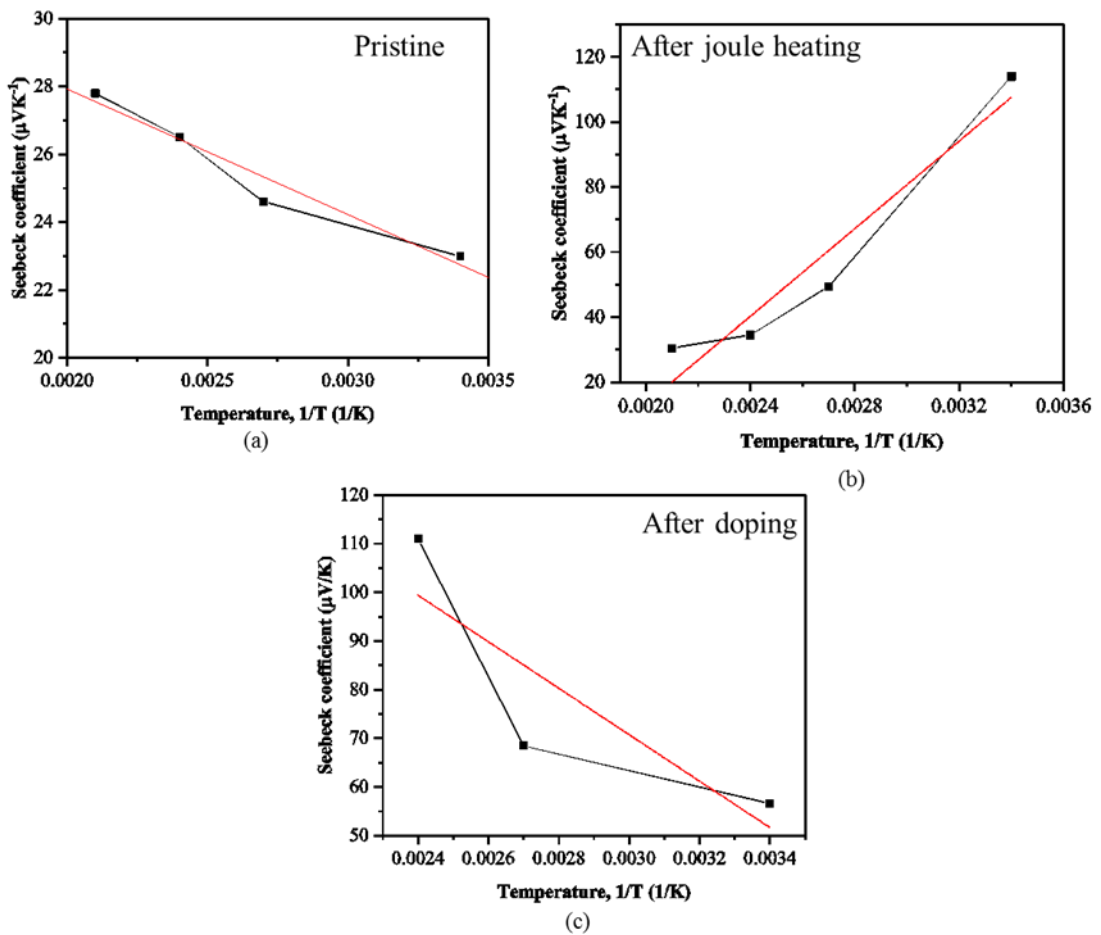


Figure 5.6: Fitted curves of temperature dependent Seebeck coefficient for (a) pristine CNT yarn and CNT yarn (b) after Joule heating and (c) doping.

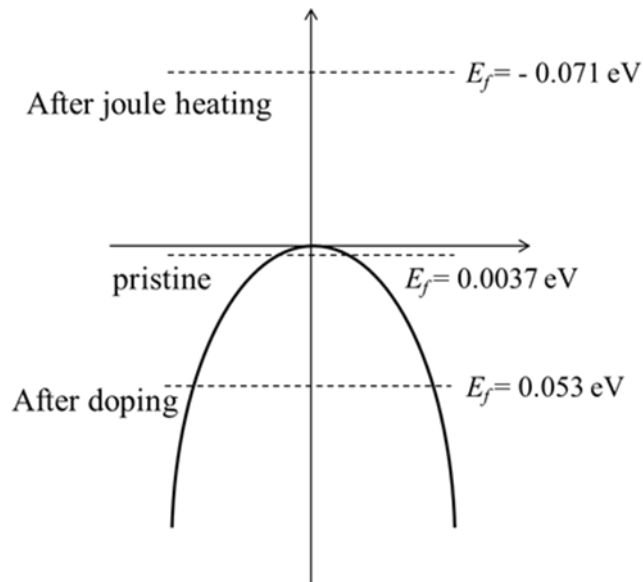


Figure 5.7: Model of single band diagram of CNT yarn.

indicates that the upper part of the valence band is filled of holes and changing of metallic nature. Therefore, the larger thermopower after Joule heating and the higher electrical conductivity after doping can be explained qualitatively from the above

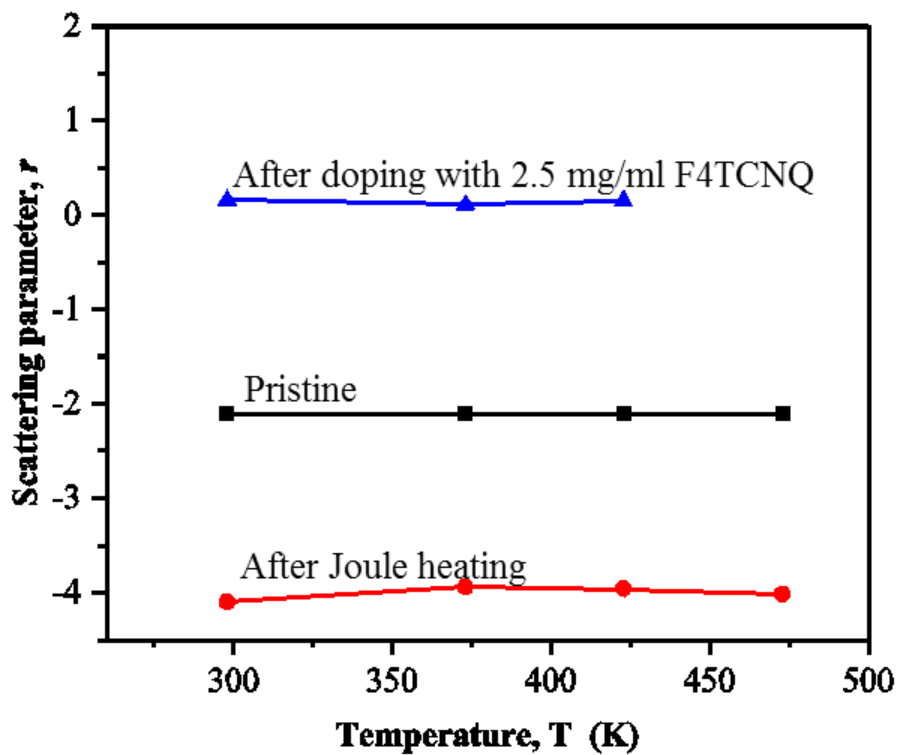


Figure 5.8: Calculated values of the scattering parameter as a function of temperature.

equations and band diagram. On the other hand, the calculated scattering parameter,  $r$  has negative (-) value and still it has negative (-) value after Joule heating. It shows the predominance of the acoustic scattering in the pristine and Joule annealed CNT yarn. This value changed to positive (+) value after doping, indicating ionized impurities scattering [106]. The calculated values of the scattering parameter as a function of temperature are shown in Figure 5.8.

Raman spectra were scanned to capture D band ( $1305\text{ cm}^{-1}$ ), G band ( $1545\text{ cm}^{-1}$ ) and G' or 2D band ( $2641\text{ cm}^{-1}$ ). G band represents in-plane bond stretching vibrations of  $sp^2$  hybridized carbon atoms of  $E_{2g}$  symmetry. D band comes from disorder or impurities in the MWCNT such as amorphous carbon with  $sp^3$  bonding and 2D band is the second order vibration mode of D band and related to structural defects in continuous graphitic sheet of the nanotubes [109-112]. Figure 5.9 shows the Raman spectra of CNT yarns annealed at various amount of heat. It can be seen that the intensity ratio of  $I_G$  to  $I_D$

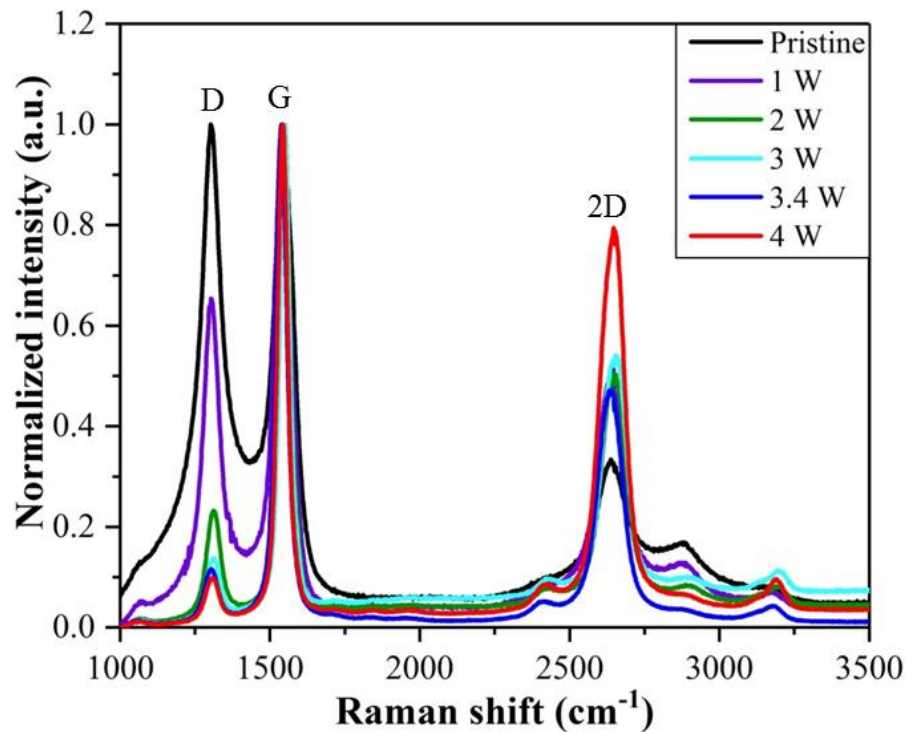


Figure 5.9: Normalized Raman spectra of CNT yarns annealed at various amount of heat such as 1, 2, 3, 3.4 and 4 W, respectively.

Table 5.1: The values of the intensity ratio of  $I_G/I_D$  and  $I_{2D}/I_G$ .

Joule Heat (W)	$I_G/I_D$	$I_{2D}/I_G$
0 (pristine)	1	0.3
1	1.6	0.5
2	5	0.5
3	11.2	0.5
3.4	15.7	0.4
4	17.8	0.7

increases from average values of 1 for the pristine CNT yarns to 11.2 and 17.8 for the yarns annealed at 3 and 4 W, respectively. But no Raman peak shift of the D band was observed after Joule annealing which is consistent with other reports [112]. The values of  $I_G/I_D$  and  $I_{2D}/I_G$  at various amounts of heats are listed in Table 5.1. These results reveal that the removal of amorphous carbon and impurities as well as improvement of crystallinity [113]. Concurrently, the intensities ratio of  $I_{2D}$  to  $I_G$  band in Raman spectra gradually increased while joule heating increased as in Figure 5.10. After Joule heating

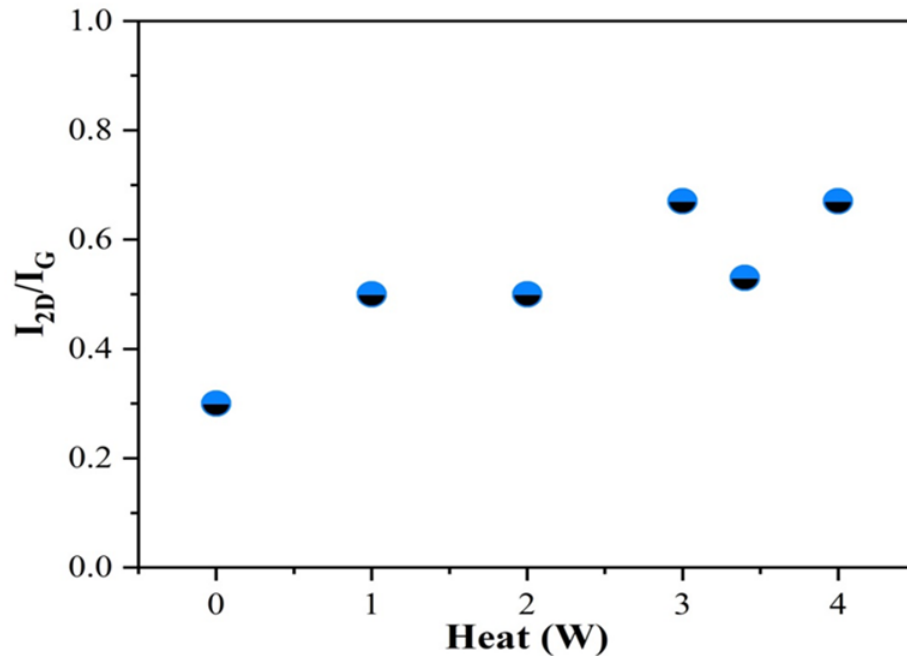


Figure 5.10: The relationship between the amount of Joule heating and the intensity of 2D band to G band in Raman spectroscopy, indication of the multi-layered graphene structure of CNT yarn.

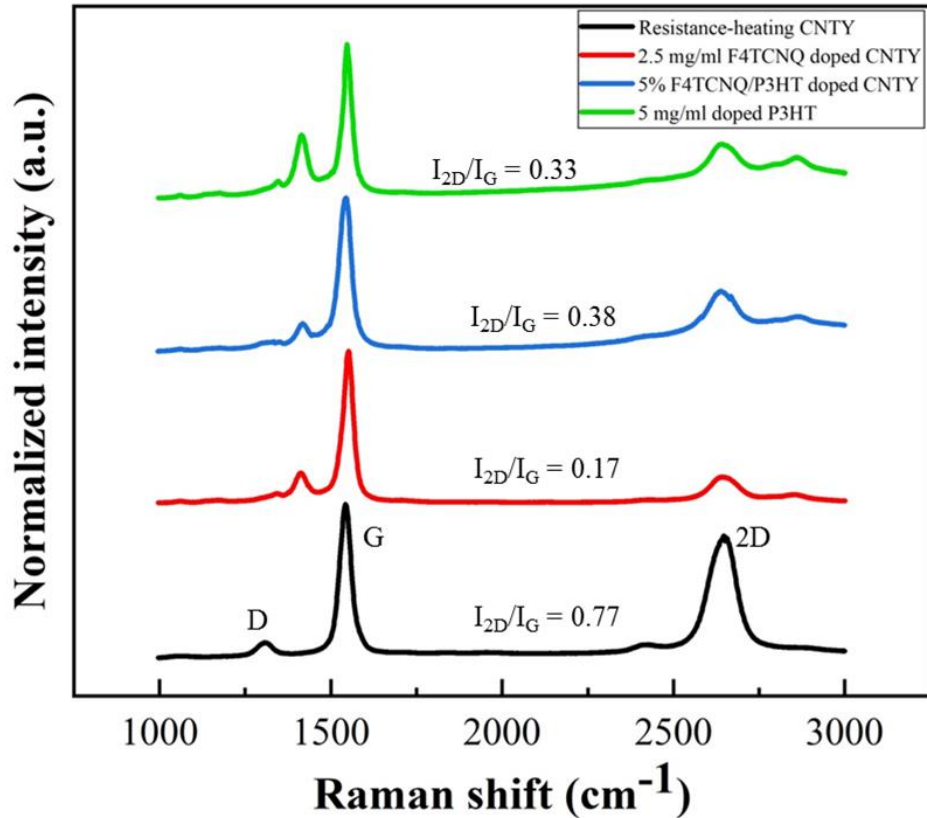


Figure 5.11: Normalized Raman spectra of annealed CNT yarn, and doped CNT yarn with 2.5 mg/ml F4TCNQ, 5% F4TCNQ/P3HT and 5mg/ml P3HT.

at 4 W, the intensity ratio of  $I_{2D}$  to  $I_G$  reaches nearly 0.8 which points out the formation of a few layer graphene structure on the surface of the CNT yarn.

Doping was confirmed by the G band shift and the intensity ratio of  $I_{2D}$  to  $I_G$  in the Raman spectra [112] as demonstrated in Figure 5.11. The G band of the samples doped with F4TCNQ (2.5 mg/ml), P3HT (5 mg/ml) and doped with both were red-shifted [114] from 1544 to 1552, 1546 and 1547  $\text{cm}^{-1}$  respectively. These G band shifts indicate the charge transfer from CNT yarn to dopant materials with the improvement of electron-phonon coupling [112, 114]. The intensity ratio of  $I_{2D}$  to  $I_G$  decreases again after doping. It points out the introduction of dopants into the CNT yarn and doping was successfully finished. After doping with 2.5 mg/ml F4TCNQ, the new peaks appeared at

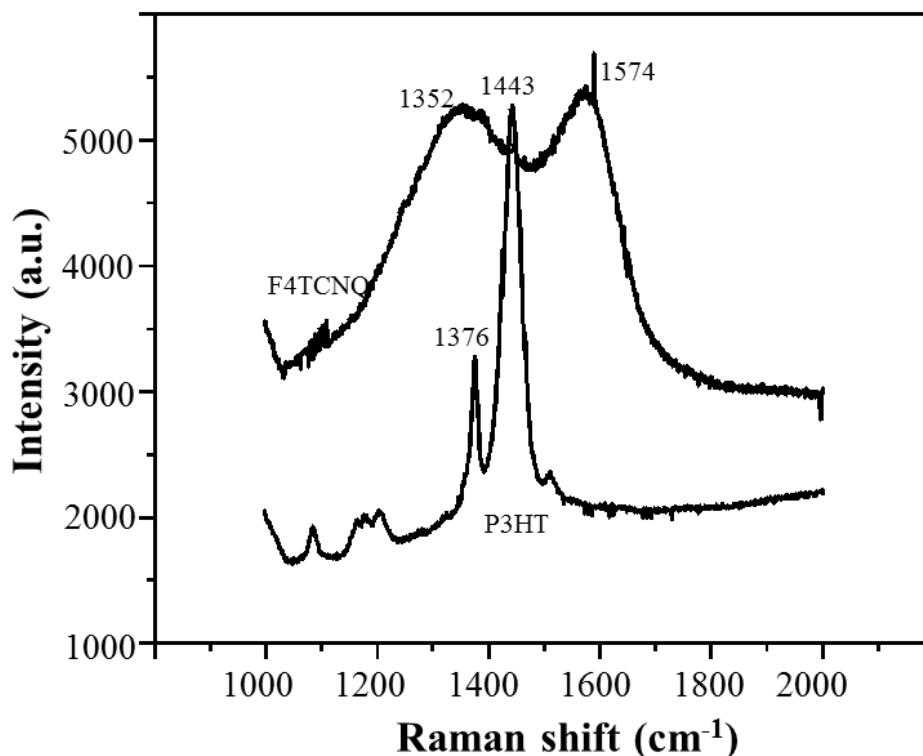


Figure 5.12: Raman spectra of pristine F4TCNQ and P3HT.

around 1345 and 1414  $\text{cm}^{-1}$  which come from the F4TCNQ. After doping with 5 % F4TCNQ and P3HT, the new peaks appeared at around 1349 and 1417  $\text{cm}^{-1}$  which come from the bond stretching between the F4TCNQ, P3HT and CNT yarn. After doping with P3HT, the new peaks appeared at around 1347 and 1415  $\text{cm}^{-1}$  which may come from the P3HT [115]. In order to compare before and after doping with CNT yarn and F4TCNQ and P3HT, the Raman spectra of pristine F4TCNQ and P3HT are shown in Figure 5.12.

Figure 5.13 shows TEM images of pristine, Joule annealed and doped CNT yarn with F4TCNQ and P3HT. We can see loosen CNTs from CNT yarn in TEM images because CNTs broke up from CNT yarn during probe sonication for sample preparation. Amorphous carbon can be seen on the surface of the pristine CNT yarn in Figure 5.13 (a). After Joule annealing, similar morphology of the CNT yarn with the pristine one is observed as in Figure 5.13 (b). This may be ascribed as graphene layer formation on the

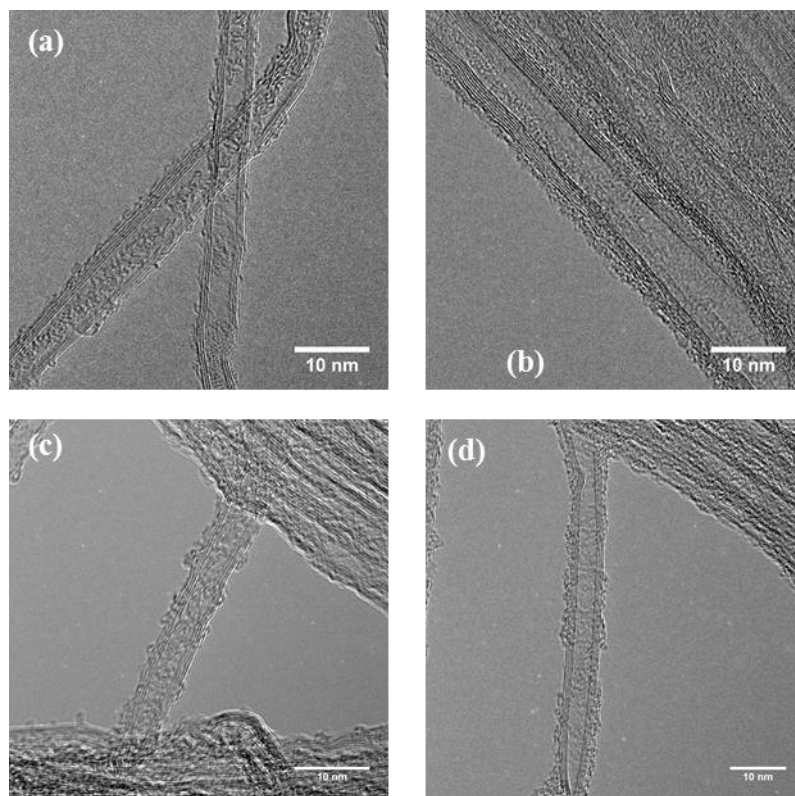


Figure 5.13: TEM images of (a) pristine, (b) Joule annealed, (c) F4TCNQ doped (2.5 mg/ml) and (d) P3HT doped (5 mg/ml) CNY yarns.

surface of the CNT yarn due to Joule heating. The improvement of the intensity ratio of 2D band to G band in Raman spectroscopy after Joule annealing also agrees well with this concept. TEM images are also acquired after doping with F4TCNQ and P3HT as in Figure 5.13 (c) and (d). Thicker coating layers observed in both figures can be attributed to the F4TCNQ and P3HT respectively. SEM images are also captured as in Figure 5.14 to get more information about morphology. After joule annealing, swelling structure is observed as demonstrated in Figure 5.14 (b). Even though smooth surface is examined after doping with 2.5 mg/ml F4TCNQ (Figure 5.14 (c)), some aggregates can be seen after doping with 10 mg/ml F4TCNQ (Figure 5.14 (d)). This is one possible reason why electrical conductivity decrease at higher concentration of F4TCNQ. Brighter and smooth surface is scanned after doping with 5 mg/ml P3HT (Figure 5.14 (e)). After

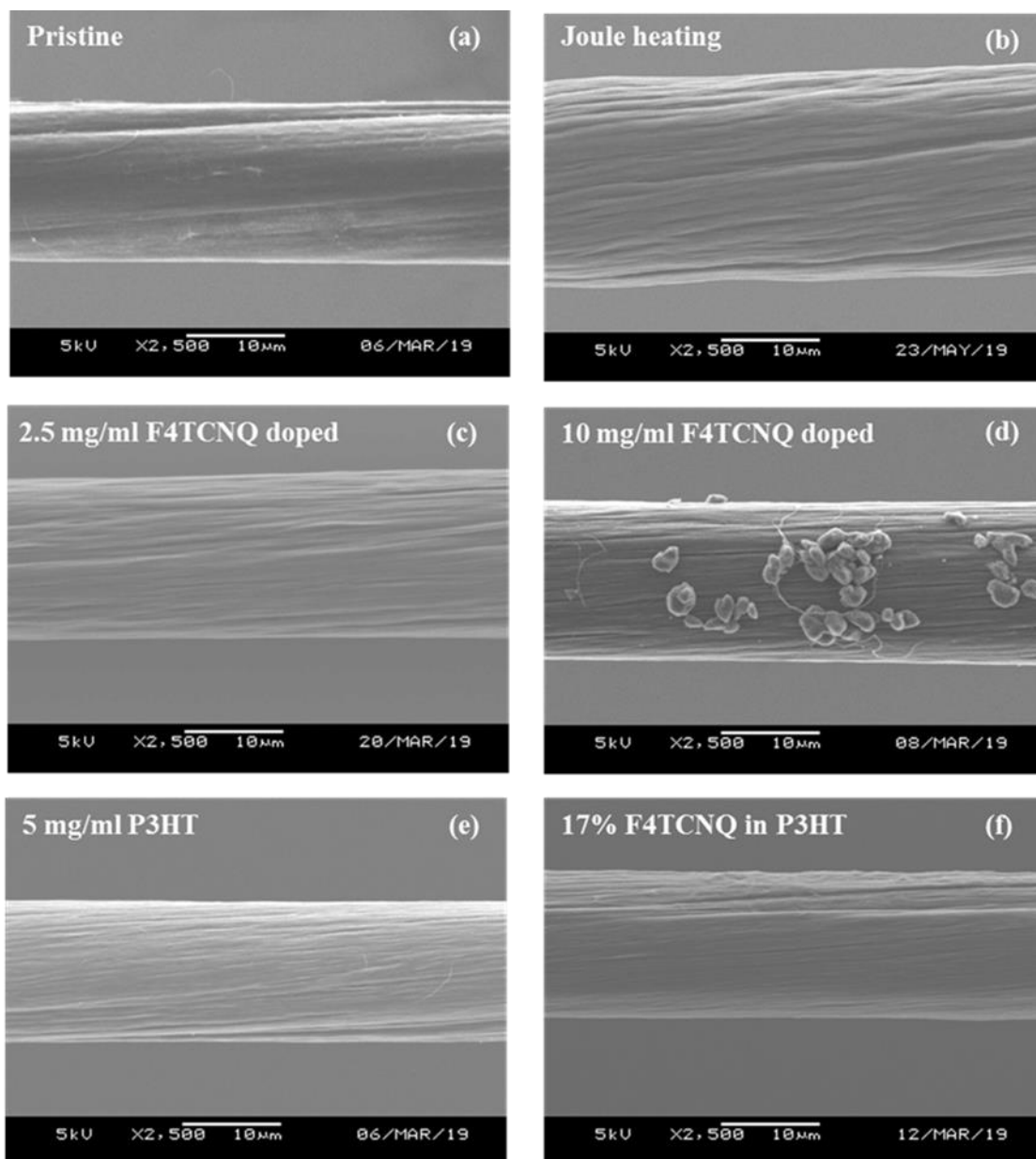


Figure 5.14: SEM images of (a) pristine, (b) Joule annealed, (c) 2.5 mg/ml F4TCNQ doped, (d) 10 mg/ml F4TCNQ doped, (e) 5 mg/ml P3HT and (f) 17 % F4TCNQ/P3HT doped CNT yarns.

doping with both F4TCNQ and P3HT, very small aggregates are observed on the surface of the CNT yarn (Figure 5.14 (f)). TGA (in air) analysis was used to analyze CNT and removal of impurity contents based on the weight changes in the CNT yarn before and after Joule annealing. The CNT content at 450° C is 92 % for pristine and 97 % after Joule heating, which is illustrated in Figure 5.15. A majority of the CNT yarn

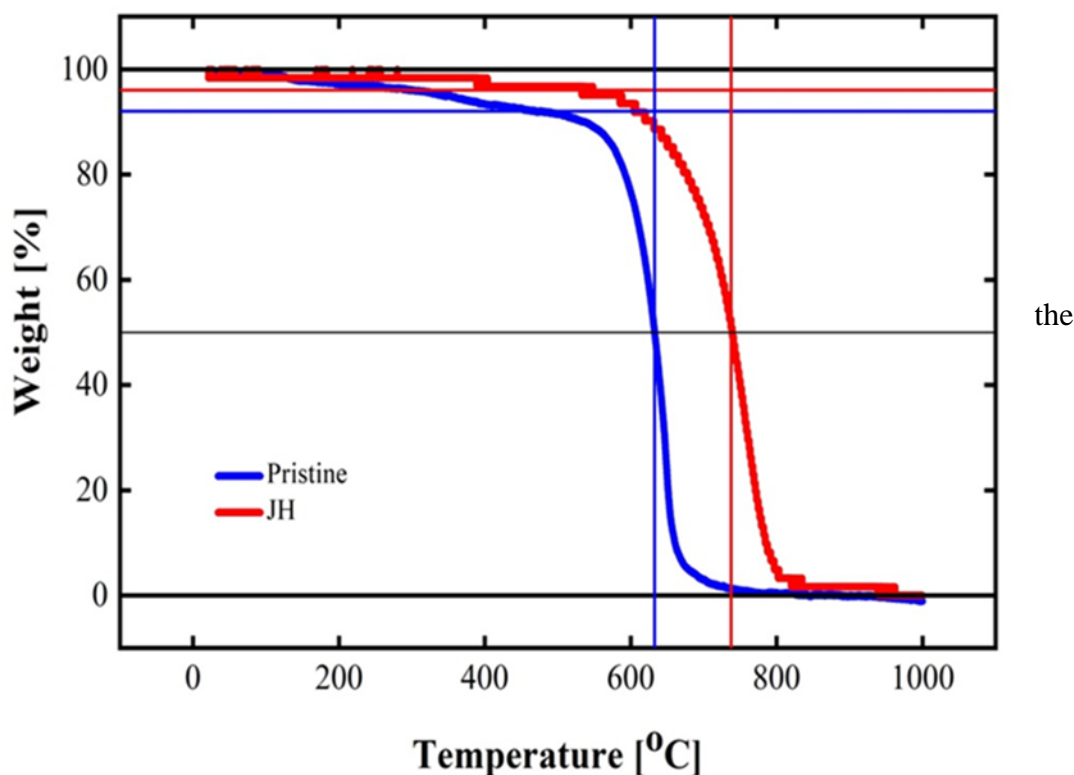


Figure 5.15: TGA analysis of the CNT yarn before and after Joule annealing.

impurities such as amorphous carbonaceous impurities are lost by 450°C in TGA [116]. This weight-loss until 450°C can be attributed to the removal of amorphous carbon. Therefore, very less amount of amorphous carbon is present in the CNT yarn after Joule heating. The temperature at which CNT combustion occurs ( $T_c$ ) is obtained from the TGA as 629 °C for pristine and 739°C for Joule heated CNT yarn.  $T_c$  upshifts after Joule annealing with  $\Delta T_c \approx 110^\circ\text{C}$ . Large amount of  $\Delta T_c$  value indicates that CNT themselves could participate in burning process associated with Joule annealing, leading to structure changes on CNT surfaces that effect  $T_c$  and hence,  $\Delta T_c$  [117].

#### 5.4. Conclusion

In this chapter, a novel approach for *p*-type doping of CNT yarn with F4TCNQ and P3HT is presented. Our results show that doping after Joule annealing can lead higher thermoelectric power factor of CNT yarn. Specifically, CNT yarn doped with 2.5 mg/ml

F4TCNQ exhibited a power factor of  $2250 \mu\text{Wm}^{-1}\text{K}^{-2}$ , which is one of the highest values among the p-typed doped MWCNT yarn. Moreover, pretreatment by Joule heating is confirmed to be effective way to improve Seebeck coefficient. Finally, combination of Joule annealing and doping can pave a way to enhance the thermoelectric properties of CNT yarn.

## CHAPTER 6

### Summary

In this thesis, how to improve thermoelectric properties of conducting polymer, PEDOT:PSS and P3HT/CNT yarn composite have been discussed. N<sub>2</sub> pressure-induced nitric acid treatment was used to improve electrical conductivity and Seebeck coefficient of PEDOT:PSS simultaneously. In PEDOT:PSS, the enhancement of electrical conductivity is due to the removal of insulating extra PSS from PEDOT:PSS and the conformation of PEDOT polymer structure from benzoid (coiled) to quinoid (linear) structure. In order to highlight the effect of N<sub>2</sub> gas pressure on the enhancement of thermoelectric properties of PEDOT:PSS, immersion in deionized (DI) water, drying in the vacuum chamber, or N<sub>2</sub> gas passing was performed after HNO<sub>3</sub> treatment. Among them, N<sub>2</sub> gas passing gave the optimum thermoelectric properties. In addition, H<sub>2</sub>SO<sub>4</sub> and HCl treatment were also performed to examine the effect of pressure of N<sub>2</sub> gas on the structure and thermoelectric properties of PEDOT:PSS. Based on our results, the conformation of PEDOT is due to the removal of PSS by acids and the pressure of N<sub>2</sub> gas. Acids are mainly responsible for the removal of insulating PSS, leading to the conformation of PEDOT while N<sub>2</sub> gas pressure is responsible for the additional conformation of PEDOT favoring the linear orientation of the polymer structure. Therefore, mechanical force such as N<sub>2</sub> blown after acids treatment makes the PEDOT:PSS films highly aligned and causes anisotropic charge transfer in the film leading to increase the electrical conductivity, regardless of the types of acids.

In P3HT/CNT yarn composite, Joule heating of CNT yarn before doping could enhance the Seebeck coefficient while doping with F4TCNQ gave the higher electrical conductivity. Joule heating can create band gap between the valence band and conduction band, leading to the higher density of states and resulting in the higher Seebeck coefficient. Doping with F4TCNQ can improve the electrical conductivity

creating the charge transfer between P3HT and CNT structure as dopant-linked semicrystalline polymer. Therefore, combination of joule heating and doping is a better approach to enhance both electrical conductivity and Seebeck coefficient of carbon-based materials.

## **Acknowledgement**

It is my pleasure to say “Thank you” to everyone who contributed in my Ph.D work.

Firstly, I would like to express my sincere gratitude to my supervisor, Professor Yasuhiko Hayashi, for providing me to join the Ph.D course and necessary assistances through the whole period of Ph.D course. Apart from my supervisor, I would like to thank to Associate Professor, Yoshifumi Yamashita and Toshihiko Kiwa for their kind supporting to accomplish this thesis.

The deep gratitude is reserved for Assistant Professor, Takeshi Nishikawa for his kind help, encouragement and valuable suggestions. I really appreciate his kind support and help whenever I have difficulties.

Special thanks are offered to Associate Professor, Aung Ko Ko Kyaw, Southern University of Science and Technology, Shenzhen, People Republic of China, who provided me great advice, comments and discussions during my Ph.D work.

I also would like to say “Thanks” to Associate Professor, Masaki Hada for giving some advices on my research.

I am also pleased to say “Thank you” to all of my colleagues in our laboratory, Nanodevices and Materials, for providing me a friendly atmosphere and for sharing knowledge and experiences, in particular, Takuma Hayashi, Hirotaka Inoue, Tatsuki Marui for their help to characterize my samples. Apart from this, I greatly appreciate for their helps which are very useful for my academic life as well as my personal life.

I also wish to express many thanks to Associate Professor, Yuta Nishina for XPS measurement, and Professor Masayoshi Umeno and Dr. Susumu Ichimura for Hall effect measurement.

This Ph.D study would not have been possible without the financial support from Japanese Government (MEXT) Scholarship, Nano devices and materials Lab. and

Okayama University. Therefore, I gratefully acknowledge to the funding received towards my Ph.D words.

Finally, there are no words to show my gratitude to my family and my friends (from MYANMAR) for their understanding, encouragement and necessary assistant.

## References

- [1]. Said, S. M.; Rahman, S. M.; Long, B. D.; Sabri, M. F. M. Preparation of TEG materials based on conducting polymer PEDOT:PSS through treatment by nitric acid. *WIT Trans. Ecol. Environ.* **2013**, *186*, 251-258.
- [2]. Eun, J. B.; Young, H. K.; Kwang-Suk, J.; Song, Y. C. Enhancement of thermoelectric properties of PEDOT:PSS and tellurium-PEDOT:PSS hybrid composites by simple chemical treatment. *Sci. Rep.* **2016**, *6*:18805.
- [3]. Salim, F.; Christophe, D.; Julien, V.; Didier, N.; Bernard, R.; Bruno, L. Organic thermoelectric device based on a stable n-type nanocomposite printed on paper. *Sustainable Energy Fuels* **2018**, *2*, 199-208.
- [4]. Nitin, S.; Mihael, C.; Anton, G.; Jan, W.; Mika, P.; Michael, K.; Martin, S. B.; Eva, M. H.; Peter, M. Morphology-function relationship of thermoelectric nanocomposite films from PEDOT:PSS with silicon nanoparticles. *Adv. Electron. Mater* **2017**, *3*, 8, 1.
- [5]. Tzounis, L.; Liebscher, M.; Mader, E.; Potschke, P.; Stamm, M.; Logothetidis, S. Thermal energy harvesting for large-scale applications using MWCNT-grafted glass fibers and polycarbonate-MWCNT nanocomposites. *AIP Conference Proceedings* **2015**, *1646*, 138.
- [6]. Haijun, S.; Congcong, L.; Jingkun, X.; Qinglin, J.; Hui, S. Fabrication of a layered nanostructure PEDOT:PSS/SWCNTs composite and its thermoelectric performance. *RSC Adv.* **2013**, *3*, 22065-22071.
- [7]. Suemori, K.; Hoshino, S.; Kamata, T. Flexible and lightweight thermoelectric generators composed of carbon nanotube-polystyrene composites printed on film substrate. *App. Phys. Lett.* **2013**, *103*, 153902.
- [8]. Gao, C.; Chen, G. Conducting polymer/carbon particle thermoelectric composites: Emerging green energy materials. *Composite Science and Technology* **2016**, *124*, 52-70.
- [9]. Yoo, D.; Kim, J.; Lee, S. H.; Cho, W.; Choi, H. H.; Kim, F. S.; Kim, J. H. Effects of one- and two- dimensional carbon hybridization of PEDOT: PSS on the power factor of polymer thermoelectric energy conversion devices. *J. Mater. Chem A.* **2015**, *3*, 6526-33
- [10]. Beretta, D.; Perego, A.; Lanzani, G.; Caironi, M. Organic flexible thermoelectric generators: From modeling, a roadmap towards applications. *Sustainable Energy Fuels* **2017**, *1*, 174-190

- [11]. Bubnova, O.; Khan, Z. U.; Malti, A.; Braun, S.; Fahlman, M.; Berggren, M.; Crispin, X. Optimization of the thermoelectric figure of merit in the conducting polymer poly(3,4-ethylenedioxythiophene). *Nat. Mater.* **2011**, *10*(6), 429–33
- [12]. Reene, K.; Desalegn, A. M.; David, K.; Jonna, H.; Jason, D. R.; Liyang, Y.; Christian, M. Thermoelectric plastics: from design to synthesis, processing and structure-properties relationships. *Chem. Soc. Rev.* **2016**, *45*, 6147-6164.
- [13]. Mario, C.; Clara, M. G.; Andres, C. Review on polymers for thermoelectric applications. *Materials* **2014**, *7*, 6701-6732.
- [14]. Bubnova, O.; Khan, Z. U.; Malti, A.; Braun, S.; Fahlman, M.; Berggren, M.; Crispin, X. Optimization of the Thermoelectric Figure of Merit in the Conducting Polymer Poly (3,4-ethylenedioxythiophene). *Nature Materials* **2011**, *10*, 429-433.
- [15]. Zheng, Y.; Luo, Y.; Du, C.; Zhu, B.; Liang, Q.; Hng, H. H.; Hippalgaonkar, K.; Xu, J.; Yan, Q. Designing hybrid architectures for advanced thermoelectric materials. *Mater. Chem. Front.* **2017**, *1*, 2457-2473.
- [16]. Yuan, L.; Zijun, S.; Qihao, Z.; Zhenxing, Z.; Yijing, T.; Lianjun, W.; Juanjuan, Z.; Wei, L.; Wan, J. Preparation of bulk AgNWs/PEDOT:PSS composites: a new model towards high performance bulk organic thermoelectric materials. *RSC Adv.* **2015**, *5*, 45106-45112.
- [17]. Xijing, S.; Yanhong, W.; Junajuan, L.; Jinghong, Z.; Lijuan, Z.; Quan, L. Ultralight conducting PEDOT:PSS/carbon nanotube aerogels doped with silver for thermoelectric materials. *Sci China Mater* **2017**, *60*(2), 159-166.
- [18]. Mahmoud, L.; Abdul, S. Y.; Alhawari, M.; Mohammad, B.; Liao, K.; Ismail, M. Combination of PVA with graphene to improve the Seebeck coefficient for thermoelectric generator applications. *Journal of ELECTRONIC MATERIALS* **2015**, *44*(1), 420-424.
- [19]. Bin, L.; Tingyu, L.; Biao, W.; Jun, L.; Tsuneyoshi, N.; Jun, Z.; Baowen, L. Thermoelectric transport in hybrid materials incorporating metallic nanowires in polymer matrix. *Appl. Phys. Lett.* **2017**, *110*, 113102.
- [20]. Lu, Z.; Tatsunari, G.; Ichiro, I.; Yasuaki, S.; Yutaka, H. Thermoelectric properties of PEDOT films prepared by electrochemical polymerization. *Journal of Polymer Science, Part B, Polymer Physics* **2017**, *55*, 524-531.
- [21]. Endou, L.; Congcong, L.; Zhengyou, Z.; Hui, S.; Qinglin, J.; Fengxing, J.; Jingkun, X.; Jinhua, X.; Yongjing, H. Enhanced thermoelectric performance of PEDOT:PSS films by solvent thermal treatment. *J Polym Res* **2015**, *22*:240.

- [22]. Qin, Y.; Lidong, C.; Sanyin, Q. Chapter 6: Conducting polymer-based nanocomposites for thermoelectric applications. *Fundamentals of conjugated polymer blends nanocomposites for thermoelectric applications* **2015**, 339-378.
- [23]. Boris, R., Annie, G.; Jeffrey, J.U.; Michael, L. C.; Rachel, A. S. Organic thermoelectric materials for energy harvesting and temperature control. *Nature Materials: Review* **2016**, *1*.
- [24]. Tzounis, L.; Gravalidis, C.; Vassiliadou, S.; Logothetidis, S. Fiber yarn/CNT hierarchical structures as thermoelectric generators. *Materials Today: Proceedings* **2017**, *4*, 7070-7075.
- [25]. Jeffery, G. S. Small thermoelectric generators. *The Electrochemical Society Interface* **2008**, 54-56.
- [26]. Mir, S. H.; Nagahara, L. A.; Thundat, T.; Mokarian-Tabari, P.; Furukawa, H.; Khosla, A. Review—Organic-Inorganic Hybrid Functional Materials: An Integrated Platform for Applied Technologies. *J. Electronchem. Soc.* **2018**, *165* (8), B3137-B3156.
- [27]. Dai, L. Intelligent macromolecules for smart devices: From materials synthesis to device applications. *Springer* **2004**.
- [28]. Crispin, X. Chapter-8: Thermoelectric Properties of Conducting Polymers. *The WSPC Reference on Organic Electronics: Organic Semiconductors* **2016**, 277-298.
- [29]. Brendan, T. M.; Alp, S.; Emily, P. Polymer composite for thermoelectric applications. *Angew Chem Int. Ed* **2015**, *54*, 1710-1723.
- [30]. Caiyan, G.; Guangming, C. Conducting polymer/carbon particle thermoelectric composites: Emerging green energy materials. *Composites Science and Technology* **2016**, *124*, 52-70.
- [31]. Yong, D.; Shirley, Z. S.; Kefeng, C.; Philip, S. C. Research progress on polymer-inorganic thermoelectric nanocomposite materials. *Progress in Polymer Science* **2012**, *37*, 820-841.
- [32]. György, I. Conducting polymers: A new era in electrochemistry. *2<sup>nd</sup> edition* **2012**.
- [33]. Li, Y. Conducting Polymers. *Organic Optoelectronic Materials, Chapter 2*, **2015**.

- [34]. Ghasemi-Mobarakeh, L.;Prabharakan, M. P.; Morshed, M.; Nasr-Esfahani, M. H.; Baharvand, H.; Kiani, S.; Al-Deyab, S. S.; Ramakrishna, S. Applications of conductive polymers, scaffolds and electrical stimulation for nerve tissue engineering. *J. Tissue Eng. Regen Med.***2011**, *5*, e17-e35.
- [35]. Balint, R.; Cassidy, N. J.; Cartmell, S. H. Conductive polymers: Towards a smart biomaterial for tissue engineering. *Acta Biomaterialia* **2014**, *10*, 2341-2353.
- [36]. Myint, M. T. Z.; Hada, M.; Inoue, H.; Marui, T.; Nishikawa, T.; Nishina, Y.; Ichimura, S.; Umeno, M.; Kyaw, A. K. K.; Hayashi, Y. Simultaneous improvement in electrical conductivity and Seebeck coefficient of PEDOT:PSS by N<sub>2</sub> pressure induced nitric acid treatment. *RSC Adv.* **2018**, *8*, 36563-36570.
- [37]. Udo, L.; Elisabeth, M.; Nicola, N.; Jurg, D.; Microscopical Investigations of PEDOT:PSS Thin Films. *Adv. Funct. Mater* **2009**, *19*, 1215-1220.
- [38]. Yao, H.; Fan, Z.; Cheng, H.; Guan, X.; Wang, C.; Sun, K. and Ouyang, J.; Recent Development of Thermoelectric Polymers and Composites. *Macromol. Rapid Commun.* **2018**, 1700727.
- [39]. Zhu, Z.; Liu, C.; Jiang, Q.; Shi, H.; Jiang, F.; Xu, J.; Xiong, J.; Liu, E. Optimizing the thermoelectric properties of PEDOT:PSS films by combining organic cosolvents with inorganics base. *J Mater Sci: Mater Electron* **2015**, *26*, 8515-8521.
- [40]. Culebras, M.; Choi, K.; Cho, C. Recent progress in flexible organic thermoelectric. *Micromachnies* **2018**, *9*, 638.
- [41]. Wang, X.; Kyaw, A. K. K.; Yin, C.; Wang, F.; Zhu, Q.; Tang, T.; Yee, P. I.; Xu, J. Enhancement of thermoelectric performance of PEDOT:PSS films by post-treatment with a superacid. *RSC Adv.* **2018**, *8*, 18334-18340.
- [42]. Fan, Z.; Li, P.; Du, D.; Ouyang, J. Significantly enhanced thermoelectric properties of PEDOT:PSS films through sequential post-treatment with common acids and bases. *Adv. Energy. Mater.* **2017**, *7* (8), 1602116.
- [43]. Meng, W.; Ge, R.; Li, Z.; Tong, J.; Liu, T.; Zhao, Q.; Xiong, S.; Jiang, F.; Mao, L.; Zhou, Y. Conductivity enhancement of PEDOT:PSS films via phosphoric acid treatment for flexible all-plastic solar cells. *ACS Appl. Mater. Interfaces* **2015**, *7* (25), 14089-14094.

- [44]. Kim, J.; Jang, J. G.; Hong, J-I.; Kim, S. H.; Kwak, J. Sulfuric acid vapour treatment for enhancing the thermoelectric properties of PEDOT:PSS thin films. *J. Mater. Sci: Mater. Electron* **2016**, *27*, 6122-6127.
- [45]. Myint, M. T. Z.; Inoue, H.; Ichimura, S.; Nishikawa, T.; Nishina, Y.; Kyaw, A. K. K.; Hayashi, Y. Influence of the pressure of nitrogen gas on the structure and thermoelectric properties of acid-treated PEDOT:PSS films. *DOI: 10.1007/s10854-019-01721-2*
- [46]. Kyaw, A. K. K.; Yemata, T. A.; Wang, X.; Lim, S. L.; Chin, W. S.; Hippalgaonkar, K.; Xu, J. Enhanced thermoelectric performance of PEDOT:PSS films by sequential post-treatment with formamide. *Macromol. Mater. Eng.* **2018**, *303*, 1700429.
- [47]. Jang, E.; Poosapati, A. Madan, D. Enhanced thermoelectric properties of F4TCNQ doped P3HT and its use as a binder for Sb<sub>2</sub>Te<sub>3</sub> based printed thermoelectric films. *ACS Appl. Energy Mater.* **2018**, *1*, 1455-1462.
- [48]. Pingel, P.; Neher, D. Comprehensive picture of *p*-type doping of P3HT with the molecular acceptor F<sub>4</sub>TCNQ. *Physical Review B* **2013**, *87*, 115209.
- [49]. Jacobs, I. E.; Aasen, E. W.; Oliveria, J. L.; Fonseca, T. N.; Roehling, J. D.; Li, J.; Zhang, G.; Augustine, M. P.; Mascall, M.; Moule, A. J. Comparison of solution-mixed and sequentially processed P3HT:F4TCNQ films: effect of doping-induced aggregation on film morphology. *J. Mater. Chem. C.* **2016**, *4*, 3454.
- [50]. Karthik, P. S.; Himaja, A. L.; Singh, S. P. Carbon-allotropes: synthesis methods, applications and future perspectives. *Carbon Letters* **2014**, *15* (4), 219-237.
- [51]. Avila, A. F.; Lacerda, G. Molecular mechanics applied to single-walled carbon nanotubes. *Materials Research* **2008**, *11* (3), 325-333.
- [52]. Saifuddin, N.; Raziah, A. Z.; Junizah, A. R. Carbon nanotubes: a review on structure and their interaction with proteins. *Journal of Chemistry* **2013**, Article ID: 676815.
- [53]. Aqel, A.; Abou EI-Nour, K. M. M.; Ammar, R. A. A.; Al-Warthan, A. Carbon nanotubes, science and technology part (1) structure, synthesis and characterization. *Arabian Journal of Chemistry* **2012**, *5*, 1-23.
- [54]. Ghemes, A.; Minami, Y.; Muramatsu, J.; Okada, M.; Mimura, H.; Inoue, Y. Fabrication and mechanical properties of carbon nanotube yarns spun from

- ultra-long multi-walled carbon nanotube arrays. *CARBON* **2012**, *50*, 4579-4587.
- [55]. Liu, K.; Zhu, F.; Liu, L.; Sun, Y.; Fan, S.; Jiang, K. Fabrication and processing of high-strength densely packed carbon nanotube yarns without solution processes. *Nanoscale* **2012**, *4*, 3389-3393.
- [56]. Duong, H. M.; Gong, F.; Liu, P.; Tran, T. Q. Chapter 2-Advanced fabrication and properties of aligned carbon nanotube composites: Experiments and Modeling. *Carbon nanotubes-current progress of their polymer composites* **2016**, 47-72.
- [57]. Wei, Q.; Mukaida, M.; Kirihara, K.; Naitoh, Y.; Ishida, T. Recent Progress on PEDOT-based Thermoelectric Materials. *Materials* **2015**, *8*, 732-750.
- [58]. Jiang, Q.; Liu, C.; Song, H.; Shi, H.; Yao, Y.; Xu, J.; Zhang, G.; Lu, B. Improved Thermoelectric Performance of PEDOT:PSS Films Prepared by Polar-solvent Vapor Annealing Method. *J. Mater. Sci: Mater. Electron.* **2013**, *24*, 4240-4246.
- [59]. Zhou, W.; Fan, Q.; Zhang, Q.; Li, K.; Cai, L.; Gu, X.; Yang, F.; Zhang, N.; Xiao, Z.; Chen, H.; Xiao, S.; Wang, Y.; Liu, H.; Zhou, W.; Xie, S. *small* **2016**, *12* (25), 3407-3414.
- [60]. Shin, N-R.; Choi, S-H.; Kim, J-Y. Highly Conductive PEDOT:PSS Electrode Films Hybridized with Gold-nanoparticles-doped-carbon Nanotubes. *Synthetic Metals* **2014**, *192*, 23-28.
- [61]. Cowen, L. M.; Atoyo, J.; Carnie, M. J.; Baran, D. ; Schroeder, B. C. Review—Organic Materials for Thermoelectric Energy Generation. *ECS Journal of Solid State Science and Technology* **2017**, *6* (3), N3080-N3088.
- [62]. Kim, J.; Jang, J. G.; Hong, J-I.; Kim, S. H.; Kwak, J. Sulfuric Acid Vapor Treatment for Enhancing the Thermoelectric Properties of PEDOT:PSS Thin-films. *J. Mater. Sci: Mater. Electron* **2016**, *27*, 6122-6127.
- [63]. Kim, G-H.; Shao, L.; Zhang, K.; Pipe, K. P. Engineer Doping of Organic Semiconductors for Enhanced Thermoelectric Efficiency. *Nature Materials* **2013**, *12* (8), 719-723.
- [64]. Mengisie, D. A.; Chen, C-H.; Boopathi, K. M.; Pranoto, F. W.; Li, L-J.; Chu, C-W. *ACS Appl. Mater. Interfaces* **2015**, *7* (1), 94-100.

- [65]. Sarath Kumar, S. R.; `Kurra, N.; Alshareef, H. N. Enhanced High Temperature Thermoelectric Response of Sulfuric Acid Treated Conducting Polymer Thin Films. *J. Mater. Chem. C* **2016**, *4*, 215-221.
- [66]. Yeon, C.; Yun, S. J.; Kim, J.; Lim, J. W. PEDOT:PSS Films with Greatly Enhanced Conductivity via Nitric Acid Treatment at Room Temperature and Their Application as Pt/TCO-Free Counter Electrodes in Dye-Sensitized Solar Cells. *Adv. Electron. Mater.* **2015**, *1*, 1500121 (1-8).
- [67]. Mengistie, D. A.; Wang, P-C.; Chu, C-W. Effect of Molecular Weight of Additives on the Conductivity of PEDOT:PSS and Efficiency for ITO-Free Organic Solar Cell. *J. Mater. Chem. A* **2013**, *1*, 9907-9915.
- [68]. Oh, H. J.; Jang, J. G.; Kim, J-G.; Hong, J-I.; Kim, J.; Kwak, J.; Kim, S. H.; Shin, S. Structural and Morphological Evaluation for Water-resistance Organic Thermoelectrics. *Scientific Reports* **2017**, *7*, 13287 (1-8)
- [69]. Fan, Z.; Du, D.; Yu, Z.; Li, P.; Xia, Y.; Ouyang, J. Significant Enhancement in the Thermoelectric Properties of PEDOT:PSS Films through at Treatment with Organic Solutions of Inorganic Salts. *ACS Appl. Mater. Interfaces* **2016**, *8* (35), 23204-23211.
- [70]. Kyaw, A. K. K.; Yemata, T. A.; Wang, X.; Lim, S. L.; Chin, W. S.; Hippalgaonkar, K.; Xu, J. Enhanced Thermoelectric Performance of PEDOT:PSS Films by Sequential Post-Treatment with Fomamide. *Macromol. Mater. Eng* **2017**, 1700429.
- [71]. Park, H.; Lee, S. H.; Kim, F. S.; Choi, H. H.; Cheong, I. W.; Kim, J. H. Enhanced Thermoelectric Properties of PEDOT:PSS Nanofilms by a Chemical Doping Process. *J. Mater. Chem. A* **2014**, *2*, 6532-6539.
- [72]. Bubnova, O.; Khan, Z. U.; Wang, H.; Braun, S.; Evans, D. R.; Fabretto, M.; Hojati-Talemi, P.; Dagnelung, D.; Arlin, J-B.; Geerts, Y. H.; Desbief, S.; Breiby, D. W.; Andreasen, J. W.; Lazzaroni, R.; Chen, W. M.; Zozoulenko, I.; Fahlman, M.; Murphy, P. J.; Berggren, M.; Crispin, X. Semi-metallic Polymers. *Nature Materials* **2014**, *13*, 190-194.
- [73]. Yu, Z.; Xia, Y.; Du, D.; Ouyang, J. PEDOT:PSS Films with Metallic Conductivity through a Treatment with Common Organic Solutions of Organic Salts and Their Application as a Transparent Electrode of Polymer Solar Cells. *ACS Appl. Mater. Interfaces* **2016**, *8*, 11629-11638.
- [74]. Andrei, V.; Bethke, K.; Madzharova, F.; Beeg, S.; Knop-Gericke, A.; Kneipp, J.; Rademann, K. Size Dependence of Electrical Conductivity and

Thermoelectric Enhancements in Spin-Coated PEDOT:PSS Single and Multiple Layers. *Adv. Electron. Mater* **2017**, 1600473 (1-8).

- [75]. Dubey, N.; Leclerc, M. Conducting Polymers: Efficient Thermoelectric Materials. *Journal of Polymer Science Part B: Polymer Physics* **2011**, 49, 467-475.
- [76]. Meng, Q.; Jiang, Q.; Cai, K.; Chen, L. Preparation and Thermoelectric Properties of PEDOT:PSS Coated Te nanoroad/PEDOT:PSS Composite Films. *Organic Electronics* **2019**, 64, 79-85.
- [77]. Shi, H.; Liu, C.; Jiang, Q.; Xu, J. Effective Approach to Improve the Electrical Conductivity of PEDOT:PSS: A Review. *Adv. Electron. Mater* **2015**, 1, 1500017 (1-16).
- [78]. Kim, J-S.; Woongsik, J.; Hwan, W. D. The Investigation of the Seebeck Effect of the Poly (3,4-Ethylenedioxythiophene)-Tosylate with the Various Concentrations of an Oxidant. *Polymers* **2019**, 11(1), 21.
- [79]. Xia, Y.; Ouyang, J.; Significant Conductivity Enhancement of Conductive Poly (3,4-ethylenedioxythiophene): Poly (styrenesulfonate) Films through a Treatment with Organic Carboxylic Acids and Inorganic Acids. *ACS Appl. Mater. Interfaces* **2010**, 2 (2), 474-483.
- [80]. Zhu, Z.; Liu, C.; Shi, H.; Jiang, Q.; Xu, J.; Jiang, F.; Xiong, J.; Liu, E. An Effective Approach to Enhance Thermoelectric Properties of PEDOT:PSS Films by a DES Post-Treatment. *Journal of Polymer Science Part B: Polymer Physics* **2015**, 53 (12), 885-892.
- [81]. Mazaheripour, A.; Majumdar, S.; Hanemann-Rawlings, D.; Thomas, E. M.; MacGuinness, C.; d'Alencon, L.; Chabinyk, M. L.; Segalman, R. A. Tailoring the Seebeck Coefficient of PEDOT:PSS by Controlling Ion Stiochometry in Ionic Liquid Additives. *Chem. Mater.* **2018**, 30 (14), 4816-4822.
- [82]. Wang, J.; Cai, K.; Shen, S. Enhanced Thermoelectric Properties of Poly (3,4-ethylenedioxythiophene) Thin Films Treated with H<sub>2</sub>SO<sub>4</sub>. *Organic Electronics* **2014**, 15 (11), 3087-3095.
- [83]. Mahajan, M. S.; Marathe, D. M.; Ghosh, S. S.; Ganesan, V.; Sali, J. V. Changes in in-plane Electrical Conductivity of PEDOT:PSS Thin Films due to Electric Field Induced Dipolar Reorientation. *RSC Advances* **2015**, 5, 86393-86401.

- [84]. Li, L.; Gao, P.; Schuermann, K. C.; Ostendorp, S.; Wang, W.; Du, C.; Lei, Y.; Fuchs, H.; Cola, L. D.; Müllen, K.; Chi, L. Controllable Growth and Field-Effect Property of Monolayer to Multilayer Microstripes of an Organic Semiconductor. *J. Am. Chem. Soc.* **2010**, *132* (26), 8807-8809.
- [85]. Kyaw, A. K. K.; Lay, L. S.; Peng, G. W.; Changyun, J.; Jie, Z. A Nanogroove-guided Slot-die Coating Technique for Highly Ordered Polymer Films and High-mobility Transistors. *Chem. Commun.* **2016**, *52*, 358-361.
- [86]. Yang, C. Y.; Soci, C.; Moses, D.; Heeger, A. J. Aligned rrP3HT Film: Structural Order and Transport Properties. *Synthetic Metals* **2005**, *155*, 639-642.
- [87]. Luo, C.; Kyaw, A. K. K.; Perez, L. A.; Patel, S.; Wang, M.; Grimm, B.; Bazan, G. C.; Kramer, E. J.; Heeger, A. J. General Strategy for Self-Assembly of Highly Oriented Nanocrystalline Semiconducting Polymers with High Mobility. *Nano. Lett.* **2014**, *14* (5), 2764-2771.
- [88]. Tsai, T-C.; Chang, H-C.; Chen, C-H.; Huang, Y-C.; Whang, W-T. A Facile Dedoping Approach for Effectively Tuning Thermoelectricity and Acidity of PEDOT:PSS Films. *Organic Electronics* **2014**, *15* (3), 641-645.
- [89]. Chang, S. H.; Chiang, C-H.; Kao, F-S.; Tien, C-L.; Wu, C-G. Unraveling the Enhanced Electrical Conductivity of PEDOT:PSS Thin Films for ITO-free Organic Photovoltaics. *IEEE Photonics* **2014**, *6* (4), 8400307.
- [90]. Mengistie, D. A.; Ibrahem, M. A.; Wang, P-C.; Chu, C-W. Highly Conductive PEDOT:PSS Treated with Fomic Acid for ITO-free Polymer Solar Cell. *ACS Appl. Mater. Interfaces* **2014**, *6* (4), 2292-2299.
- [91]. Sarker, A. K.; Kim, J.; Wee, B-H.; Song, H-J.; Lee, Y.; Hong, J-D.; Lee, C. Hydroiodic Acid Treated PEDOT:PSS Thin Films as Transparent Electrodes: An Approach Towards ITO Free Organic Photovoltaics. *RSC Adv.* **2015**, *5*, 52019-52025.
- [92]. Hu, A.; Tan, L.; Hu, X.; Hu, L.; Ai, Q.; Meng, X.; Chen L.; Chen, Y. Crystallization and Conformation Engineering of Solution-processed Polymer Transparent Electrodes with High Conductivity. *J. Mater. Chem. C.* **2017**, *5*, 382-389.
- [93]. Beretta, D.; Perego, A.; Lanzani, G.; Caironi, M. Organic Flexible Thermoelectric Generators: from Modeling, A Roadmap Towards Application. *Sustainable Energy Fuels.* **2017**, *1*, 174-190.

- [94]. Bahk, J-H.; Fang, H.; Yazawa, K.; Shakouri, A. Flexible Thermoelectric Materials and Device Optimization for Wearable Energy Harvesting. *J. Mater. Chem. C* **2015**, *3*, 10362-10374.
- [95]. An, C. J.; Kang, Y. H.; Song, H.; Jeong, Y.; Cho, S. Y. High-Performance Flexible Thermoelectric Generator by Control of Electronic Structure of Directly Spun Carbon Nanotube Webs with Various Molecular Dopants. *J. Mater. Chem. A* **2017**, *5*, 15631-15639.
- [96]. Du, Y.; Xu, J.; Paul, B.; Eklund, P. Flexible Thermoelectric Materials and Devices. *Applied Materials Today* **2018**, *12*, 366-388.
- [97]. Choi, J.; Jung, Y.; Yang, S. J.; Oh, J. Y.; Oh, J.; Jo, K.; Son, J. G.; Moon, S. E.; Park, C. R.; Kim, H. Flexible and Robust Thermoelectric Generators Based on All-Carbon Nanotube Yarn without Metal Electrodes. *ACS Nano* **2017**, *11*, 7608-7614.
- [98]. Min, C.; Shen, X.; Shi, Z.; Chen, L.; Xu, Z. The Electrical Properties and Conducting Mechanisms of Carbon Nanotube/Polymer Nanocomposites: A Review. *Polymer-Plastics Technology and Engineering* **2010**, *49*, 1172-1181.
- [99]. Cho, C.; Wallace, K. L.; Tzeng, P.; Hsu, J-H.; Yu, C.; Grunlan, J. C. Outstanding Low Temperature Thermoelectric Power Factor from Completely Organic Thin Films Enabled by Multidimensional Conjugated Nanomaterials. *Adv. Energy Mater.* **2016**, 1502168.
- [100]. MacLeod, B. A.; Stanton, N. J.; Gould, I. E.; Wesenberg, D.; Ihly, R.; Owczarczyk, Z. R.; Hurst, K. E.; Fewox, C. S.; Folmar, C. N.; Hughes, K. H.; Zink, B. L.; Blackburn, J. L.; Ferguson, A. J. Large n- and p-type Thermoelectric Power Factors from Doped Semiconducting Single-walled Carbon Nanotube Thin Films. *Energy Environ. Sci.* **2017**, *10*, 2168-2179.
- [101]. Inoue, H.; Yoshiyama, T.; Hada, M.; Chujo, D.; Saito, Y.; Nishikawa, T.; Yamashita, Y.; Takarada, W.; Matsumoto, H.; Hayashi, Y. High-Performance Structure of a Coiled-Shaped Soft-Actuator Consisting of Polymer Threads and Carbon Nanotube Yarns. *AIP Advances* **2018**, *8*, 075316.
- [102]. Maik, S.; Hayashi, Y.; Vyacheslav, K.; Chujo, D.; Inoue, H.; Hada, M.; Albrecht, L.; Bernd, B.; Silke, H. Resistance-Heating of Carbon Nanotube Yarns in Different Atmospheres. *Carbon* **2018**, *133*, 232-238.
- [103]. Jang, E.; Poosapati, A.; Madan, D. Enhanced Thermoelectric Properties of F4TCNQ Doped P3HT and Its Use as a Binder for Sb<sub>2</sub>Te<sub>3</sub> Based Printed Thermoelectric Films. *ACS Appl. Energy Mater.* **2018**, *1*, 1455-1462.

- [104]. Jacobs, I. E.; Aasen, E. W.; Oliveira, J. L.; Fonseca, T. N.; Roehling, J. D.; Li, J.; Zhang, G.; Augustine, M. P.; Mascal, M.; Moule, A. J. Comparison of Solution-Mixed and Sequentially Processed P3HT:F4TCNQ Films: Effect of Doping-Induced Aggregation on Film Morphology. *J. Mater. Chem. C* **2016**, *4*, 3454.
- [105]. Randeniya, L. K.; Bendavid, A.; Martin, P. J.; Tran, C-D. Composite Yarns of Multiwalled Carbon Nanotubes with Metallic Electrical Conductivity. *small* **2010**, *6* (16), 1806-1811.
- [106]. Lee, H. Thermoelectric Transport Properties for Electrons, Chapter 12. *Thermoelectrics: Design and Materials* **2017**.
- [107]. Hung, N. T.; Nugraha, A. R. T.; Hasdeo, E. H.; Dresselhaus, M. S.; Saito, R. Diameter Dependence of Thermoelectric Power of Semiconducting Carbon Nanotubes. *Physical Review B* **2015**, *92*, 165426.
- [108]. Hone, J.; Ellwood, I.; Munro, M.; Mizel, A.; Cohen, M. L.; Zettl, A. Thermoelectric Power of Single-Walled Carbon Nanotubes. *Physical Review Letters* **1998**, *80*(5), 1042-1045.
- [109]. Hopkins, A. R.; Labatete-Goeppinger, A. C.; Kim, H.; Katzman, H. A. Space Survivability of Carbon Nanotube Yarn Material in Low Earth Orbit. *Carbon* **2016**, *107*, 77-86.
- [110]. Rebelo, S. L. H.; Guedes, A.; Szeftczyk, M. E.; Pereira, A. M.; Araujo, J. P.; Freire, C. Progress in the Raman Spectra Analysis of Covalently Functionalized Multiwalled Carbon Nanotubes: Unraveling Disorder in Graphitic Materials. *Phys. Chem. Chem. Phys.* **2016**, *18*, 12784-12796.
- [111]. Pierlot, A. P.; Woodhead, A. L.; Church, J. S. Thermal Annealing Effects on Multi-walled Carbon Nanotube Yarns Probed by Raman Spectroscopy. *Spectrochimica Acta Part A: Molecular and Biomolecular Spectroscopy* **2014**, *117*, 598-603.
- [112]. An, C. J.; Kang, Y. H.; Song, H.; Jeong, Y.; Cho, S. Y. High-performance Flexible Thermoelectric Generator by Control of Electronic Structure of Directly Spun Carbon Nanotube Webs with Various Molecular Dopants. *J. Mater. Chem. A* **2017**, *5*, 15631-15639.
- [113]. Niven, J. F.; Johnson, M. B.; Juckes, S. M.; White, M. A.; Alvarez, N. T.; Shanov, V. Influence of Annealing on Thermal and Electrical Properties of Carbon Nanotube Yarns. *Carbon* **2016**, *99*, 485-490.

- [114]. Mahakul, P. C.; Mahanandia, P. Structural and Electrical Characteristics of Solution Processed P3HT-Carbon Nanotube Composite. *IOP Conf. Ser.:Mater. Sci. Eng.* **2017**, *178*, 012024.
- [115]. Giulianini, M.; Waclawik, E. R.; Bell, J. M.; Scarselli, M.; Castrucci, P.; Crescenzi, M. D.; Motta, N. Microscopic and Spectroscopic Investigation of Poly (3-hexylthiophene) Interaction with Carbon Nanotube. *Polymers* **2011**, *3*, 1433-1446.
- [116]. Pang, L. S. K.; Saxby, J. D.; Chatfield, S. P. Thermogravimetric Analysis of Carbon Nanotubes and Nanoparticles. *The Journal of Physical Chemistry* **1993**, *97*(27), 6941-6942.
- [117]. Sundaram, R.; Yamada, T.; Hata, K.; Sekiguchi, Atsuko. Purifying Carbon Nanotube Wires by Vacuum Annealing. *Materials Today: Proceedings* **2018**, *5*, 27316-27326.

## List of Publications

### Refereed Papers

(1) “Simultaneous Improvement in Electrical Conductivity and Seebeck Coefficient of PEDOT:PSS by N<sub>2</sub> Pressure-induced Nitric Acid Treatment”

**May Thu Zar Myint**, Masaki Hada, Hirotaka Inoue, Tatsuki Marui, Takeshi Nishikawa, Yuta Nishina, Susumu Ichimura, Mayoshi Umeno, Aung Ko Ko Kyaw and Yasuhiko Hayashi.

*RSC Adv.* **2018**, 8, 36563-36570.

(2) “Influence of pressure of nitrogen gas on structure and thermoelectric properties of acid-treated PEDOT:PSS films”

**May Thu Zar Myint**, Hirotaka Inoue, Susumu Ichimura, Takeshi Nishikawa, Yuta Nishina, Aung Ko Ko Kyaw and Yasuhiko Hayashi.

*J. Mater Sci: Mater Electron* **2019**, 30 (14), 13534-13542.

### List of Oral and Poster Presentations

(1) Investigation on the Effects of PSS Loading on PEDOT:PSS/MWCNTs Composite for Thermoelectric Applications (Oral Presentation only)

**May Thu Zar Myint**, Karthik PS, Zaw Lin, Venkata Krishina Rao, Venkata Abhinav K, Takuma Hayashi, Hirotaka Inoue, Takeshi Nishikawa, Masaki Hada, Yasuhiko Hayashi

*International Conference on Applied Science (ICAS 2017)*, Higher Education Forum, (Hokkaido, Japan, 19-21 January, **2017**).

(2) Dedoping of PSS from PEDOT:PSS/MWCNT Composite to Improve Thermoelectric Properties (Oral Presentation only)

**May Thu Zar Myint**, V. A. Korada, M. M. Peter, M. Hada, T. Nishikawa, Y. Hayashi  
*The 4<sup>th</sup> International Symposium on Microwave/Terahertz Science and Applications & the 8<sup>th</sup> International Symposium on Terahertz Nanoscience (MTSA 2017 & Tera Nano 8)*. (Okayama, Japan, 19-23 November, **2017**).

(3) A Facile Approach to Enhance the Thermoelectric Properties of PEDOT:PSS through Post-Treatment with Nitric Acid (Oral Presentation only)

**May Thu Zar Myint**, Masaki Hada, Takeshi Nishikawa, Aung Ko Ko Kyaw, Yasuhiko Hayashi

*4<sup>th</sup> International Conference on Mechanical Structures and Smart Materials (ICMSSM 2018)*, X-Academy, (Shenzhen, China, 22-23 September, **2018**).

(4) Significant Improvement of the Thermoelectric Properties of PEDOT:PSS by the Synergetic Effect of Nitric Acid and the Pressure of N<sub>2</sub> Gas. (Poster Presentation only)

**May Thu Zar Myint**, Aung Ko Ko Kyaw, Takayuki Yoshiyama, Hiroataka Inoue, Takeshi Nishikawa, Masaki Hada and Yasuhiko Hayashi

*31<sup>st</sup> International Microprocesses and Nanotechnology Conference (MNC 2018)*, The Japan Society of Applied Physics (Sapporo, Hokkaido, Japan, 13-16 November, **2018**).

(5) Effect *p*-type doping on thermoelectric properties of carbon nanotube yarn devices. (Oral Presentation only)

**May Thu Zar Myint**, Aung Ko Ko Kyaw, Takayuki Yoshiyama, Hiroataka Inoue, Takeshi Nishikawa, Masaki Hada and Yasuhiko Hayashi

*The 38<sup>th</sup> International Conference on Thermoelectrics and The 4<sup>th</sup> Asian Conference on Thermoelectrics (ICT/ACT 2019)*, International Thermoelectric Societies (ITS), Asian Association of Thermoelectrics (AAT), Korea Thermoelectric Society (KTS), The Korean Institute of Metals and Materials (Gyeongju, Korea, 30 June - 4 July, **2019**).